IEEE ComSoc IEEE Communications Society | IEEE Open Journal of the Communications Society

Received 6 February 2026; accepted 1 March 2026. Date of publication 4 March 2026; date of current version 12 March 2026.

Digital Object Identifier 10.1109/OJCOMS.2026.3670414

An Ecosystemic Approach for the Seamless Integration of Terrestrial and Non-Terrestrial Network Connections

CLAUDIO SACCHI[1,2] (Senior Member, IEEE), CARMEN D'ANDREA[3,4] (Member, IEEE), ELISA CONTI[4,5], TOMMASO FOGGI[4,5], AMINA PIEMONTESE[4,5], ALESSANDRO UGOLINI[4,5], ARMANDO VANNUCCI[4,5], CAMILO ROJAS[6] (Graduate Student Member, IEEE), NOUR BADINI[6] (Member, IEEE), FABIO PATRONE[6] (Member, IEEE), MARIO MARCHESE[6] (Senior Member, IEEE), FULVIO BABICH[4,7] (Senior Member, IEEE), MASSIMILIANO COMISSO[4,7] (Member, IEEE), ALBERTO CARINI[4,7] (Senior Member, IEEE), FRANCESCO ADAMO[8,9,10], SIMONE PAULETTO[7,10], HENOK BERHANU TSEGAYE[2] (Member, IEEE), PETRO MUSHIDI TSHAKWANDA[2] (Senior Member, IEEE), AND MICHAEL DEVETSIKIOTIS[2] (Fellow, IEEE)

[1]Department of Information Engineering and Computer Science (DISI), University of Trento, 318123 Trento, Italy
[2]Department of Electrical and Computer Engineering, The University of New Mexico, Albuquerque, NM 87131 USA
[3]Department of Electrical and Information Engineering, University of Cassino and Lazio Meridionale, 03043 Cassino, Italy
[4]Consorzio Nazionale Interuniversitario per le Telecomunicazioni (CNIT), 43124 Parma, Italy
[5]Department of Engineering and Architecture, University of Parma, 43124 Parma, Italy
[6]University of Genova, 16145 Genoa, Italy
[7]Department of Engineering and Architecture, University of Trieste, 34127 Trieste, Italy
[8]University of Trento, 38122 Trento, Italy
[9]University of Trieste, 34127 Trieste, Italy
[10]PicoSats s.r.l., 34149 Trieste, Italy

CORRESPONDING AUTHOR: C. SACCHI (claudio.sacchi@unitn.it)

This work was supported by European Union through Italian National Recovery and Resilience Plan (NRRP) of NextGenerationEU, partnership on "Telecommunications of the Future" (program "RESearch and innovation on future Telecommunications systems and networks, to make Italy more smART (RESTART)") under Grant PE00000001; in part by the Ph.D. Program in Space Science and Technology at the University of Trento, Cycle XXXVIII, co-financed by the Ministerial Decree no. 352 of April 2022, based on NRRP Mission 4 "Education and Research," Component 2 "From Research to Business," Investment 3.3, under Grant CUP E63C22001350008; and in part by the company PicoSaTs s.r.l.

ABSTRACT An unrestricted, global, and ubiquitous connectivity, available to anyone, everywhere, and anytime, is a key objective of the 6G vision. A true, seamless integration of terrestrial (T) and non-terrestrial (NT) networks is mandatory to reach such an ambitious target. From this perspective, the three-year ITA-NTN project (2023-2025), funded by the European Union within the framework of NextGenerationEU work program, aims to investigate advanced solutions for the seamless integration of Terrestrial and Non-Terrestrial networks. This paper considers the project aspects concerning the provision of seamless *connectivity* across the heterogeneous T and NT layers by proposing an integrated *ecosystem*, which enables transparent information exchange among the various communicating nodes belonging to each layer. The ecosystem relies on the software-based management of fully reconfigurable network architectures based on disruptive concepts like cell-free multiple-input multiple-output (MIMO), full software-defined radio (SDR)-based multi-waveforms physical layer design, use of aggressive capacity-oriented radio resource management strategies based on Non Orthogonal Multiple Access (NOMA), extended use of Software-Defined Networking (SDN), and Artificial Intelligence (AI) to monitor and manage the entire network architecture. The discussion of the achieved results validates the proposed ecosystemic approach both in terms of viability and quantitative performance improvement.

INDEX TERMS Artificial intelligence, cell-free MIMO, NOMA non-terrestrial networks, seamless connectivity, 6G, software-defined networking, cloud computing, MEC, software-defined radio.

I. INTRODUCTION

THE proclaimed objective of the Sixth Generation (6G) telecommunication standard is to guarantee access to ICT services as a universal right. For this reason, 6G network infrastructures aim to reach every point on the terrestrial globe at any time [1]. Nowadays, terrestrial networks can

provide broadband connectivity to many areas in the World. However, they are still far from achieving global coverage, which means that two geographical locations, arbitrarily placed in the globe, must be reached by a connection with guaranteed Quality-of-Service (QoS). Unfortunately, many geographical areas are not currently connected (islands, forests, seas, mountains, plains, and remote areas). The data reported by the International Telecommunication Union (ITU) in 2024 regarding the percentage of individuals using the Internet highlighted the well-known disparity between developed and developing countries, as well as a dramatic access gap between rural and urban areas [2]. Globally, 83 percent of urban dwellers used the Internet in 2024, compared with less than half of the rural population (48 percent). Of the 2.6 billion people not using the Internet, 1.8 billion reside in rural areas, against 800 million in urban areas. Such numbers indicate a true emergency that is not limited to the economically depressed areas of the globe. Moreover, [2] highlights a strict correlation between the accessibility of the Internet and the per-capita income. Therefore, the efficient access to Internetworking services is not only a technical matter, as clearly remarked by the UNO [1]. On the contrary, it involves highly critical societal issues.

From another side, the recent COVID-19 outbreak also convinced the most skeptical that, nowadays, connectivity is a vital factor. Indeed, if everyday life was only partially suspended during the pandemic emergency, this was ascribed to the capillary diffusion of fixed and mobile communication services, at least in the developed countries. Indeed, commercial activities, didactics, public administration offices, and private companies survived thanks to the virtualization and the remotization of the workload, also known as *smart working*. The lesson was immediately learned. Indeed, in 2020, during the peak of the pandemic outbreak, the European Union decided to launch a very rich R&D program called NextGenerationEU [3], aimed at restarting life after the sanitary shock. In such a program, a special role has been assigned to accelerate the update of existing networking infrastructures from the perspective of 6G, accepting the big challenge of global and ubiquitous connectivity.

The objective of NextGenerationEU was to restart the European life and economy, and RESTART is indeed the acronym of the Italian branch of NextGenerationEU dedicated to innovation in the field of Telecommunications and Networking systems targeted at improving everyday life [4]. The RESTART programme is articulated into 32 research sub-projects: 14 of them are big structural projects, and 18 are smaller, focused projects. Among the structural projects, ITA-NTN (the acronym stands for ''Integrated Terrestrial and Non-Terrestrial Networks'') focuses on the aspects related to the study and development of innovative integrated T-NT architectures. The RESTART programme also considers cascade-call projects, which tackle some specific research aspects within the field of interest of the structural projects. This is the case of INFINITE, a two-year project (2024-2025), whose acronym stands for: ''An Integrated and Sustainable Terrestrial/Non-Terrestrial Ecosystem for Anytime/Anywhere 6G Connectivity.'' As made clear by the title, INFINITE was targeted at addressing the R&D aspects more related to the *connectivity* among the various terrestrial and non-terrestrial nodes composing the network architectures investigated in the originating structural project.

In this paper, the main results of the cascade-call project will be reviewed and critically discussed, along with the contributions they yield in the framework of future 6G system standardization.

A. LITERATURE BACKGROUND

Several recent papers have been published on topics concerning 6G connectivity. In [5], Chen et al. illustrated the advancement from 5G to 6G, focused on the extensive adoption of massive multiple-input multiple-output (MIMO), multi-user MIMOs, New Radio (NR) positioning, and AI tools. Non-terrestrial networks have been introduced in 5G NR release 17 as part of a unified standard for both terrestrial and satellite communications. The paper of Giordani and Zorzi [6] addresses the open challenges and opportunities for NTNs in the 6G era, highlighting, in particular, the requirements of communication resilience and service continuity. The most critical aspects concerning the integration of terrestrial and non-terrestrial networks are analyzed in [7], with a focus on the role of UAVs in such an integration process. In the same framework, the work of Nguyen, Saputra, et al. [8] provides a comprehensive survey on the utilization of network slicing, AI, Open Radio Access Networks (ORAN) to address the diverse challenges of 6G NTNs from the perspective of both Academia and Industry. The way paved by AI toward more intelligent network planning, resource allocation, and interference management has been thoroughly discussed in [9]. The adoption of Integrated Access Backhaul (IAB) technology in NTNs has been proposed and analyzed in [10]. In particular, a two-layer Uncrewed Aerial Vehicle (UAV)-based architecture is presented, which consists of a lower layer comprising flying users and a UAV Base Station (BS), and an upper layer designed to provide both wireless access for flying users and backhaul connectivity for the BS. A challenging aspect of T-NT integration will certainly be the vertical handover. In [11], a vertical handover approach based on multiple factors (received signal strength, signal-to-noise ratio, and elevation angle) is proposed to determine the optimal time and location for a handover between a terrestrial BS and the satellite links.

One of the technologies that gained renewed interest in 6G is the Direct-to-Smartphone transmission. Indeed, such services are consolidated thanks to satellite constellations like Iridium and Globalstar. However, the unprecedented connection availability brought by new megaconstellations, such as Starlink, opened the road to a new broadband vision of Direct-to-Smartphone communications capable of supporting Mbps transmission speeds. The recent article of He et al. [12] proposed some key technical solutions

for next-generation Direct-to-Smartphone services (adaptive radio interface systems, spaceborn multi-beam antennas, on-demand scheduling of narrow beams for random access, etc.)

As far as non-terrestrial 6G transmission aspects are concerned, it is worth mentioning the paper of Noh et al. [13], where the required features for 6G NTN repeaters are investigated. Satellite swarm-based antenna arrays are proposed in [14] to be launched in the LEO orbit. Reconfigurable intelligent surfaces (RIS) will be a key enabler of multi-gigabit communications in the terahertz (THz) bands. In [15], technical advances and applications of RIS in THz NTNs are surveyed. The recent work [16] considers RIS and Rate-Splitting Multiple Access (RSMA) to improve the radio resource utilization in space-aerial-terrestrial relay networks. Federated Deep Reinforcement Learning is employed in [16] to optimize active beamforming vectors, RIS reflection coefficients, UAV trajectories, and power splitting ratios. Similarly, RIS and RSMA are jointly introduced in [17] to implement secure beamforming in the presence of multiple eavesdroppers; system parameters are optimized by means of Deep Reinforcement Learning. Self-powered absorptive Reconfigurable Intelligent Surfaces (RISs) are considered in [18] to maximize the achievable secrecy rate of the earth station, while satisfying the signal reception constraints in terms of harvested power threshold and available power budget.

The increasing demand for 6G connectivity is expected to involve a massive number of users, characterized by highly heterogeneous demands and services. The range is from a few Kb/s supported IoT devices and the Tb/s capacities required by Virtual Reality applications. It is clear that in such scenarios, asynchronous and flexible multi-user radio resource management is mandatory. Non-Orthogonal Multiple Access (NOMA) may provide an effective solution to such a demand, in particular when heterogeneous terrestrial/non-terrestrial links are involved in the data exchange. In this framework, the survey of Belemeki and Alouini [19] discusses the synergistic integration and interplay between non-terrestrial networks and NOMA techniques.

B. PAPER CONTRIBUTION

The above-reviewed state-of-the-art background addresses most of the technical challenges related to 6G NTNs and their integration with terrestrial networks. In our paper, we aim to provide readers with a global, ecosystemic vision of the future integrated T-NT 6G connectivity, in agreement with novel cutting-edge concepts concerning "Space 2.0" [20] and space networking as "glue technology" interconnecting sparse terrestrial network segments [21]. The present work can be regarded as a review paper, providing an organic overview of the project results already published in the literature.

We aim at introducing the various research tasks addressed by the INFINITE project as integrated parts of a non-terrestrial connectivity framework based on innovative concepts like software-defined implementation (SDR, SDN), cell-free network design, AI-based network orchestration, and link monitoring. The expected innovative contribution concerns the definition of a 6G-driven vision of Space as an integrated communication environment, where connectivity is adaptive, transparent, ubiquitous, and available to users at any time. In conjunction with the vision, the paper also aims to provide some concrete technical guidelines for implementing it. The presentation and discussion of the project results will form the basis for specific proofs of concept that will be the subject of future work.

C. PAPER STRUCTURE AND ORGANIZATION

The organization of the rest of the paper reflects the research vision of the authors toward a renewed concept of "6G Space." Section II will outline the proposed ecosystemic approach for the seamless integration of terrestrial and non-terrestrial networks. This will draw the framework where the technical sections of the paper will be inserted, namely:

- Section III describing the proposed cell-free MIMO NTN architecture.
- Section IV proposing a global, modular PHY-layer design based on SDR, focusing on a specific case study of advanced multicarrier waveform design for NTNs.
- Section V analyzing techniques for efficient NOMA radio access.
- Section VI detailing the approach for a multi-modal transceiver implementation.
- Section VII encompasses the higher-layer networking aspects concerning SDN, cloud computing, and multi-access edge computing for orchestration and link monitoring.

The rest of the paper is dedicated to the review and discussion of the most representative project results (Section VIII), while Section IX concludes the paper with the lessons learned from the project activities and an open door to future R&D directions and realizations.

II. THE PROPOSED ECOSYSTEMIC APPROACH FOR T-NT INTEGRATION

In Fig. 1, a pictorial description of a typical 6G global coverage scenario is shown. Three remote sites are connected: two located in Europe (for instance, Germany and Italy) and one located in the USA.

In the first use case, a residential user, located in the US building, wants to communicate with a residential correspondent located in one of the Italian small houses (blue connection). The data exchange is related to document transmission as an email attachment. Such a connection is not highly delay sensitive and, therefore, can exploit a direct uplink connection with a geostationary satellite that can cover the long distance between Italy and the USA. The geostationary satellite reverses in the downlink to an Italian 6G hub, which provides mobile communication services and residential fiber-based services. A terrestrial fiber connection will

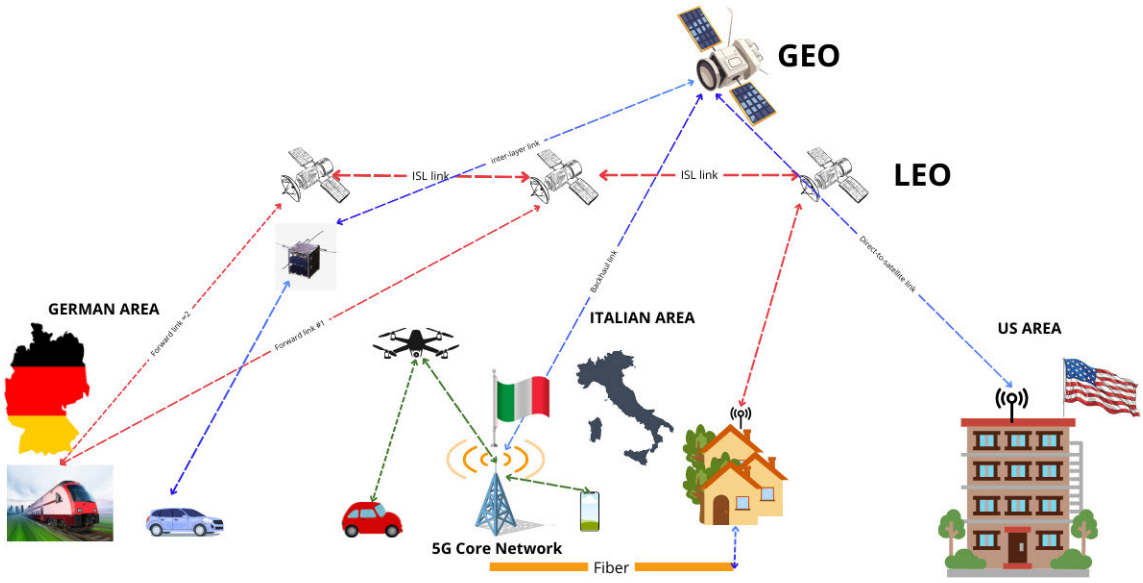

FIGURE 1. A possible scenario of global coverage targeted by 6G.

reach the residential destination. In the German area, there is another recipient of the material produced in the US building, and this recipient is moving in a car. A small satellite, connected to the GEO by means of an inter-layer link, can provide the required information route for this connection.

Let's suppose that another residential user in the Italian village wants to communicate by video chat with a user traveling on a high-speed train reaching a German town. Such a connection might be conveniently provided by a Low Earth Orbit (LEO) satellite constellation, like Starlink, which exploits inter-satellite connections and satellite diversity to cope with the fast motion of trains.

One last use case may consider vehicular communication in the Italian area. The small car is traveling in a zone where the terrestrial cellular coverage is absent. In such a case, a drone can work as a donor relay node connecting the terrestrial gNB with the vehicular terminal. Then, the terrestrial gNB dispatches the information to the smartphone by means of a terrestrial downlink.

The effective support of the use cases addressed in Fig. 1 requires a reconfigurable, multi-layered, and integrated T-NT architecture. For this reason, the ITA-NTN project proposes the deployment of a cluster constellation-based NTN (CCB-NTN) architecture [22] (see Fig. 2) as a viable solution capable of providing spatial diversity, scalability, and ease of maintenance in the case of node failure. The primary node of a cluster connects with the nearest cluster primary in the intra-layer and inter-layer to minimize the number of ground stations and point-to-point links. The NTN gateway provides data relaying between the NTN and the terrestrial core network to enable a unified network coverage. The interconnection of the various network nodes requires an accurate balance between optical wireless links - these last well suited for intra-layer communications - and Radio Frequency (RF) links, necessary to bring connectivity from the Sky to the Earth [22].

The system model adopted in this work primarily focuses on communication scenarios where terrestrial and non-terrestrial networks interact through indirect links, such as satellite gateways, relay nodes, or multi-hop paths across heterogeneous network segments. This modeling choice reflects challenging yet realistic operational conditions, including remote-area connectivity, intermittent line-of-sight availability, and highly dynamic user mobility, where direct links cannot always be guaranteed. Nevertheless, the proposed ecosystemic framework is not restricted to indirect-link-only communication. On the contrary, it naturally supports the coexistence of direct and indirect links, which can be dynamically exploited depending on channel conditions, network topology, and service requirements. In scenarios where a direct link between terrestrial and non-terrestrial nodes is available (e.g., direct satellite-to-device or UAV-to-user communication), such links can be seamlessly incorporated into the ecosystem as additional access options.

To cope with the connectivity requirements of the architecture of Fig. 2, the INFINITE project investigates a new ecosystemic approach based on the synergic combination of innovative transmission architectures and cloud-computing tools, as shown in Fig. 3. The due degree of flexibility and reconfigurability of the NTN architecture is provided by innovative transmission structures, based on advanced concepts like user-centric cell-free (UC-CF) MIMO, NOMA multi-access management, and full software-defined radio interface design. The physical architecture is orchestrated by an upper layer comprising SDN, cloud computing, and artificial intelligence, which dynamically configures the network topology

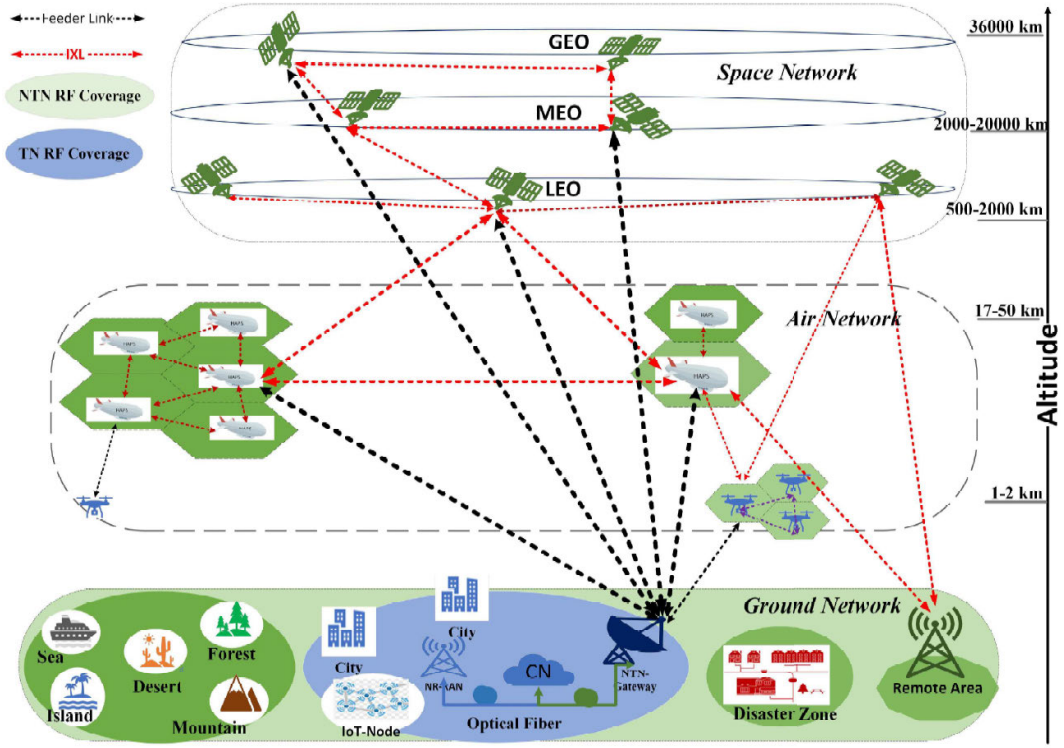

FIGURE 2. ITA-NTN architecture with a balanced mix of RF and optical wireless links (courtesy of [22]).

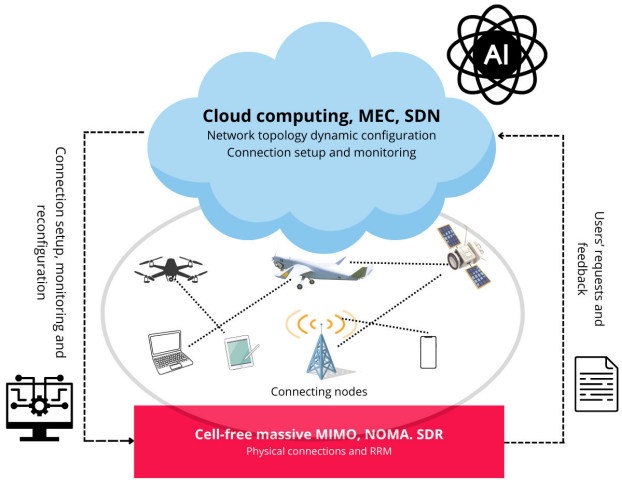

FIGURE 3. The INFINITE vision of reconfigurable global connectivity management.

and the radio interface, providing adaptive traffic rerouting, link monitoring, and access control. Such an "immanent" layer represents an initial step of practical implementation of the "Space Network Intelligence" of the "New-Space" architecture described in [21]. The technology framework that targets the implementation of the ecosystemic vision of global connectivity, as described in Fig. 3, is shown in Fig. 4. The project task was to investigate the technologies required for the intelligent part of the ecosystem immersed in a "Space cloud" (namely: the "immanent" layer) and for the physical part of it residing in the NTN flying nodes and in the ground transceivers (ground stations and user equipment). As shown in Fig. 4, the "Space cloud" is an SDN architecture relying on cloud computing, multi-access edge computing, and AI. Such a layer monitors and controls the underlying section of the integrated T-NT network system, consisting of programmable and reconfigurable payloads that physically transfer data. The common design basis for the two system sections is the full software-defined approach (SDN for network management and SDR for physical data transmission), which targets the full reconfigurability of network connections through an adaptive selection of the best information route and the optimal radio interface setup to convey information over this route. The investigated technologies will be assessed by means of some quantifiable metrics, which can be listed according to the guidelines contained in [23]:

- *Link performance metrics*: Bit-Error-Rate (BER), Signal-plus-Noise to Interference Ratio (SINR), outage probability.
- *Quality-of-Service (QoS) metrics*: throughput, pragmatic capacity, Packet Loss Ratio (PLR), latency.
- *RF hardware/modulation metrics*: Error-Vector Magnitude (EVM), TX spurios emission, peak power consumption.
- *Computational metrics*: computational complexity, CPU usage.

In the following sections of our work, the research achievements related to the various components of the physical and

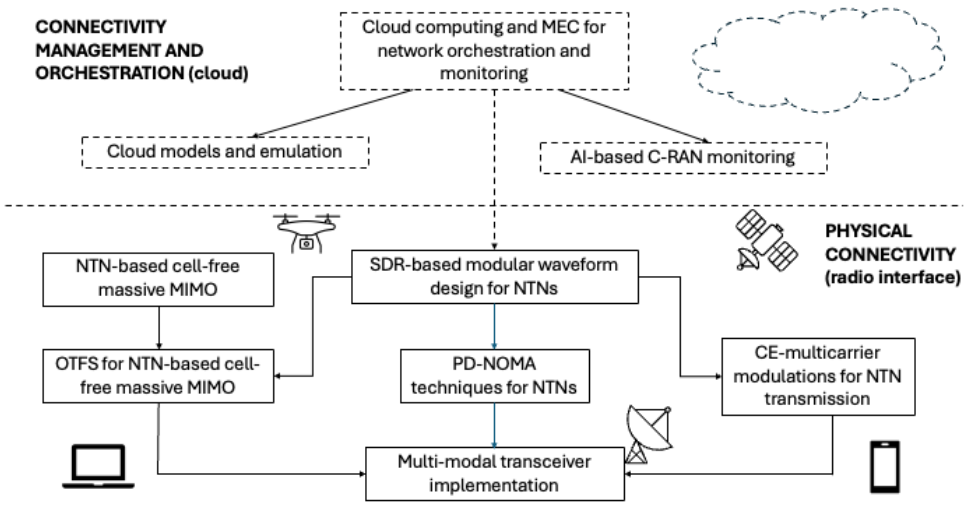

FIGURE 4. The INFINITE technology framework implementing the vision of Fig. 3.

cloud computing layers of the ecosystem will be discussed in detail. Before starting the technical overview, which will form the core of the paper, let's try to discuss in the following subsection the proposed ecosystemic approach in the framework of the evolution of T-NT integration. This will be useful to readers to better understand the innovative contribution of our study.

A. THE PROPOSED ECOSYSTEM IN THE EVOLUTION OF T-NT INTEGRATION

The ecosystemic approach followed in the INFINITE project clearly proceeds toward the direction drawn by the ''6G and beyond'' evolution of T-NT integration. As highlighted in [24], the evolution of such an integration process was marked by three distinct epochs:

- the interworking era (3G and 4G), where the target was to exploit Space segments for backhauling support, roaming of special satellite phones, and support for satellite-based IP services.
- the integration era (5G), where seamless integration was tackled along with the 5G support across various radio access technologies.
- the native NTN era (6G and beyond), where native NTN components are nested in the global infrastructure.

Interworking schemes clearly suffered from the incompatibility of terrestrial and non-terrestrial networking protocols. Some solutions targeted to smoothing such an incompatibility have been devised and implemented; for instance, the use of performance-enhancing proxies and special versions of the IP protocol more resilient to latency. Such solutions achieved suboptimal performance, as they are impaired by the violation of the end-to-end principle characterizing Internet protocols. 5G exploited SDN and NFV to combine seamlessly terrestrial and non-terrestrial segments (some examples can be found in [25], [26], and [27]), although treating the heterogeneous segments as separate entities.

In contrast, the native NTN vision emerging in the context of 6G aims at embedding non-terrestrial components directly into the global networking fabric, rather than interfacing them as external extensions. Many current 6G integration approaches address this objective by focusing on individual technological enablers, such as advanced waveform design, AI-assisted resource management, or network slicing, yet they often lack a unifying architectural framework capable of jointly optimizing physical-layer adaptability, multi-user access, and network-wide orchestration. As a consequence, performance degradation may still arise in practical scenarios characterized by extreme mobility, heterogeneous service requirements, and stringent reliability constraints.

The proposed ecosystemic approach overcomes these limitations by natively integrating terrestrial and non-terrestrial components within a unified, software-defined, and AI-assisted architecture. Unlike state-of-the-art solutions that optimize isolated layers or functions, the proposed framework jointly addresses physical-layer reconfigurability, robust multi-user access, and global network orchestration. A key novelty of the proposed approach lies in the tight and continuous collaboration among its enabling technologies, rather than in their isolated adoption. In particular, the ecosystem is designed to couple software-defined networking, AI-based monitoring, cloud/MEC computing, and reconfigurable PHY-layer techniques into a closed-loop control framework capable of dynamically optimizing resource allocation across heterogeneous terrestrial and non-terrestrial segments.

At the core of this collaboration is the software-defined abstraction of the network, which provides a global and programmable view of both terrestrial and non-terrestrial resources. SDN enables the decoupling of the control and

data planes, allowing network decisions to be centrally coordinated while being executed in a distributed manner. This abstraction is essential in T–NT scenarios, where link characteristics, topology, and node availability vary rapidly due to satellite motion, aerial mobility, and heterogeneous access technologies. AI-based monitoring functions operate on top of this software-defined substrate and continuously collect multi-layer KPIs, including physical-layer metrics, network-layer indicators, and computing-resource usage. Machine-learning models process this information to infer network states, predict future resource demands, and detect anomalies or performance degradation trends.

The AI modules provide predictions and recommendations, which are fed into the SDN controller. Based on this information, the SDN layer dynamically enforces reconfiguration actions, including traffic rerouting across terrestrial and non-terrestrial paths, adaptive association of users to multiple access points or satellites, and redistribution of computational tasks among terrestrial and space-based MEC nodes. This tight integration allows the network to move from a reactive management paradigm to a proactive and predictive one, which is particularly crucial in high-dynamic user scenarios and in remote-area deployments where connectivity margins are limited.

The collaborative mechanism extends down to the physical layer through the SDR framework. Decisions taken at the SDN and AI levels can trigger real-time reconfiguration of waveform parameters, modulation formats, access schemes (e.g., OMA vs. NOMA), and macro-diversity strategies (e.g., cell-free MIMO). In this sense, the PHY layer becomes an adaptive actuator of the ecosystem, implementing the high-level policies derived from network-wide intelligence. Cloud computing and MEC play a complementary role by hosting both AI models and virtualized network functions close to where decisions are needed. MEC placement enables low-latency inference and control, while cloud-based coordination ensures global consistency and long-term optimization. The joint use of centralized and distributed intelligence allows the ecosystem to scale efficiently while preserving responsiveness, even in large-scale LEO constellations and heterogeneous T–NT deployments.

Overall, the proposed ecosystemic framework does not merely juxtapose SDN, AI, SDR, and advanced access technologies; rather, it orchestrates them within a unified control loop in which monitoring, learning, decision-making, and actuation are intrinsically interdependent. This collaborative operation represents a key differentiating factor with respect to existing 6G integration approaches, which often consider these technologies in isolation, and it is instrumental in achieving resilient, efficient, and truly seamless T–NT connectivity in practical 6G scenarios.

III. CELL-FREE MIMO T-NT ARCHITECTURE

As already mentioned in Section I, significant interest is currently emerging around NTNs, which can integrate non-terrestrial devices (NTDs), including uncrewed aerial vehicles (UAVs), high-altitude platforms (HAPs), and LEO satellites, to facilitate efficient and ubiquitous global connectivity [6], [28]. The presence of multiple and cooperating NTDs can be leveraged to enhance the reliability and macro-diversity of communication systems. Specifically, when considering mobile user terminals (UTs), a line-of-sight (LOS) link between the generic NTD and the terrestrial UT is not always guaranteed: due to the fast movement, the LOS link can indeed be unexpectedly shadowed/obstructed by physical objects nearby the UT. In the INFINITE project, we mainly refer to LEO satellites.

The structural similarities between a network of cooperating LEO satellites and UC-CF MIMO terrestrial systems, relying on dense access points (APs) deployments, have sparked growing interest in the adaptation of UC-CF-inspired macro-diversity strategies to NTNs. In terrestrial UC-CF networks, coherent processing is widely adopted, leading to the following assumptions [29], [30], [31], [32]: i) time division duplex (TDD), ii) APs estimate the uplink channel through training sequences transmitted by the users, and iii) APs exploit channel reciprocity for downlink beamforming and uplink combining. Macro-diversity schemes, i.e., the joint use of several LEO satellites to serve the same UT, can be widely used in order to increase the system reliability and efficiency.

References [33], [34], [35], [36] show that, under the assumption of a wide angular separation between the satellites, the blockage events for each UT-satellite link are statistically independent, leading to an exponential decrease of the outage probability. When applying UC-CF MIMO concepts to LEO NTNs, some challenges emerge. Indeed, in the NTNs scenario, uplink channel estimation and phase compensation are extremely challenging due to satellite mobility and propagation delays [33], [34]. While Doppler and timing compensation can be accurately performed at known ground locations, phase alignment across multiple satellites is generally impractical. Thus, applying terrestrial UC-CF designs to satellite-based NTNs is not straightforward, since novel solutions to fully leverage macro-diversity are needed. These limits are explored in [37] by comparing coherent and non-coherent joint transmissions and highlighting the need for at least coarse phase alignment to approach satisfactory performance. The research work on this topic carried out in the INFINITE project can be divided into two main research lines, as discussed in the following subsections.

A. MACRO-DIVERSITY SCHEMES IN LEO NTNs WITH OTFS AND OFDM MODULATION

In this scenario, we consider a terrestrial area containing Q UTs equipped with uniform planar arrays (UPAs) with multiple antennas, N_{UT} say. The Q UTs are in possible visibility with P satellites, all equipped with UPAs having the same number N_S of antennas. In general, some paths from satellites to UTs can be blocked by the presence of obstacles. We consider multicarrier and multisymbol transmissions, denoting with M the number of subcarriers, Δ_f the subcarrier spacing, N the number of symbols, and T the symbol duration.

The downlink time-varying channel between the q-th UT and the p-th satellite is the following vector-valued ($N_{UT} \times N_S$)-dimensional function:

$$\mathbf{H}_{p,q}(t,\tau) = \rho_{p,q}\mathbf{a}_{UT}(\phi_{p,q}^{UT}, \theta_{p,q}^{UT})\mathbf{a}_S^T(\phi_{p,q}^S\theta_{p,q}^S) \times \delta(\tau - \tau_{p,q})e^{j2\pi\nu_{p,q}t} \quad (1)$$

where $\rho_{p,q}$ is the *complex gain* containing the path-loss, log-normal shadowing loss, and clutter loss, i.e., the attenuation due to surrounding objects on the ground. The azimuth and elevation angles corresponding to the direction of departure (DoD) and to the direction of arrival (DoA) are denoted by $\phi_{p,q}^S$ and $\theta_{p,q}^S$ and by $\phi_{p,q}^{UT}$ and $\theta_{p,q}^{UT}$, respectively. The UPA array response at the generic array is $\mathbf{a}_x(\varphi,\vartheta)$ with $x \in \{S, UT\}$ and defined similarly as in reference [37]. The number of antennas at the satellite is $N_S = N_{S,v}N_{S,h}$ with $N_{S,v}$ and $N_{S,h}$ the number of antennas on the vertical and horizontal axis, and the number of antennas at the UT is $N_{UT} = N_{UT,v}N_{UT,h}$ with $N_{UT,v}$ and $N_{UT,h}$ the number of antennas on the vertical and horizontal axis. Finally, $\tau_{p,q}$ and $\nu_{p,q}$ are the *residual* propagation delay and the Doppler shift of the q-th UT with respect to the p-th satellite. Note that $\nu_{p,q}$ is a *relative Doppler shift* that takes into account the movement of the p-th satellite and the q-th UT. Regarding the meaning of residual delay and Doppler shift, we assume that the satellites perfectly compensate for delay and Doppler shift in one specific location, namely, the *ideal UT position*. The *offset distance* of the UT from the ideal position is $r_{p,q}$, which entails residual uncompensated delay and Doppler shifts, i.e., $\tau_{p,q}$ and $\nu_{p,q}$.

In this paper, we do not report all the details of the derivations of OTFS and OFDM signal models, which follow the derivations in [38]. In both cases, the whole observable at the q-th UT from the p^*-th satellite, $\mathbf{y}^{(p^*,q)}$ say, obtained by stacking the NM observable at the receiver, can be expressed as

$$\mathbf{y}^{(p^*,q)} = \underbrace{\alpha_{p^*,q}\overline{\mathbf{\Psi}}_{p^*,p^*,q,q}\mathbf{x}^{(q)}}_{\text{intended signal to the } q\text{-th UT from the } p^*\text{-th satellite}} + \underbrace{\sum_{\substack{p=0 \\ p\neq p^*}}^{P-1} \alpha_{p,q}\overline{\mathbf{\Psi}}_{p^*,p,q,q}\mathbf{x}^{(q)}}_{\text{intended signal to the } q\text{-th UT from the other satellites}} + \underbrace{\sum_{p=0}^{P-1}\sum_{\substack{q'=0 \\ q'\neq q}}^{Q-1} \alpha_{p,q'}\overline{\mathbf{\Psi}}_{p^*,p,q,q}\mathbf{x}^{(q')}}_{\text{interference from the other downlink transmissions}} + \mathbf{z}^{(p^*,q)}$$

with $\alpha_{p,q}$ a binary variable being 1 if the p-th satellite serves the q-th UT and 0 otherwise, the NM-dimensional vector $\mathbf{x}^{(q')}$ contains the information symbols intended to the q'-th UT, $\mathbf{z}^{(p^*,q)}$ contains the AWGN contribution and the $NM \times NM$-dimensional matrix $\overline{\mathbf{\Psi}}_{p^*,p^*,q,q}$ follows the structure in reference [39]. Upon defining $\mathcal{S}_q : \{p^* : \alpha_{p^*,q} = 1\}$ as the set containing the serving satellites for the q-th UT, the estimation of the symbols intended for the q-th UT can be obtained by combining the contributions from the serving satellites [39]:

$$\widehat{\mathbf{y}}^{(q)} = \sum_{p^*\in\mathcal{S}_q} \mathbf{y}^{(p^*,q)} \quad (2)$$

To detect the information symbols stacked in the vector $\mathbf{x}^{(q)}$, the q-th UT employs a practical minimum mean square error (MMSE) detector, assuming knowledge only of the channels from its serving satellites. After straightforward algebraic manipulations, the expression of the generic ℓ-th symbol estimate at the q-th UT can be derived as in [39]; the full expression is omitted here for brevity. Regarding the design of the beamforming and combining vectors for the p-th satellite–q-th UT pair, we assume imperfect knowledge of the UT positions at the satellites and of the satellite positions at the UTs, and adopt a zero-forcing (ZF) approach to mitigate inter-UT interference. For the transmit power coefficients, each satellite is assumed to uniformly allocate its available power budget among the UTs it serves. The binary association variables $\alpha_{p,q}$ are defined according to the user-centric cell-free (UC-CF) paradigm [29]. Specifically, the q-th UT is served by the N_{UC} closest satellites, subject to a maximum number of UTs per satellite, denoted by $N_{UT,MAX}$. In Section VIII-A, we report the performance in terms of SINR of the ℓ-th symbol at the q-th UT, defined as the ratio between the intended signal power and the interference-plus-noise power, as well as in terms of pragmatic capacity [37], [38], [39].

B. OTFS DETECTOR DESIGN IN CELL-FREE NTN FRAMEWORKS

We consider the scenario of Sec. III-A under the assumption that the UT is equipped with a single antenna, i.e., $N_{UT} = 1$. Therefore, only transmit beamforming is employed. We denote with $\mathbf{y}$ the whole received signal, defined as the superposition of the useful signals transmitted from the satellites in visibility with the UT and the interference signals deriving from the other downlink transmissions, i.e., with reference to a generic UT,

$$\mathbf{y} = \Psi\mathbf{x} + \tilde{\mathbf{z}} \quad (3)$$

where Ψ is the channel matrix associated with the intended signal, whereas $\tilde{\mathbf{z}}$ accounts for undesired effects, i.e., interference and AWGN. Equation (3) defines the input-output relation according to the Forney observation model [40]. However, an alternative sufficient statistic on which the detector can operate is

$$\tilde{\mathbf{y}} = \Psi^H\mathbf{y} = \mathbf{G}\mathbf{x} + \tilde{\mathbf{w}} \quad (4)$$

where

$$\tilde{\mathbf{w}} = \Psi^H\tilde{\mathbf{z}}, \quad (5)$$

$$\mathbf{G} = \Psi^H\Psi \quad (6)$$

The operation in (4) corresponds to a matched filtering, and the resulting observation model is the Ungerboeck one [41],

[42]. The processed channel matrix $\boldsymbol{G}$ presents a compact structure which can be advantageous for the detection process, as discussed in [43] and [44].

Here, we focus on detection strategies under the assumption of perfect channel state information at the receiver. We highlight the differences among the state-of-the-art approaches. With reference to the scenario described above, employing both the OTFS and OFDM modulation formats, we test the algorithm with the lowest computational load and compare its performance with that of the high-complexity MMSE benchmark. In fact, for the OTFS modulation, this last detector - derived under the assumption that $\mathbf{x}$ is a Gaussian vector- requires the inversion of a $NM \times NM$ matrix, since the optimal estimator $\hat{\mathbf{x}}$ of $\mathbf{x}$ is given by

$$\hat{\mathbf{x}} = \Psi^H \left[\Psi \Psi^H + 2\sigma^2 \mathbb{I}_{NM} \right]^{-1} \mathbf{y} \tag{7}$$

and thus involves an overall complexity of $\mathcal{O}\left((NM)^3\right)$. Although this approach offers very good performance, as will be shown in the following, its huge required computational load is typically unaffordable in realistic time-varying scenarios, where the channel matrix Ψ changes at every block. For this reason, some low-complexity techniques, e.g., approximate message-passing algorithms working on factor graphs (FGs) have been deeply studied in recent research (see, e.g., [45], [46], [47], [48], [49] and references therein). They can be classified not only by the kind of employed approximation, e.g., on messages and/or variable distributions, but also by the observation model used for the implementation of the maximum a posteriori (MAP) symbol detection strategy, namely either the Forney [40] or the Ungerboeck [41] model.

Among the algorithms of the first kind, the most successful one in terms of both complexity and performance is that of [45]. The detection strategy proposed in [45] is graph-based and consists of approximating the interference term plus thermal noise through a Gaussian random variable. This approximating technique is used to reduce the complexity of the exact sum-product algorithm (SPA) applied on the FG relative to the Forney observation model, which otherwise would lead to an impractical computational load. The complexity required by the approach of [45] results in being linear in the number of interferers per symbol S and in the constellation cardinality Q. Differently, the detection strategy proposed in [47] is based on the Ungerboeck observation model and, therefore, operates on the processed channel matrix $\mathbf{G}$. This algorithm directly derives from the application of the exact SPA on the associated FG. There are no approximations involved; however, the resulting complexity depends linearly on S and quadratically on Q. An alternative solution working on the same FG has been proposed in [43]. This last solution exploits the structure of $\mathbf{G}$, where the main entries, i.e., the terms with the largest magnitudes, are located along diagonals. Moreover, the adoption of a hierarchical scheduling allows for achieving faster convergence and superior performance of the algorithm proposed in [47], as discussed in [43] and [44]. However, its quadratic dependence on the constellation size hinders its adoption in low-complexity applications with large alphabet cardinality.

We here focus on a recently proposed detector [44] characterized by an extremely low complexity, which also outperforms all the above-mentioned algorithms, as demonstrated in [44] with reference to a standard 3GPP channel profile [50]. This strategy works on the Ungerboeck observation model as the approaches in [43] and [47], and its effectiveness is enabled by the compact structure of $\mathbf{G}$. This scheme is developed on the principle of interference cancellation and will be referred to as $\text{IC}_{\boldsymbol{G}}$. Through multiple iterations, the interference term is estimated and subsequently removed from the observable. Furthermore, the use of damping ensures convergence. Again, in Section VIII-A we report the performance of the detectors discussed above in terms of pragmatic capacity[1] [37], [38].

IV. SDR-BASED MODULAR WAVEFORM DESIGN

A. MODULAR DECOMPOSITION OF NTN TRANSCEIVERS

The ecosystemic approach considered in INFINITE aims to offer to various transmission applications supported by NTN links a smart PHY-layer capable of dynamically reconfiguring itself based on user needs in terms of capacity and availability. This is one of the key features of NR systems, which straightforwardly involves the design and implementation of software-defined NTN data transmission functions. The starting point has been the comprehensive lattice structure proposed in [51], which provides a generalized, modular, backward-compatible, forward-looking PHY layer framework for 6G networks. The corresponding multi-waveform modular-decomposed transmitter for NTNs is pictorially described in Fig. 5. The transmitter is divided into macroblocks, which are structured in processing slices. The first macroblock forms the time-frequency resource grid and consists of three slices:

- *Reshaping*, which organizes the modulated symbols into a lattice of $\frac{N}{L_2} \times \frac{M}{L_1}$ elements, M and N being the number of resources in the frequency (subcarriers) and in the time domain respectively, while L_1 and L_2 account the reshaping granularity. Reshaping parameters determine the mapping type: one-to-one (scalar), one-to-many (orthogonal), and many-to-one (non-orthogonal). The pictorial example of Fig. 5 shows the OTFS reshaping, leading to the symbol mapping in the two-dimensional Delay-Doppler domain. DFT-based multicarrier modulations – OFDM, DFT-spread-OFDM, and OFDM-inspired waveforms, like Filter-Bank Multi-Carrier (FBMC) [52] – perform serial-to-parallel (S/P) reshaping, forming the vector of the symbols which are transmitted in the discrete frequency domain. In Multicarrier Spread Spectrum (MC-SS) transmission, the

[1]The pragmatic capacity is the mutual information of the virtual channel with constellation symbols as input and received samples after the LMMSE processing as soft output.

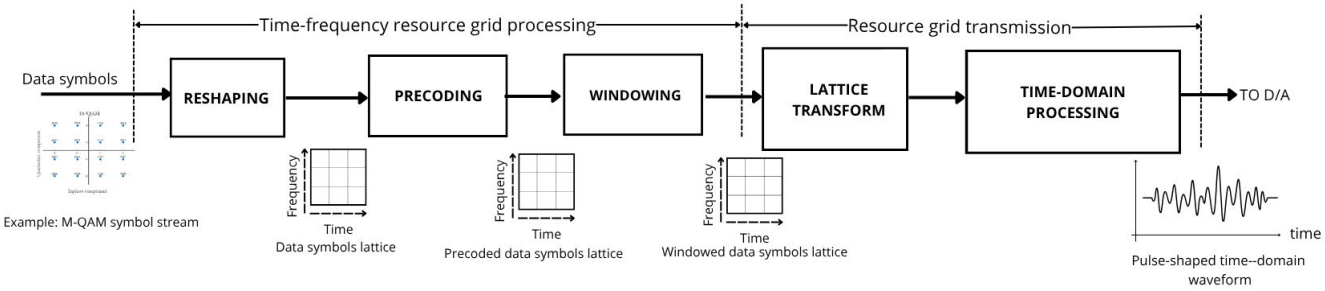

FIGURE 5. The modular decomposition of PHY-layer for 6G NTNs.

reshaping blocks perform a S/P symbol repetition [53]. In such a case, the symbol S_k is transmitted in parallel during the signaling interval of duration $kT, k = 0, 1, 2 \cdots$ over the M assigned subcarriers. According to [51], it is possible to consider a reshaping operation also for single carrier modulations, like, e.g., LoRA chirp. In such a case, the reshaped symbol vector is made by a first, nonzero, element consisting of the information symbol followed by $M - 1$ zero-padding.

- *Precoding* converts the symbols mapped in the multidimensional lattice to PHY-layer resources in the Time-Frequency (T-F) grid. The conversion is performed by transforming and/or combining symbols located at different points of the lattice. A well-known example is the DFT precoding employed by the DFT-spread-OFDM, known as single-carrier (SC)-OFDM, or SC-FDMA in the multi-user case [54]. Other examples are the M-point Hadamard-Walsh (HW) transformation employed by MC-SS, required to realize the Spread Spectrum randomization of the transmitted signal [53], the $M \times N$-points Inverse Sympletic FFT (ISFFT) inherent to OTFS [55], and the combination of N-point HW transformation followed by the M-point DFT used by Orthogonal Time Sequency Modulation (OTSM) [56].
- *Windowing* slice performs some sort of transformation of the precoded T-F lattice, leading to signal scaling or rotation, selected based on specific applications or requirements [51]. Windowing operations are the zero-padding required by DFT-s-OFDM before the ML_1-point – L_1 is conventionally denoted as *spreading factor* [54], usually set as a power of 2 –, and the $\frac{\pi}{4}$ rotation imposed on the chirp lattice. We can also extend the concept of windowing proposed in [51] to the zero-padded conjugate symmetric vector formation required by Constant-Envelope OFDM (CE-OFDM) [57] and Constant-Envelope SC-OFDM (CE-SC-OFDM) [58] to obtain, after the IDFT operation, a real-valued multicarrier signal suitable for the subsequent nonlinear phase modulation.

The T-F resource grid obtained by the aforesaid modules is characterized by three basic quantities: the minimum frequency spacing Δf, the minimum sampling rate T_s, and the maximum frame duration T_f. Such quantities impose the duration of the symbol $T = \frac{1}{\Delta f}$, the transmission bandwidth $B = \frac{1}{T_s}$, and relate the duration of the frame to the reshaping parameter N, i.e.: $T_f = NT$.

The second macroblock actually converts the T-F resource grid into the complex baseband waveform that will then be processed by the RF section of the transceiver and sent to the channel. It consists of two slices:

- *Lattice transform* converts the T-F grid to a signal in the time domain by performing a pulse-shaped transformation of the samples in the grid. Typical examples of such an operation are the IDFT used in the basic multicarrier modulations and the Heisenberg transform in the OTFS.
- *Time-domain processing* performs some fundamental operations in the time domain before the D/A conversion. The common operations for all the waveform formats are the Parallel to Serial (P/S) conversion and the Cyclic Prefix (CP) insertion. The slice may optionally filter the signal before the RF conversion (for example, in the case of filtered OFDM and FBMC). In the case of CE-OFDM and CE-SC-OFDM transmission, it also performs the nonlinear phase modulation of the real-valued multicarrier signal obtained by the transform slice. As far as the LoRA chirp waveform is considered, the time-domain processing slice performs the Chirp Spread-Spectrum modulation.

The generic multi-waveform numerical receiver scheme of Fig. 6 is matched to the modular decomposition of the transmitter shown in Fig. 5. After the A/D conversion, the inverse transformation returns the lattice in the discrete frequency domain, where equalization, de-windowing, and inverse precoding are performed. Finally, de-shaping, which is actually the inverse of reshaping, converts the received lattice to the time domain. The last RX processing tasks are synchronization, matched filtering (with the pulse shaping imposed by the time-domain processing slice of the transmitter), and symbol detection to complete the chain. As shown in two recent contributions [59], [60], the proposed modular framework enables the synthesis of a wide plethora of single-carrier and multi-carrier waveforms that are regarded as good candidates to support differentiated 6G NTN PHY-layer configurations. In Fig. 7, we summarize the practical modular decomposition

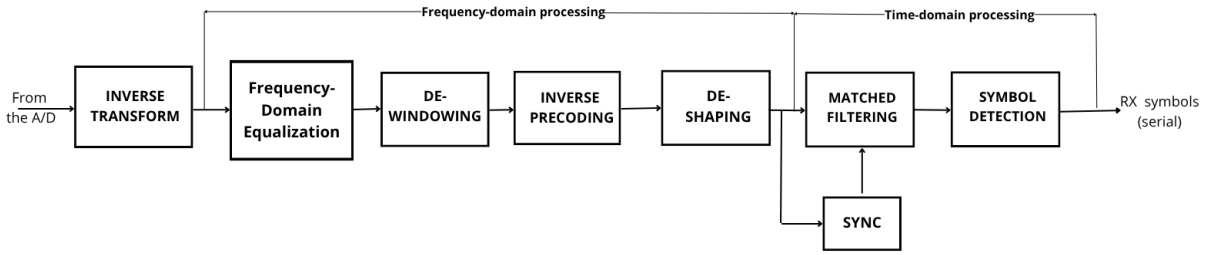

FIGURE 6. Receiver scheme matched to the modular decomposition of the waveform transmission shown in Fig. 5.

Waveform	Reshaping	Precoding	Windowing	Lattice Transform	Time-domain processing
OFDM	Mx1 (S/P)	None	None	M-point IDFT	P/S and CP insertion
DFT-s-OFDM	Mx1 (S/P)	M-point DFT	(ML_1-M) zero-padding (L_1>1)	ML_1-point IDFT	P/S and CP insertion
MC-SS	Mx1 (S/P symbol repetition)	Hadamard-Walsh (HW) transform	None	M-point IDFT	P/S, CP insertion
Filtered-OFDM	M/L_k x1 (k=1,..,K, L_k>1) (S/P)	None	None	M/L_k-point IDFT	Sub-band filtering, P/S and CP insertion
FBMC	Mx1 (S/P)	None	None	M-point IDFT	Subcarrier filtering (filter bank), P/S
LoRA chirp	1x1 + (M-1) zero-padding (S/P)	None	Widowing with $\pi/4$ phase rotation	M-point IDFT	Chirp SS modulation, P/S and CP insertion
Constant Envelope-OFDM	Mx1 (S/P)	None	$2F_{ov}$ (M +1)x1 (zero-padded conjugate symmetric vector)	$2F_{ov}$ (M +1)-point IDFT	Nonlinear phase modulation, P/S and CP insertion
Constant Envelope-SC-OFDM	Mx1 (S/P)	M-point DFT	$2F_{ov}$ (M+1) x1 (zero-padded conjugate symmetric vector)	$2F_{ov}$ (M +1)-point IDFT	Nonlinear phase modulation, P/S and CP insertion
OTFS	MxN buffering	MxN Inverse Sympletic FFT	None	MxN Heisenberg transform	P/S and CP insertion
OTSM	MxN buffering	N-point HW transform and M-point DFT	None	M-point IDFT	P/S and CP insertion
NOMA (power-domain) with OFDM	M/L_1 x 1 (L_1<1) (S/P)	None	None	M-point IDFT	P/S and CP insertion

FIGURE 7. Modular decomposition of the candidate waveforms for 6G NTN transmission: processing slices instantiations.

of some of these waveforms, with the appropriate instantiation of each slice.

B. SDR IMPLEMENTATION OF THE CANDIDATE NTN WAVEFORMS

The modular decomposition of the 6G NTN waveforms shown in Fig. 7 can be straightforwardly translated into an agile SDR-based PHY-layer implementation, driven by an intelligent agent, as shown in Fig. 8. The transmitting unit includes a waveform selection module that receives input information on application requirements, such as data rate, terminal mobility, bit-error rate, latency, etc. Based on this information, the module assembles a PHY-layer report that is sent through a dedicated channel to an intelligent SDN-programmed agent. The agent reads the report and decides which waveform to use to establish the connection. The consequential action is to retrieve the related set of PHY-layer procedures (reshaping, precoding, windowing, lattice transform, and time-domain processing) from the SDR library. Then, the agent packs the code into an SDR package, which is sent to the transmitting unit. Finally, the code is executed by the baseband SDR processor, and the data is transmitted onto the NTN link.

To make the work of the PHY-orchestrator easier, an agile organization of the SDR library should be considered. We propose to organize the library into sub-libraries. One of these should contain general-purpose functions (reshaping and CP insertion), a generic lattice transform (typically: the IFFT) that can be reused for different PHY-layer formats

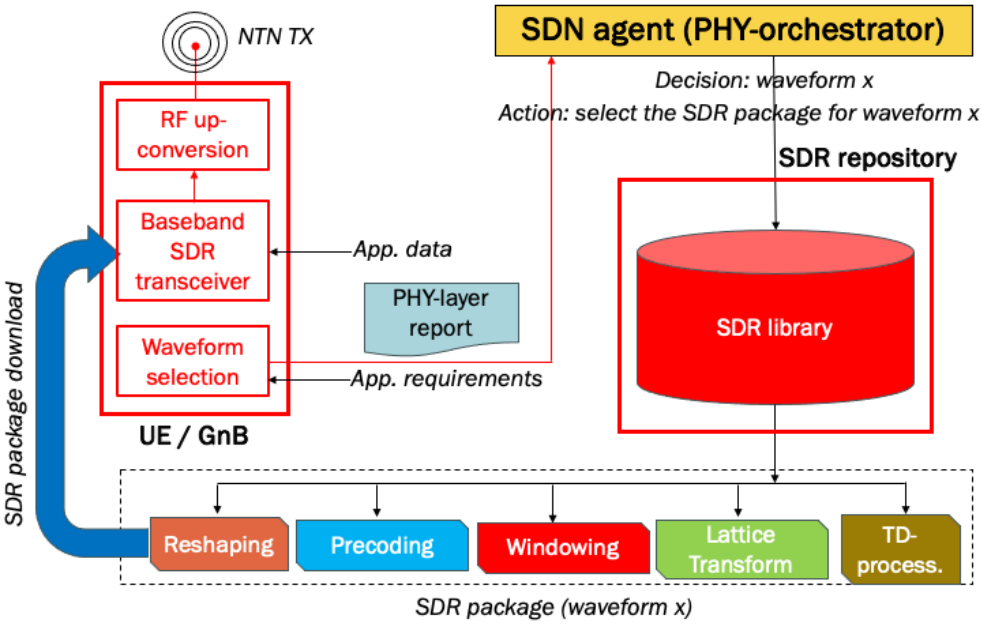

FIGURE 8. The proposed SDR-based PHY-layer implementation framework for 6G NTNs.

simply by changing their parameters. Then, specific sub-libraries should be established for each waveform, containing the appropriate instantiations of precoding, windowing, lattice transformation, and filtering. Substantially, the network orchestrator plays the role of the "librarian." who selects the right "volumes" (namely: the SDR modules) from the appropriate "racks" (namely: the sub-libraries) and delivers them in a package to the node asking for connection. The use of AI tools to drive the decision of the SDN orchestrator will represent an interesting and challenging matter for future research.

C. IMPLEMENTATION ISSUES

The research work concerning the modular SDR-based waveform decomposition has focused on the system design methodology and did not address aspects related to practical implementation. These aspects will be considered in future follow-up activities. In the present work, we want to highlight some critical issues to be tackled during the successive implementation phase:

- *Waveform switching*: if the PHY-orchestrator decides that the waveform format should be changed, a sort of handover should be issued by the network manager so that the PHY-layer reconfiguration is prepared in advance. Buffering mechanisms should be considered for user data during the transition from one transmission format to another. The switching procedure should be as soft as possible without a perceivable service interruption. This process would involve an increase in overhead and computational complexity that should be carefully assessed by taking into account that some transceiver nodes are installed in flying and/or orbiting payloads.
- *Synchronization*: the PHY-layer architecture of Fig. 8 requires a double synchronization that we can denominate as "horizontal" and "vertical". The "horizontal" synchronization concerns the current transmitting waveform and should be implemented by using efficient state-of-the-art techniques. The "vertical" synchronization is inherent to the waveform switching operation and should be governed by the PHY-layer orchestrator in a centralized manner. Again, such a procedure looks critical in terms of computability, latency, and overhead.
- *Compatibility*: different standard waveform formats generally support different transmission applications, characterized by varied requirements in terms of bit-rate and bit-error-rate. The PHY-layer orchestrator should also manage the waveform compatibility before a reconfiguration issue. To this aim, appropriate procedures of data formatting and rate scaling should be implemented by following a cross-layer approach. Another compatibility issue concerns the design and implementation of an RF front-end capable of supporting the different baseband transmission formats of Fig. 7. A viable and concrete solution for the design and implementation of a waveform-agnostic RF section, ready to be integrated with the SDR-based PHY-layer framework of Fig. 8 will be presented and discussed in Section VI-A.
- *Energy efficiency*: It is commonly recognized that the physical layer is the energy-hungriest part of a networking system. In our vision, the physical layer is an intelligent structure provided with autonomous reconfiguration capabilities. The increase in conceptual complexity may turn into an increase in energy demand. But it might also represent an opportunity to design a more

sustainable and energy-efficient system. Sustainability should be introduced ''by design'' in the considered software-defined approach, as shown in some recently published contributions dealing with a more sustainable vision of Space systems [61]. Some considerations about energy supply and power budgeting of the RF section of non-terrestrial nodes have been drawn in Section VI-B.

- *Security*: the PHY-layer security is a critical aspect in satellite-aerial-ground integrated networks (SAGINs). Some valuable contributions have been published in the recent literature. In [62], covert communication performance for SAGINs has been investigated in the presence of non-ideal behaviors of the HW/SW components of the transmission chain. In [63], the tradeoff between ubiquitous access targeted by 6G NTNs and secure communications is analyzed, and potential solutions based on Wireless Endogenous Security (WES) are proposed. Machine Learning tools are also considered in [64] to enhance the SAGIN security. In particular, Federated Learning is used to update covert communication parameters to dynamically react to eavesdroppers' attacks. It is clear that the software-defined PHY-layer architecture of Fig. 8 exhibits some evident vulnerabilities in terms of security. The potential critical issues concern both data transmission and dynamic link reconfiguration. The second one appears as the most critical. Indeed, an attacker may interfere with the SDR updating process, introducing fake software, malware, viruses, etc. Of course, such adversarial actions can severely compromise both system and data integrity, involving potentially catastrophic effects. Suitable countermeasures should therefore be adopted. A valuable example is shown in [65], where a blockchain-based authentication mechanism has been exploited to secure the firmware updates of LEO satellites. The adoption of similar solutions can be profitably extended to secure the SDR-based PHY-layer software update depicted in Fig. 8. This would be an attractive topic for future research.

D. CASE-STUDY FOR ADVANCED SDR-BASED NTN PHY-LAYER DESIGN: CONSTANT-ENVELOPE MULTICARRIER MODULATIONS (CE-MC)

Among the waveforms included in the modular SDR-based PHY-layer framework of Figs. 7-8, Constant-Envelope (CE) multicarrier modulations have particular relevance for non-terrestrial transmission scenarios. A detailed analysis of the pros and cons of the use of CE-MC waveforms in non-terrestrial networks has been presented in [66]. In the present paper, we shall summarize the main outcomes of such an analysis.

Constant-Envelope Orthogonal Frequency Division Multiplexing (CE-OFDM) was originally proposed by Thompson et al. in 2008 [57]. CE-OFDM offers a radical solution to the problem of the high Peak-to-Average Power Ratio (PAPR) of multicarrier modulations by transmitting a $0dB$-PAPR waveform, generated from an OFDM signal. In this way, the immunity to nonlinear amplification is guaranteed. CE-OFDM is obtained by applying a non-linear phase modulation to a normalized real-valued OFDM signal. The block diagram of the CE-OFDM transmitter is given in Fig. 9. You can notice that the processing blocks of the modular waveform decomposition of Fig. 7 are highlighted. The input of the transmission process is a data sequence (AKA: *symbol block*) made of M symbols $\{D_1, \cdots, D_M\}$, each one belonging to a squared K-levels QAM constellation (K is an even integer power of 2). The symbol duration is denoted by T_S. After the serial-to-parallel conversion (*reshaping*), no precoding is applied to the lattice that is passed unaltered to the windowing module. The CE-OFDM instantiation of windowing converts the original symbol lattice into a zero-padded hermitian-symmetric lattice, as follows:

$$\underline{D}_H = \left[0, D_1, \cdots, D_M, \underline{Z}_p, 0, D_M^*, \cdots, D_1^*\right] \tag{8}$$

$\underline{Z}_p$ denotes the zero-padding vector of length N_{zp}. Substantially the original lattice is zero-padded and mirrored so that $D_H(k) = D_H^*(-k)$. The length of $\underline{D}_H$ is expressed in [57] as follows:

$$N_{IFFT} = 2(M+1) + N_{zp} = 2(M+1)F_{ov} \tag{9}$$

where F_{ov} is the *oversampling factor*, defined in [57]. The oversampling factor (a power of 2) is typically chosen to be 4 or 8 [57].

The next processing module is the lattice transform from the frequency to the time domain, which applies the I-FFT operator to $\underline{D}_H$. The output of this step is a real-valued OFDM signal in the digital domain:

$$\begin{aligned} x[n] &= \sum_{k=0}^{N_{IFFT}-1} D_H[k]\, e^{2\pi j\left(\frac{kn}{N_{IFFT}}\right)} \\ &= 2\sum_{k=1}^{M} \Re\{D_k\} \cos\left(\frac{2\pi kn}{N_{IFFT}}\right) \\ &\quad - \Im\{D_k\} \sin\left(\frac{2\pi kn}{N_{IFFT}}\right) \end{aligned} \tag{10}$$

It is interesting to highlight that, adopting a squared multi-level QAM constellation, we have two independent real-valued $\sqrt{K}$-PAM symbol streams, which modulate the in-phase and carrier components of $x[n]$. The subsequent time-domain processing module generates the phase-modulated numerical signal $s[n]$ as follows:

$$s[n] = e^{j2\pi h(\Lambda x[n])} \quad n = 1, 2, \cdots, M \tag{11}$$

where $2\pi h$ is the *angular modulation index* measured in radians and $\Lambda = \sqrt{\frac{3}{M(K-1)}}$ is the normalization constant, defined in [57]. The insertion of the cyclic prefix concludes the numerical waveform generation.

The final step of the transmission is analog, with the Digital-to-Analog (D/A) conversion, performed at a sampling

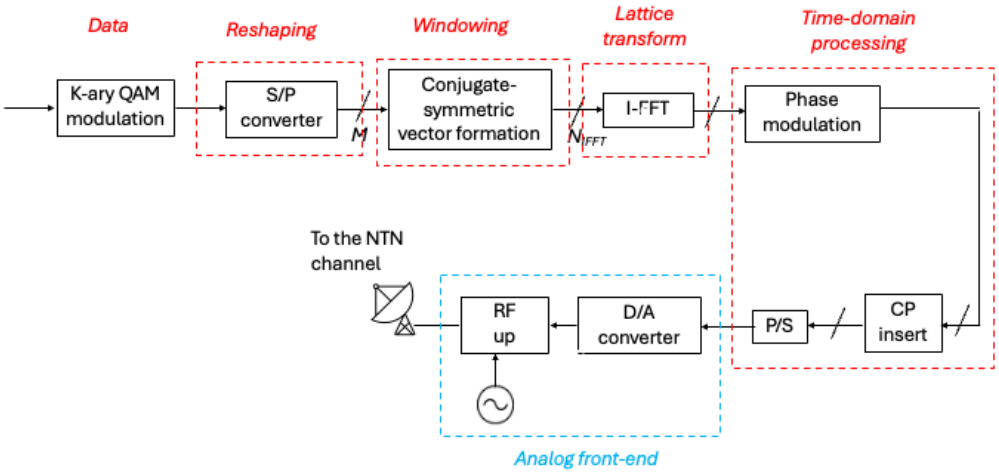

FIGURE 9. Block diagram of the CE-OFDM transmitter.

rate $1/T_S$. The transmitted CE-OFDM signal is thus given by:

$$s(t) = A_c \Re\left\{e^{j[2\pi f_0 t + \phi(t) + \vartheta]}\right\}, -T_{cp} \le t \le T \tag{12}$$

where $T = M \times T_S A_c, f_0$, and ϑ are the amplitude, frequency, and phase of the carrier signal, respectively, while $\phi(t) = 2\pi h \Lambda x(t)$ is the analog real-valued OFDM signal modulating the carrier phase. Just for the sake of completeness, $x(t)$ is the D/A converted sequence $x[n]$ of (10).

We can immediately notice the strongest point of the CE-OFDM transmission, i.e., the constant envelope. A CE-OFDM signal can be transmitted at the saturation point of a nonlinear amplifier, thereby avoiding the *SNR* decrease due to the insertion of the input back-off (IBO), which is required by OFDM and DFT-s-OFDM to mitigate nonlinear distortion effects. Moreover, under some conditions of high pre-detection carrier-to-noise ratio $\frac{C}{N_0}$, the use of a modulation index larger than 1 rad may turn into a post-detection signal-to-noise ratio gain, as is typical of analog angular PM and FM systems [57].

CE-OFDM is intrinsically resilient to frequency-selective multipath propagation for two main peculiarities. As shown in Fig. 10, the frequency-domain equalization (FDE) is applied to the received single-carrier phase-modulated signal. Such an arrangement offers a diversity gain, as formally demonstrated in [67], whereas OFDM with FDE does not. Moreover, the phase modulation introduces a sort of spectrum spreading. Indeed, if we consider the Taylor series expansion of the low-pass equivalent phase-modulated signal CE-OFDM signal, we can see that:

$$\begin{aligned} s_{lp}(t) = A_c e^{j\phi(t)} &\simeq A_c\left[1 + j(2\pi h)\Lambda x(t)\right] + \\ &- A_c\left[\frac{(2\pi h)^2 \Lambda^2}{2!} x^2(t) + j\frac{(2\pi h)^3 \Lambda^3}{3!} x^3(t) + \cdots\right] \end{aligned} \tag{13}$$

$x(t)$ being the analog real-valued OFDM signal. The corresponding approximation of the CE-OFDM low-pass equivalent spectrum is consequently obtained:

$$\begin{aligned} S_{lp}(f) \simeq\ & A_c \delta(f) \\ & + jA_c(2\pi h)\Lambda X(f) \\ & - A_c\left[\frac{(2\pi h)^2 \Lambda^2}{2!}\{X(f) * X(f)\}\right] + \\ & - jA_c\frac{(2\pi h)^3 \Lambda^3}{3!}[\{X(f) * X(f)\} * X(f)] + \cdots \end{aligned} \tag{14}$$

$X(f)$ is the spectrum of $x(t)$. As heuristically demonstrated in [57], such a spreading turns into a further increase of multipath diversity, similarly to what happens for wideband Spread Spectrum transmission. Indeed, the phase demodulation recompacts the "dispersed" spectrum of $s_{lp}(t)$ into the baseband spectrum of $x(t)$), thus providing augmented resiliency to frequency-selective channel effects.

The impact of phase noise on CE-OFDM transmission has been investigated in [68]. The arctangent function converts the complex exponential multiplicative phase noise term into an additive Gaussian term. Thus, the impact of phase noise on CE-OFDM link performance is generally mitigated as compared to that experienced by OFDM, where phase noise can destroy subcarrier orthogonality, inducing inter-channel interference [69]. On the other hand, the intrinsic single-carrier nature of the transmitted DFT-s-OFDM signal makes such a waveform more resilient to frequency and phase drifts, including phase noise, which remains, anyway, a relevant non-additive source of signal degradation.

Despite these advantages, CE-OFDM entails trade-offs that need careful evaluation. Orthogonal multiple access (OMA) is one of the strongest assets of OFDM (and DFT-s-OFDM). CE-OFDM enables OMA only in the downlink. CE-OFDM signals transmitted in uplink from the User Equipments (UEs) to the Access Point (AP) are truly independent and non-slotted single-carrier signals, which can be multiplexed only in the time (TDMA) or

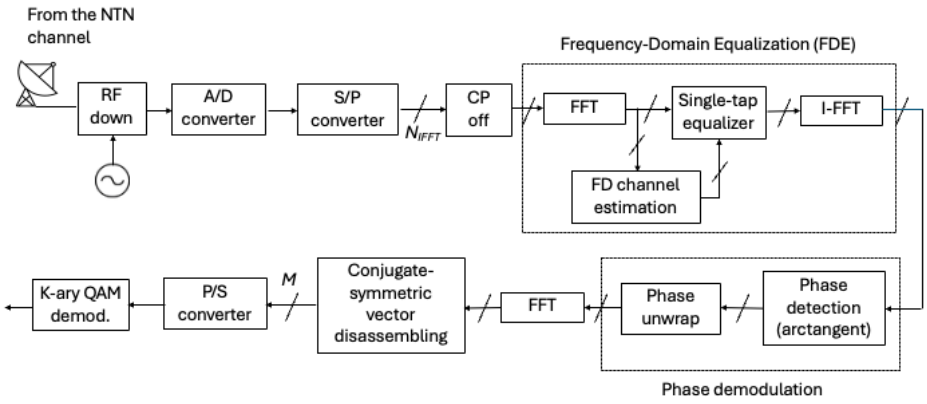

FIGURE 10. Basic receiver scheme for CE-OFDM signals.

frequency (FDMA) domain. More trendy and efficient NOMA solutions for multi-user CE-OFDM uplink transmission are currently under investigation and matter for future work.

The second point concerns the CE-OFDM detection. The block diagram of Fig. 10 clearly indicates that the CE-OFDM receiver is *nonlinear*, because the phase demodulation is a nonlinear processing task. Therefore, nonlinear effects on the symbol detection should be carefully evaluated. One of these is the *threshold effect*, typical of angular modulations, which degrades the system performance at low SNRs for any value of the modulation index. The threshold effect is due to the non-additivity of the background noise caused by the nonlinearity of phase detection [70]. Another nonlinear detection effect is the *phase wrapping*. The phase demodulator based on the nonlinear arctangent function works on a range of output values falling within the limited interval $[-\pi, \pi]$. If the transmitted signal exhibits phases falling outside such an interval (this occurs with very high probability when $2\pi h > 1$), these phases "wrap around." Substantially, they are shown as phases in the opposite direction or falling within the standard range. Phase wrapping involves a form of aliasing in phase demodulation that turns into inter-channel interference at the output of the CE-OFDM receiver. For this reason, CE-OFDM considers two basic countermeasures: the zero-padding of D_H, which reduces the PAPR of the real-valued OFDM signal, and the phase unwrapping adopted at the receiver side [57]. As previously mentioned, oversampling factors of 4 and 8 are regarded as convenient; further increase of this parameter turns into an increase of the computational burden, but is generally ineffective, and may even be detrimental. Phase unwrapping is a useful tool to solve phase ambiguities. However, phase unwrapping is, in turn, a nonlinear block that may introduce further degradations. An example is related to circular phase slips, where a 2π ambiguity is incorrectly resolved, typically by failing to add the correct integer multiple of 2π. In general, it is not convenient to increase the modulation index too much, as unsolved ambiguities in the phase detection might severely impair the demodulation process.

The DFT precoding of the input symbol sequence has been proposed in [58] as an alternative solution to make CE-OFDM more robust to the incorrect phase detection. Such a precoded CE-OFDM waveform has been denoted as *Constant-Envelope Single-Carrier OFDM (CE-SC-OFDM)*, and CE-SCFDMA in the multi-user version. An M-point DFT precoding is applied before the formation of the oversampled conjugate-symmetric symbol vector. Such an arrangement significantly reduces the probability of crossing the $\pm\pi$ boundary and, therefore, of encountering phase wrapping at the receiver side. Of course, the dual DFT decoding should be applied at the receiver side before the symbol detection. In [71], the analysis of the empirical complementary cumulative distribution function (CCDF) of the peak absolute value of $\phi(t)$ evidences a considerably reduced probability of crossing the critical π boundary, in particular for lower-order constellations and low modulation indexes.

Another important tradeoff concerns the increased bandwidth occupation of CE multicarrier modulations. The main lobe of the CE-MC signal spectrum occupies a bandwidth at least twice that of conventional multicarrier transmission formats. Such an increase is formally motivated by the two-sided RF spectrum, which characterizes $s(t)$. A reliable quantitative estimation of the bandwidth B occupied by the main spectral lobe of the CE-OFDM and CE-SC-OFDM RF signals is reported in the following equation [57]:

$$B = \max\{2\pi h, 1\} \times \left(\frac{2}{T_S}\right) \quad [Hz] \tag{15}$$

Increasing the modulation index beyond 1 rad, the performance of the CE-MC transmission (namely: CE-OFDM and CE-SC-OFDM) might improve, in particular if higher-order QAM constellations are adopted, but at the price of further reduction of spectral efficiency. The comparative performance and complexity analysis of CE-MC vs. conventional MC waveforms will be detailed in Section VIII.

V. EFFICIENT NOMA-BASED RADIO ACCESS

The full implementation of the massive Internet-of-things (mIoT) paradigm in the 6G ecosystem necessarily requires

the allocation of large numbers of packet flows across shared resources [6]. This problem has been deeply addressed at the terrestrial level during the 5G standardization process, but remains partly open for the NT contexts, where massive random access is expected to become crucial to manage swarms of UAVs or nanosatellites supported by high-altitude platforms or space motherships [72], [73], [74]. Some recent works have been published related to massive IoT access in air-ground integrated networks. In [75], the collision of ranging signals in massive IoT concurrent access is addressed in multi-frequency TDMA satellite communication systems. The devised solution comprises a multi-objective anti-collision algorithm that optimizes the concurrent access ranging process by minimizing the collision probability. In [76], the potential of AI is leveraged to manage the limited spectrum resources and constrained energy supply, which characterize massive IoT access in SAGINs. Multi-objective Deep Reinforcement Learning has been adopted in [77] for efficient time-frequency resource allocation in massive access multi-beam satellite communications.

These scenarios may specifically benefit from the interference cancellation (IC) capabilities implemented in forthcoming microwave (μWave) and millimeter-wave (mmWave) radio receivers, which represent the enabling functionality of NOMA technology. Power-domain NOMA (PD-NOMA) manages, in fact, the packets colliding within the same time slot by moving from the attempt to capture that associated with the highest received power. If this first decoding process is successful, the acquired packet is canceled, and the decoder moves to the packet associated with the second-highest received power by attempting its capture and subsequent cancellation. If, at a certain iteration, the decoding results are unsuccessful, the procedure is terminated, and the remaining packets are considered involved in an unresolvable collision. This evolution of the NOMA scheme enables significant throughput improvements with respect to the commonly adopted slotted Aloha (SA)-based protocols implemented in 2-4G random access channels (RACHs), Accordingly, many valuable contributions have been recently presented to highlight the potential and the perspectives of the PD-NOMA technology [78], [79], [80], [81], [82], [83], [84], [85]. These works mainly address the design problem, while thr modeling one has received less attention, with few valuable studies that have presented theoretical estimations of the PD-NOMA performance [86]. This latter task is, in fact, considerably challenging because of the characteristics of the IC decoding process, which is influenced by the correlation among the powers associated with the packets hosted in the same slot. Moreover, the unreliability of the communication channel, characterized by the influence of different statistical phenomena, makes the problem harder to deal with. As a consequence, the development of a fully analytical framework for the throughput evaluation of a PD-NOMA scheme often may represent a prohibitive problem, specifically in high-mobility NT scenarios. A partial addressing of this issue might be realized by adopting a semi-analytical approach [87]. According to this strategy, the PD-NOMA model may be subdivided into two parts: an analytical one, focused on the theoretical evaluation of the power statistics, and a simulated one, focused on the throughput calculation by exploiting the analytical power distributions. The benefits of this approach concern, on the one hand, the reduction of the overall computational time, thanks to the replacement of the channel simulator by a suitably generated random variable, and, on the other hand, the possibility of taking into account the correlations among the ordered powers during the IC process.

A. ANALYTICAL TASK

The conceived semi-analytical strategy becomes specifically profitable when the CDF of the power statistic is available in closed-form. For the aerial and space scenarios, this possibility can be realized, for example, by considering swarms of vehicles moving within a disk of radius ρ and center O that send information towards a common destination located in O. Since LoS conditions can be reasonably assumed, the power received by the destination from the generic transmitting user can be compactly written as:

$$P = \frac{\theta}{R^2}\,\Psi, \tag{16}$$

where $\theta = P_{\mathrm{T}} G_{\mathrm{T}} G_{\mathrm{R}} / \alpha$ is a constant accounting for the transmitting power P_{T}, the transmitting/receiving antenna gains $G_{\mathrm{T}}/G_{\mathrm{R}}$, and the path-loss floating intercept α, while R and Ψ are random variables modeling, respectively, the random location of the vehicles and the statistical fluctuation of the power.

For an aerial context, random way-point UAV mobility [88], and Nakagami-m fading [89], can be adopted to respectively describe R and Ψ. According to the these choices, the CDF of (16), for $p > 0$, can be expressed as [87]:

$$F_P(p) = \frac{1}{\Gamma(m)} \sum_{k=0}^{2} \frac{(-1)^k\,(1+\delta_{k1})}{\hat{\chi}^k(p)}\,\gamma\left[m+k;\,\hat{\chi}(p)\right], \tag{17}$$

where $\Gamma(\cdot)$ and $\gamma(\cdot;\cdot)$ are the complete and lower incomplete gamma functions, respectively, δ_{kj} is the Kronecker delta, and:

$$\hat{\chi}(p) = \frac{mp}{\theta\rho^2}. \tag{18}$$

For a space context, R and Ψ may be instead respectively described by a uniform distribution [74], and a generalized gamma distribution [90], where the first one models a lattice swarm of small satellites around a receiving mothership, while the second one models ionospheric scintillation. In this case, the CDF of (16), still for $p > 0$, can be written as [87]:

$$F_P(p) = \frac{1}{\Gamma(\mu_1)} \sum_{k=0}^{1} \frac{(-1)^k}{\tilde{\chi}^k(p)}\,\gamma\left[\mu_1+\frac{\delta_{k1}}{\mu_2};\,\tilde{\chi}^{\mu_2}(p)\right], \tag{19}$$

where μ_1 and μ_2 are the shape parameters of the generalized gamma distribution, and:

$$\tilde{\chi}(p) = \frac{p}{\theta\rho^2\Gamma(\mu_1)}\Gamma\left(\mu_1 + \frac{1}{\mu_2}\right). \tag{20}$$

B. SIMULATION TASK

The integration of the analytical CDFs inside the network simulator may be carried out by firstly generating, for a given offered load ς, the random number n of users hosted in a slot according to a Poisson-based traffic model. Subsequently, the corresponding independent and identically distributed (iid) received powers $p_{1,n}, \ldots, p_{n,n}$ may be generated according to (17) or (19). The successful or unsuccessful decoding of each of the n packets can be established by reorganizing them in ascending order. This leads to an ordered realization $p_{(1),n}, \ldots, p_{(n),n}$, where $p_{(n),n}$ is the highest generated power. Assuming perfect IC, the SINR at the l-th iteration, can be determined, for $l = 1, \ldots, n$, as:

$$\upsilon_{l,n} = \frac{p_{(l),n}}{\sum_{l'=1}^{l-1} p_{(l'),n} + N_0}, \tag{21}$$

where N_0 is the noise power. The (l)-th packet is usually considered successful if its SINR is larger than or equal to a predefined threshold. A more reliable criterion can, however, be established by considering the actual rate achievable by that SINR. For a Shannon-based limit ($i = 0$) and a QPSK modulation combined with an efficient channel code ($i = 1$), this rate can be expressed as [91]:

$$\xi_i(\upsilon_{l,n}) = \begin{cases} \log_2(1+\upsilon_{l,n}) & i = 0 \\ 2 - 2\exp\left[a_3 - a_1\left(\frac{\upsilon_{l,n}}{2}\right)^{a_2}\right] & i = 1 \end{cases} \tag{22}$$

where $a_1 \cong 1.2860$, $a_2 \cong 0.9308$, $a_3 \cong 0.0102$ are approximating coefficients, and the case $i = 1$ remains accurate for SINR values larger than -20 dB. According to this criterion, the (l)-th packet can now be considered successful if:

$$\xi_i(\upsilon_{l,n}) \geq \varrho, \tag{23}$$

where $\varrho = \varrho_c \log_2 \varrho_m$ accounts for selected code rate ϱ_c and the modulation order ϱ_m. The satisfaction of the sole condition in (23) is, however, not sufficient to guarantee that the corresponding packet actually contributes to the aggregate network throughput. The possibility that the IC process arrives at the (l)-th step is, in fact, correlated to the success of all the previously processed packets (from (m) to $(l+1)$) and the consequent complete removal of the corresponding interference powers. Otherwise, i.e., if at least one of the previous $m - l + 1$ packets is unsuccessful, the (l)-th one will not be processed because of the already occurred termination of the IC process. This correlation implies that the success event for the (l)-th IC iteration (or packet) can be modeled, for $i = 0, 1$, by the Boolean function:

$$S_{l,n}^i = \begin{cases} 1 \;\; \xi_i(\upsilon_{l',n}) \geq \varrho, \; l' = l, \ldots, n \\ 0 \;\; \text{otherwise} \end{cases}, \tag{24}$$

which allows one to express the throughput as:

$$\eta_i = \varrho \; \mathbf{E}_N\left[\sum_{l=1}^{n} S_{l,n}^i\right]\varsigma, \tag{25}$$

where $\mathbf{E}[\cdot]$ is the expectation over the rv N (whose realization is n). This latter numerical quantity provides, in information bits/transmission, the average amount of traffic successfully delivered to the target receiver as a function of the offered load for each of the two code-modulation models in (22). The expression in the brackets simply denotes the total number of successfully decoded packets per realization, which is subsequently averaged over the number of simulations performed for each considered value of the load. The results obtained by the here described semi-analytical approach for the air and space scenarios will be presented in Subsection VIII-C.

VI. MULTI-MODAL TRANSCEIVER IMPLEMENTATION

In the path from 5G to 6G, spectral efficiency becomes a key parameter for evaluating and selecting emerging technologies to be incorporated in the standard specifications. Non-Orthogonal Multiple Access (NOMA) has shown higher spectral efficiency compared to conventional OFDMA [92], which is the actual baseline of 5G waveform. At the same time, the shift to higher frequency bands allows for larger signal bandwidths, enabling higher data rates. However, this evolution is constrained by hardware impairments, as practical devices deviate from ideal behavior. Power amplifier nonlinearities (such as AM-AM and AM-PM distortion), phase noise, and IQ imbalance can degrade signal integrity. These imperfections lead to increased out-of-band emissions and reduced in-band SINR (Signal-to-Interference-and-Noise Ratio). In NOMA systems, such degradation affects the general signal quality and the effectiveness of Successive Interference Cancellation (SIC), which is a critical process that allows users to separate and decode individual data streams. The probability for a user to experience a SINR lower than the minimum required to ensure a certain QoS is known as the outage probability. It is increased by hardware non-idealities, compromising the overall network data capacity and fairness in resource allocation among users [93]. In our paper, a proof-of-concept of a TDD satellite transceiver for the 5G FR2 frequency bands n257, n258 an n261 [94] is proposed. The transceiver is composed of COTS components for a cost-effective solution. The proof-of-concept comprises evaluation boards (EVB) of the selected RF chain hardware components. A measurement campaign is performed to extract the proposed system key parameters, which are then integrated in a simulator to assess phase noise, AM-AM, and AM-PM impairments on a NOMA waveform.

A. HARDWARE ARCHITECTURE AND SDR COMPATIBILITY FOR MODULAR WAVEFORMS

The proposed RF Front-End (FE) employs a hybrid architecture that couples a direct-sampling modem/SDR interface at the intermediate frequency (IF) with a Ka-band

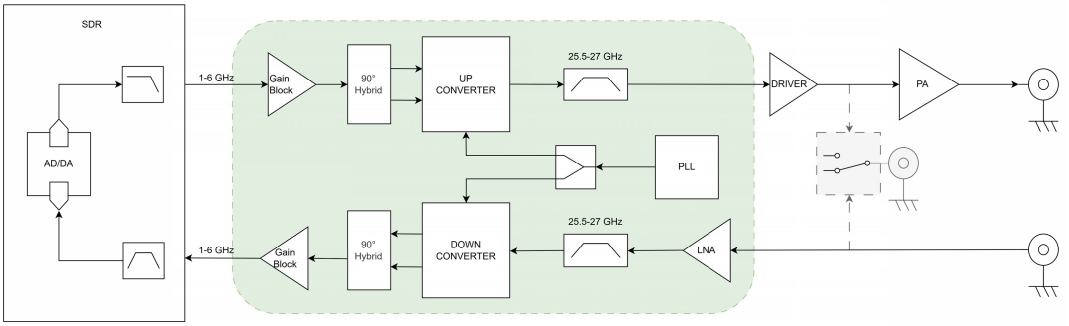

FIGURE 11. Ka-band FE PoC architecture: SDR/IF interface and RF conversion/amplification chains.

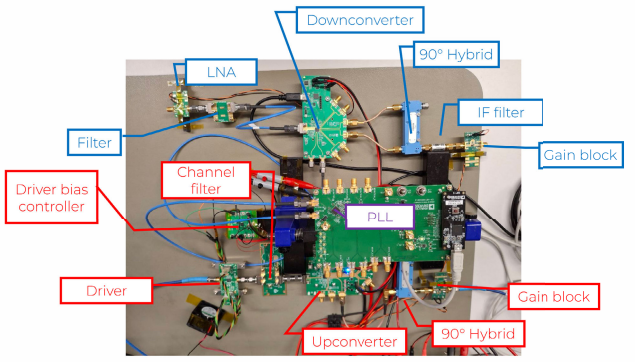

FIGURE 12. PoC implementation based on COTS building blocks (evaluation boards / modular RF components).

superheterodyne RF chain performing IF-to-RF and RF-to-IF conversion. Fig. 11 and Fig. 12 show the block diagram of the designed FE architecture and its hardware implementation using COTS building blocks, respectively. We believe that our choice provides a good tradeoff among performance, flexibility, and component availability at Ka-band, while remaining naturally compatible with software-defined, modular waveform generation and detection.

The RF section adopts highly integrated Ka-band frequency-conversion ICs, enabling compactness and reduced component count. A key design goal is to keep the RF chain as much *waveform-agnostic* as possible. In such a way, different waveform formats (including modular waveforms assembled in the SDR domain) can be accommodated by selecting bandwidth, sampling rate, and digital channel filtering at baseband/IF, while the RF chain provides wideband conversion and amplification. In particular, the IF plan is selected to avoid undesired LO-related tones within the target RF band, and upper-sideband conversion is employed to minimize the need for spectrum inversion at the SDR level.

The designed TX chain comprises: IF input conditioning/variable gain (to set the drive level), IF filtering, IF-to-Ka upconversion (superheterodyne), driver amplification, power amplification, and an output band-pass filter. This chain is dimensioned so that the FE can deliver high-throughput modulated signals while maintaining sufficient linearity margin, also guaranteed by the output detector that ensures the ability to maintain constant output power by implementing an automatic level control (ALC). The designed chain is shown in Fig. 13.

From a requirements standpoint, the PoC targets an output power at the Ka-band port in excess of 37 dBm under representative operating conditions, and modulation-quality preservation for high-order modulations (e.g., 32APSK), which translates into adequate output back-off (OBO) and stage-level headroom from compression. In practice, following the DVB-S2 standard, the design keeps the nominal operating point at least 3–5 dB below the effective $P_{1\mathrm{dB}}$ of the stages that dominantly affect EVM (e.g., driver/PA), while ensuring that spurious emissions remain below the target mask (e.g., < -40 dBc) after output filtering. The linearity analysis is shown in Fig. 14.

The RX path is designed to maximize sensitivity through low-noise front-end conditioning and provide sufficient dynamic range to accommodate varying link conditions without saturating the SDR/ADC. A representative RX chain comprises: input band-pass filtering, low-noise amplification (LNA), Ka-to-IF downconversion (superheterodyne), IF filtering, variable-gain amplification (VGA/AGC), and IF output conditioning toward the SDR/modem. The block diagram of the designed chain is shown in Fig. 15.

At a requirement level, the RX chain is dimensioned to cover a broad input power range (link-dependent) while keeping the IF output within the SDR/ADC linear region. Key driver targets include: a low overall noise figure to preserve G/T at the terminal, sufficient gain to overcome downstream noise contributions, and adequate compression and intermodulation margin at the stages most exposed to strong inputs (e.g., LNA/mixer/VGA). The gain and compression analysis is shown in Fig. 16. Section VIII will show and discuss further in-lab measurement results that will definitely provide validation to the PoC.

B. ENERGY SUPPLY AND POWER BUDGETING OF NON-TERRESTRIAL NODES

Non-terrestrial nodes (e.g., small satellites) operate under stringent energy constraints dictated by the spacecraft electrical power subsystem (EPS), which must balance generation (solar arrays), storage (battery), and loads over the orbit.

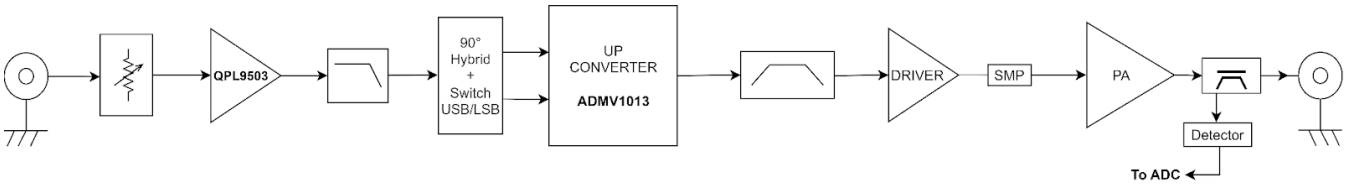

FIGURE 13. TX chain decomposition (IF conditioning, upconversion, driver, output filtering), PA, detector.

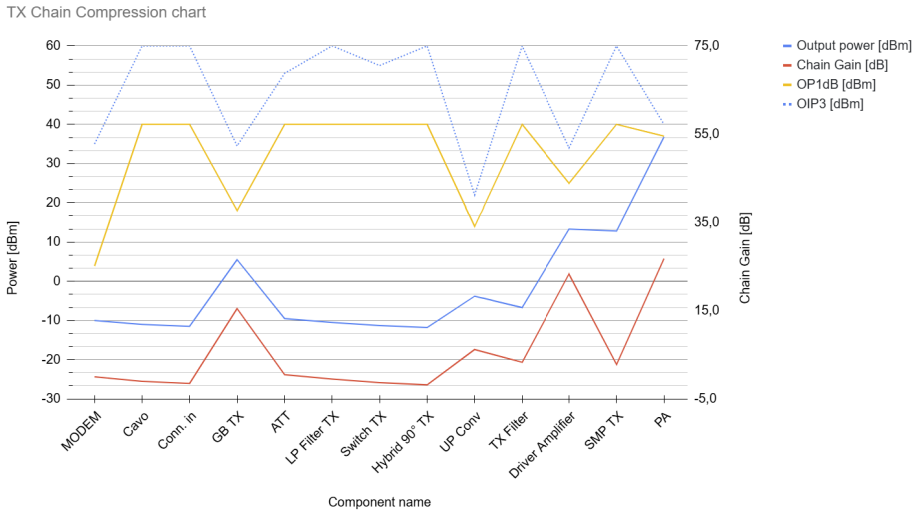

FIGURE 14. TX stage-by-stage power budget and compression headroom (e.g., P_{in}, gain, P_{out}, P_{1dB}).

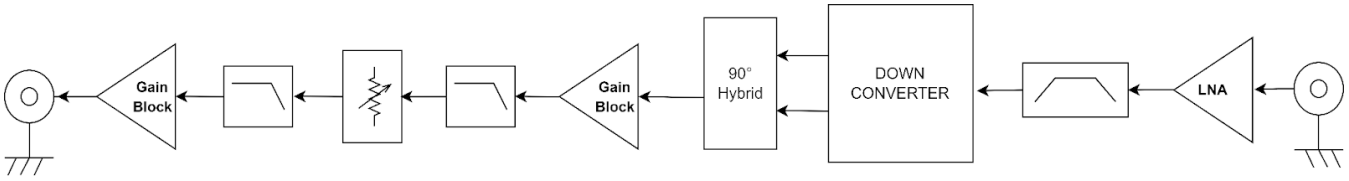

FIGURE 15. RX chain decomposition (input filtering, LNA, downconversion, IF filtering/VGA, SDR interface).

In this context, the RF payload is typically one of the dominant contributors to the power budget due to the power amplifier (PA) and the frequency-generation chain. The proposed PoC FE consumes less than 35 W in peak operation while targeting point-to-point Ka-band links above 1 Gbps (both inter-satellite and feeder links), enabled by the availability of large bandwidths and by the adoption of suitable modulation/coding techniques. From an operational standpoint, the same hardware naturally supports energy-aware strategies such as duty cycling (i.e., activating high-power RF stages only during scheduled transmission/reception windows), which reduces average power while preserving peak throughput when the link is active.

C. COST AND INTEGRATION OVERHEAD OF MULTI-TECHNOLOGY SUPPORT

The proposed multi-technology integration is achieved primarily through a *common* RF/IF platform and a software-defined baseband section. This limits hardware overhead when enabling multiple technologies: the RF chain need not be replicated for each waveform/access scheme, while waveform switching and protocol agility are primarily handled in the SDR domain (compute/FPGA resources and software). Moreover, the PoC has been implemented using consumer-grade COTS building blocks to reduce lead time and non-recurring engineering costs, while preserving a clear migration path toward an integrated custom board once the target architecture and RF plan are consolidated.

VII. CLOUD COMPUTING AND MEC FOR NETWORK ORCHESTRATION AND CONNECTION MONITORING

The massive increment of users in 5G and beyond NTNs made the traditional centralized computing techniques obsolete. Indeed, such techniques are being replaced by multi-access edge computing (MEC). MEC provides cloud computing capabilities close to the network edge [95]. It is

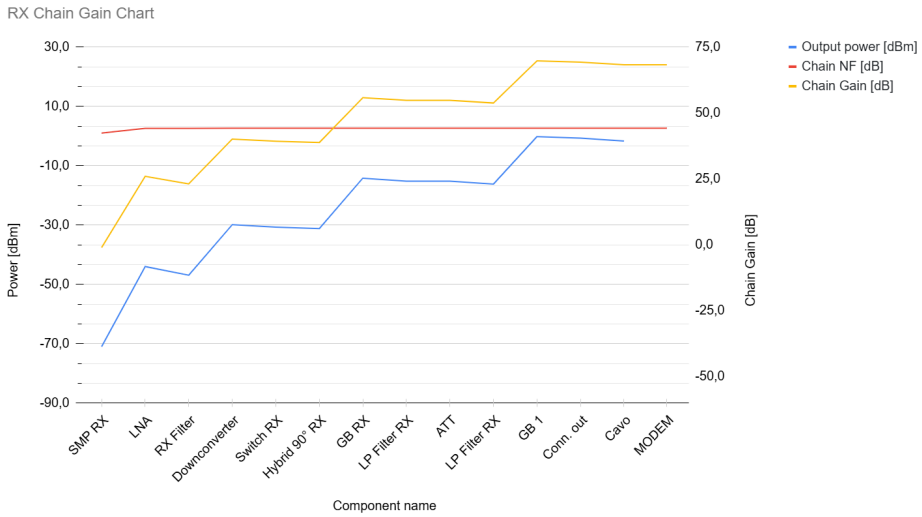

FIGURE 16. RX stage-by-stage characterization placeholders (gain plan, compression headroom).

known that satellite networks often struggle with extended delays and limited data capacity, causing connection issues. Thanks to its proximity to end-users and geographically distributed deployments, MEC can solve these problems by reducing latency, increasing data capacity, enhancing security, and ultimately improving the network efficiency [96]. During the INFINITE project, two main activities concerned the aspects of cloud computing and MEC:

- Development of a MEC emulation platform to evaluate MEC placement strategies in Space networks.
- Synergetic combination of AI and MEC for Cloud-RAN monitoring and resource management.

In the following subsections, the research core concerning these two activities will be presented.

A. METEORNET: AN EMULATION PLATFORM

In this subsection, we present MeteorNet [97], an open-source emulation framework we developed to support the study of Non-Terrestrial Networks (NTNs). MeteorNet integrates virtual networking, containerized applications, and orbital dynamics into a cohesive platform specifically designed for evaluating Multi-access Edge Computing (MEC) placement strategies in space-based networks. Unlike traditional discrete-time simulators, MeteorNet operates in continuous time and leverages real-time emulation with multi-threaded execution. By using production-grade virtualization technologies at both the network and system levels, the framework provides a realistic and scalable environment for testing edge computing solutions. This ensures that proposed strategies can meet the stringent timing and operational requirements of modern and future LEO satellite constellations.

MeteorNet models a space-based cloud system distributed across a LEO satellite constellation. Its core architecture comprises the following modules:

1) **Orbit Propagation Module**: it simulates satellite motion and orbital dynamics in real time.
2) **Software-Defined Networking (SDN) Controller**: it manages the virtual network topology using Mininet [98], enabling centralized and programmable routing control.
3) **Containerized Software Environment**: it uses Docker to deploy isolated computing services within lightweight OS-level virtual environments [99].
4) **Network Performance Monitoring**: it captures metrics such as throughput, latency, jitter, and packet loss to support system evaluation and tuning.

Each MeteorNet node consists of an OpenFlow-enabled [100] virtual switch interface. Nodes are interconnected through virtual links with configurable properties such as bandwidth, delay, and packet loss. MEC-enabled nodes also run a Docker container attached to the switch, with its own operating system and software stack. When Line-of-Sight conditions change, MeteorNet dynamically adjusts or disables links to emulate realistic network disruptions. Satellite nodes may function as compute-enabled endpoints or host-less switches that forward traffic via the SDN controller. MeteorNet does not simulate physical data transmission; instead, it models link properties such as availability and delay using empirically derived statistical approximations.

Moreover, MeteorNet supports the emulation of edge computing deployments in both terrestrial and space-based cloud architectures. In the following subsection, we focus on comparing the following two paradigms:

1) **Terrestrial Cloud**: Tasks are processed by a data center connected to the Internet via a single ground gateway in Italy.
2) **Space Cloud**: One or more satellites serve as computing nodes, executing tasks directly in orbit.

In both architectures, user devices connect to the network via the nearest satellite in line-of-sight. Inter-satellite routing is

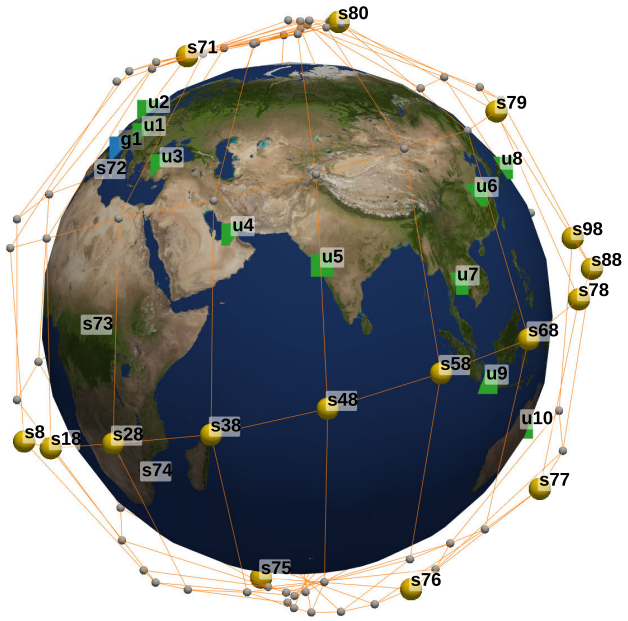

FIGURE 17. 3D view of the satellite constellation and network nodes.

handled by ONOS [101], which uses a reactive algorithm based on Dijkstra's shortest latency path [102] to compute data flows across the constellation.

B. TERRESTRIAL VS. SPACE CLOUD MODEL

This subsection presents the system model used to compare the performance of space and terrestrial edge computing architectures using the MeteorNet framework.

1) SPACE SEGMENT MODEL

We simulate a constellation of S satellites using a Walker Delta pattern with ten orbital planes evenly distributed across half the equator's circumference. Each orbital plane hosts ten satellites uniformly spaced along its orbit. Inter-Satellite Links (ISLs) connect each node to its two nearest neighbors within the same orbital plane and to two satellites in adjacent planes, forming a mesh with four direct links per node.

2) GROUND SEGMENT MODEL

User devices, defined as $\mathcal{U} = \{u_j \mid 1 \leq j \leq U\}$, are deployed at fixed locations on Earth and generate tasks that must be offloaded to external computing servers. Users lack direct access to the terrestrial Internet and hence rely on the satellite network for uplink. Each device connects via the first satellite in Line-of-Sight. Figure 17 illustrates the geographic locations and network topology. Table 1 lists the considered user coordinates and their corresponding distances to the ground gateway.

We evaluate four configurations based on server placement strategy:

1) **Terrestrial Cloud**: processing occurs on a ground server linked to the Italy gateway, with a fixed latency of 5 ms.

TABLE 1. Ground nodes locations.

Location	Latitude [°]	Longitude [°]	Name	Distance [km]
Italy	44.41	8.93	g1	-
Austria	48.2	16.3666	u1	709
UK	55.9483	-3.2191	u2	1543
Turkey	39.9272	32.8644	u3	2027
U. Arab Emirates	25.23	55.28	u4	4660
India	19.017	72.857	u5	6489
China	30.58	114.27	u6	8770
Thailand	13.75	100.5166	u7	9069
Japan	35.685	139.7514	u8	9826
Indonesia	-6.1744	106.8294	u9	11117
Australia	-27.4550	153.0351	u10	16321

TABLE 2. Constellation parameters for test cases.

Parameter	Value	Description
S	100	Number of satellites
U	10	Number of user locations
D	20	Devices per user location
T	45 minutes	Emulation duration
r	2 tasks/minute	Task generation rate per device
N_j	≈ 200	Tasks per user u_j
N	≈ 1800	Total tasks per test case

2) **Space Cloud, Single**: a single satellite (ID 78) hosts the edge server.
3) **Space Cloud, Along Orbit (AO) Distribution**: ten satellites in one orbital plane act as servers (IDs 71–80), spaced 36° apart in mean anomaly.
4) **Space Cloud, Cross Plane (CP) Distribution)**: ten satellites in adjacent orbital planes serve as compute nodes (IDs 8, 18, 28, …, 98), separated by 18° in right ascension of the ascending node [103].

All architectures share the same constellation and task generation settings, summarized in Table 2. Each user location hosts D devices, generating tasks at a rate r following a Poisson process. Let N_j be the number of tasks from user u_j, and $N = \sum_j^U N_j$ the total tasks during the emulation period T. We define $\lambda_{i,j}$ as the end-to-end network latency for a task i by user u_j. It corresponds to the shortest path delay between the user and the nearest latency MEC server. We evaluate each architecture by computing the average task latency per user u_j:

$$\bar{\lambda}_j = \frac{\sum_{i=1}^{N_j} \lambda_{i,j}}{N_j} \tag{26}$$

This setup enables a systematic comparison of edge architecture designs and helps identify when space-based computing outperforms traditional terrestrial approaches.

C. ML AND MEC-ASSISTED MONITORING AND RESOURCE PREDICTION FOR DISAGGREGATED NGRAN

One emerging trend in NTNs is the disaggregated Next-Generation Radio Access Network (NGRAN). 3GPP has proposed the disaggregated NGRAN to optimize resource management in 5G networks [104]. Substantially, in a

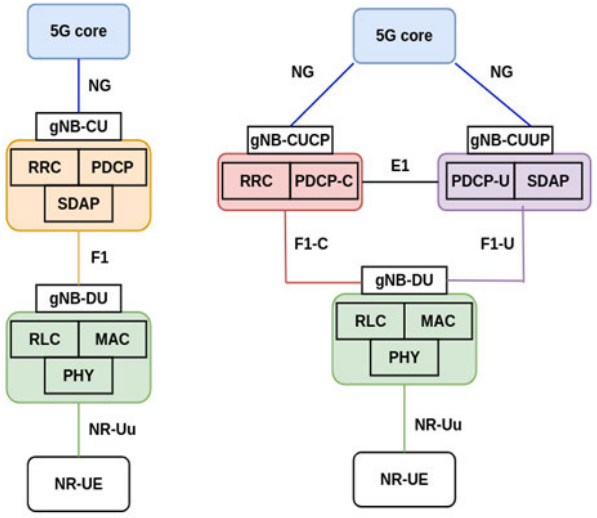

FIGURE 18. Disaggregated NGRAN split option of 3GPP: baseline option (on the left), enhanced option (on the right). NOMENCLATURE: RRC: Radio Resource Control, PDPC: Packet Data Convergence Protocol, SDAP: Service Data Adaptation Protocol, RLC: Radio Link Control, MAC: Medium Access Control, PHY: Physical layer functions (courtesy of [105]).

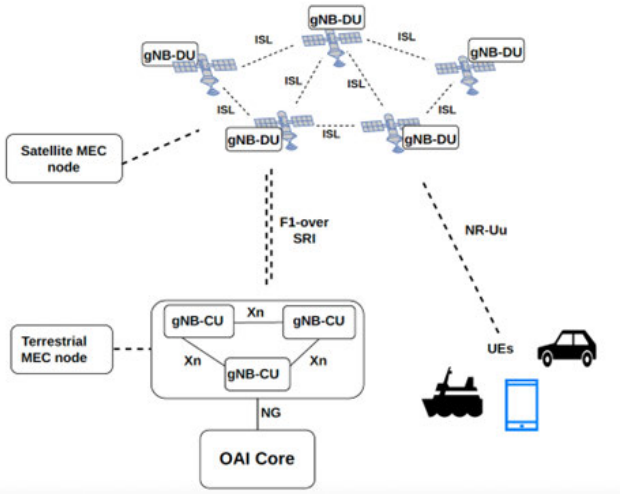

FIGURE 19. Pictorial description of the disaggregated NGRAN NTN architecture (courtesy of [107]).

disaggregated NGRAN, the gNB is split into a Central Unit (CU), a Distributed Unit (DU), and, in Open RAN-style decompositions, a Radio Unit (RU). CU hosts the higher-layer RAN protocol functions, such as RRC and PDCP/SDAP, and is commonly implemented as a virtualized network function deployed in a centralized or edge-cloud location. DU hosts the lower-layer functions such as RLC, MAC, and PHY, and performs time-sensitive baseband processing closer to the radio site, under partial control of the CU. The RU provides radio-frequency (RF) transmission/reception and typically implements RF and low-layer PHY processing near the antenna site. In Fig. 18, the different options for NGRAN disaggregation planned by 3GPP are shown. In the enhanced version, the gNB-CU is further split into gNB-CUCP and gNB-CUUP, where the gNB-CUCP handles the RRC and control plane tasks of PDCP (PDCP-C), and the gNB-CUUP handles the SDAP and PDCP user plane (PDCP-U) tasks. The disaggregation of the NGRAN is essential for optimizing resource management in 5G NTN, particularly within LEO satellite constellations operating in regenerative mode. However, this disaggregation, combined with satellite mobility and limited processing power, presents challenges in ensuring network resilience and addressing Quality of Service (QoS) requirements. During the INFINITE project timeline, relevant research efforts have been spent to exploit the full potential of AI and MEC to efficiently monitor the link status and the resource allocation in non-terrestrial NGRAN configurations. In particular, AI-based monitoring continuously ingests NGRAN and transport KPIs and translates them into actionable intents (e.g., fault localization, alternative routing decisions, and resource forecasts) that can be enforced by software-defined orchestration for adaptive rerouting and resource allocation. The related results have been published in some very recent works [105], [106], and [107]. The starting point of the research work is the cloud-native NTN architecture of Fig. 19. The gNB-DU is embarked on a regenerative LEO satellite payload, and the gNB-CU is deployed in the terrestrial network to form an end-to-end 5G NTN network, as shown in Fig. 20. In addition, the training dataset for the AI models is collected from a cloud-native 5G NGRAN testbed deployed in the lab, where the gNB-CU and gNB-DU functions run as containerized network functions and export real-time telemetry for monitoring and orchestration. In [106], a Graph Convolutional Network (GCN) is used to identify the faulty NGRAN component based on link delay and identify the shortest routing (alternative) path across the network. GCN is a typology of deep learning Graph Neural Network (GNN) that learns the graph structure representation of the deployed network [108]. A graph can be denoted as $G = (V, E)$, where V represents the set of nodes, E the links connecting the nodes, and $G(\bullet)$ a nonlinear mathematical activation function. The disaggregated NTN NGRAN is represented as a graph, with the nodes representing terrestrial gNB-CUs and satellite gNB-DUs, while the edges feature the connections between them. The key advantage of using GCNs for this task is their ability to effectively capture the local neighborhood information around each node and identify faulty edges based on the training data. More specifically, the training data consist of time-stamped NGRAN/transport KPIs collected from the deployed testbed, which are preprocessed and mapped into a KPI-attributed graph representation; representative traffic is generated, and controlled degradations/faults (e.g., delay/loss/bandwidth constraints) are introduced to obtain training/validation labels. The resulting measurements are modeled in NetworkX as a graph $G(V, E)$ with metrics stored as node/edge attributes, and then exported as adjacency and feature matrices for the GCN-based monitoring pipeline. The GCN output (fault localization and alternative

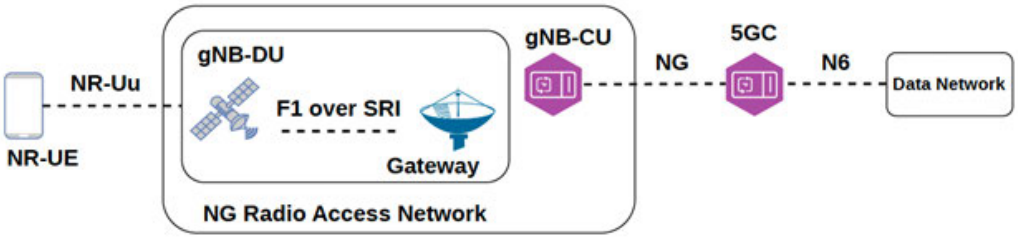

FIGURE 20. The end-to-end 5G NGRAN network model (courtesy of [107]).

routing/traffic-steering decision) can then be exploited by a software-defined orchestration layer to enforce adaptive rerouting and link monitoring.

An improvement of the approach mentioned above has been proposed in [107], where the GCN model has been used in a federated learning (FL) ML architecture, which has been supported by MEC. FL is a machine learning technique that enables algorithmic training on decentralized devices (servers) that store and process data without the need to exchange it. FL is opposed to conventional centralized learning techniques and to distributed learning with an identical distribution of data on the decentralized devices. As shown in [106], GCN utilizes graph-based learning for real-time fault detection and traffic optimization in dynamic NGRAN environments. FL enables decentralized, privacy-preserving model training while minimizing communication overhead, thus increasing the potential of GCN. On the other hand, edge-centric processing with MEC deploys local GCN models at MEC nodes, thus minimizing latency and enhancing real-time decision-making. As shown in Fig. 21, FL and MEC have been combined to improve the efficiency of disaggregated NGRAN monitoring. From a generalization standpoint, federated training across heterogeneous terrestrial/satellite MEC nodes aggregates diverse operating conditions without sharing raw data, improving robustness to topology changes and mobility dynamics. Consistent gains across training rounds under LEO mobility further indicate adaptation beyond a single static scenario.

Another essential task in NTN-based disaggregated NGRAN is the resource prediction. Cloud-native networking and disaggregated NGRAN enable the implementation of flexible, scalable, and resilient NTNs. However, the processing capabilities of satellite payloads are limited, as well as the bandwidth availability of front-haul links. This involves a significant problem of efficient network resource allocation. For this reason, proactive monitoring and network resource utilization prediction are crucial tasks to enhance efficiency and resilience. In [105], an ML-based solution for resource utilization prediction in NTN disaggregated NGRAN has been proposed, based on Long-Short Term Memory (LSTM) neural networks. LSTM is a type of recurrent neural network (RNN) aimed at mitigating the vanishing gradient problem commonly encountered by traditional RNNs [109]. It aims to provide a short-term memory for RNN that can

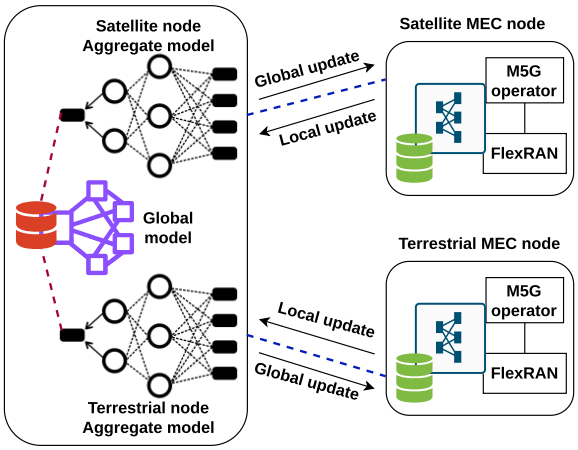

FIGURE 21. Combination of Federated Learning and MEC to improve the monitoring of disaggregated NGRAN in 5G NTNs (courtesy of [107]).

last thousands of timesteps (thus: "long short-term memory"). An LSTM unit is typically composed of a cell and three gates: an input gate, an output gate, and a forget gate. The cell remembers values over arbitrary time intervals, and the gates regulate the flow of information into and out of the cell. Selectively outputting relevant information from the current state allows the LSTM network to maintain useful, long-term dependencies to make predictions, both in current and future time-steps. Two different splits have been simulated in [105]: the first one corresponds to the baseline 3GPP NGRAN architecture of Fig. 18 (gNB-DU virtualized on the LEO satellite and gNB-CU executed on the terrestrial gateway), while the second one corresponds to the enhanced architecture with gNB-CUUP virtualized on the LEO satellite and gNB-CUCUP executed on the terrestrial gateway. With LSTM-driven utilization forecasts, a network operator can decide which disaggregated NGRAN network function is feasible to deploy on the satellite payload under limited onboard computing, while accounting for payload and fronthaul constraints. The LSTM-based resource consumption prediction model of [105] is shown in algorithm 1.

In the following section, accurate simulation results will provide a credible assessment of the considered MEC-based and AI-based network management policies.

Algorithm 1 LSTM for Resource Consumption Prediction

Input: Data (CPU, Mem), seq_length, epochs
for each epoch **do**
  Load data
  data.columns ← strip names
  data(Bandwidth) ← $\frac{data[CPU] \cdot data[Mem]}{10^6}$
  Initialize: MinMaxScaler
  scaled_data ← scaler.fit(data)
  x, y ← create_sequences(seq_length)
  x_train, x_test, y_train, y_test ← split(scaled_data, 0.2)
  Initialize: Sequential(LSTM, Dropout, Dense)
  Initialize Adam
  model.compile(loss='mse', optimizer=Adam)
  early_stopping, reduce_lr ← set callbacks
  model.fit(x_train, y_train, callbacks=[early_stopping, reduce_lr])
  test_loss, test_mae ← model.evaluate(x_test, y_test)
  Predictions ← model.predict(x_test)
  y_test_original ← inverse_transform(y_test)
end for
Output: Trained model with metrics (test_loss, test_mae) and reconstructed labels (y_test_original)

VIII. REVIEW AND DISCUSSION OF THE PROJECT RESULTS

During the INFINITE project activities, a wide series of results has been achieved and published concerning the various technologies under investigation. In this section, a representative subset of these results is presented and discussed, dealing with:

- Cell-free MIMO in integrated terrestrial and non-terrestrial scenarios (VIII.A).
- Performance assessment of advanced PHY-layer formats for NTNs, considering the Constant-Envelope Multicarrier case (VIII.B).
- Evaluation of the attainable throughput of PD-NOMA systems in NTN transmission applications (VIII.C).
- In-lab measurements concerning the Ka-band FE PoC (VIII.D).
- Comparison between terrestrial-based and Space-based edge computing architectures (VIII.E).
- AI-based Cloud-RAN monitoring in NTNs (VIII.F).

A. CELL-FREE MIMO IN T-NT SCENARIOS

In this subsection, the numerical results obtained from the cell-free architecture detailed in Section III are presented and commented on. Please notice that here we did not include the thorough and detailed analysis of the NTN cell-free MIMO environment due to the lack of space. The reader can refer to [39] for a more exhaustive investigation. For example, aspects on the mitigation of phase misalignments to preserve signal integrity between satellites and UTs are discussed in [110] and [111], and a suitable per-satellite synchronization scheme can be found in [112] exploiting space–time block coding. Regarding the performance of the macro-diversity schemes, we have considered a constellation similar to Starlink. The simulated scenario envisaged an observed fixed UT surrounded by 50 interfering UTs randomly placed within a radius of 670 km, each with an estimated positioning offset (therefore, the satellite delay and Doppler precompensation include a residual error). The offset distance $r_{p,q}$ from the exact UT position was set as a random point within a circle of radius 500 meters $\forall p, q$. Concerning the waveform, the carrier frequency was set to $f = 20$ GHz (Ka-band), the subcarrier spacing to $\Delta f = 120$ kHz, the symbol time to $T = 8.33\mu$s, with $M = 32$ and $N = 16$. The power spectral density of the noise was $N_0 = -174$ dBm/Hz, and the noise figure at the receiver was $F = 5$ dB. We assumed $N_{S,X} = N_{S,Y} = 16$, i.e., $N_S = 256$, $\Gamma_{SAT} = 23$ dB at the satellites, and $N_{UT,X} = N_{UT,Y} = 4$, i.e., $N_{UT} = 16$, $\Gamma_{UT} = 10$ dB at the UTs. We assume that all the satellites have the same power budget, i.e., $P_{p,SAT} = P_{SAT}$, $\forall p = 1, \ldots, P$. The propagation channel is modeled following the two-state semi-Markov model described in ITU-R Recommendation P.681-11 [113], with particular reference to the parameters for the highway environment.

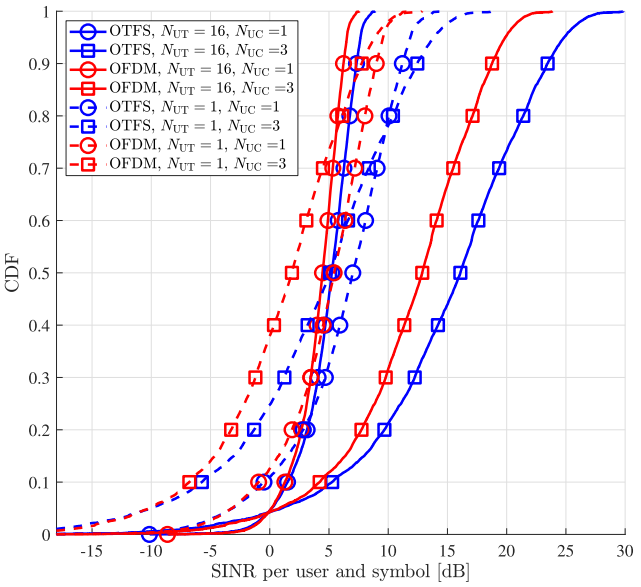

FIGURE 22. CDF of the SINR per user and symbol for OFDM and OTFS for different values of N_{UC} ans N_{UT}, ZF beamforming and combining, $P_{SAT} = 15$ dBW, and $N_{UT,MAX} = 10$.

We report in Fig. 22 the cumulative distribution functions (CDFs) of the SINR per user and symbol defined in Section III-A in the case of single-antenna and multiple antennas UTs, assuming ZF beamforming (and combining) and different values of N_{UC} for both OTFS and OFDM. We can observe that with single-antenna UTs and no phase compensation, we cannot exploit the macro-diversity benefits since the different contributions from the serving satellites destructively combine, resulting in a reduced power of the useful signal compared with the baseline ($N_{UC} = 1$). In the

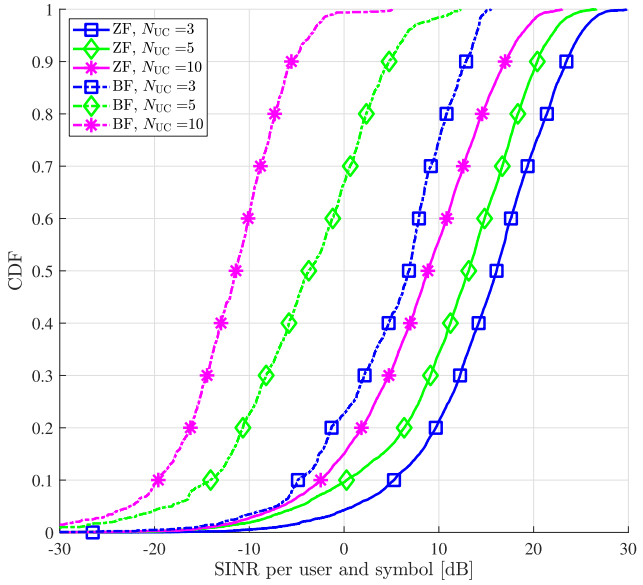

FIGURE 23. CDF of the SINR per user and symbol for OTFS for different beamforming and combining strategies, P_{SAT} = 15 dBW, N_{UT} = 16, and $N_{UT,MAX}$ = 10.

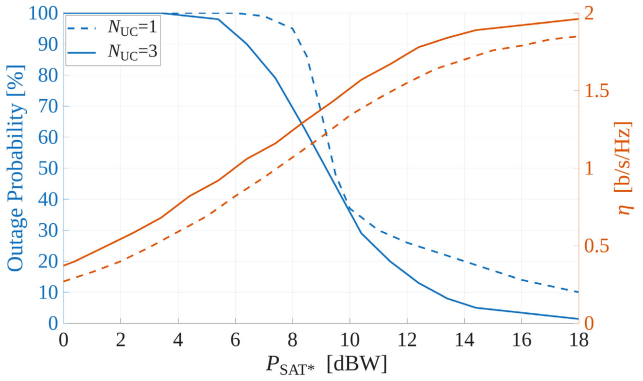

FIGURE 24. OTFS outage probability (left) and pragmatic capacity (right) as a function of the normalized transmitted power, comparison for two respective cases: a) N_{UC} = 1, $N_{UT,MAX}$ = 1 b) N_{UC} = 3, $N_{UT,MAX}$ = 5.

case of multiple antennas UTs, the use of zero-forcing can isolate the contributions from different satellites and thus, thanks to the spatial filtering, we are able to exploit the benefits of the macro-diversity for the vast majority of the UTs. This behavior was also observed in [37] and [39].

In Fig. 23, we again report the CDFs of the SINR per user and symbol, focusing now only on the case of OTFS, $N_{UC} = 3$, and $N_{UT} = 16$ (the best performance configuration, according to Fig. 22) showing the impact of the beamforming and combining techniques used at the satellites and UTs. In particular, by inspecting the figure, we can observe that, as expected, the best performance is obtained in the case of ZF approaches aimed at nulling the interference in the directions corresponding to the approximate position of the interfering UTs and satellites with respect to the simple beam-focus (BF) aimed at pointing a beam in the approximate positions of UTs and satellites. Fig. 24 presents a comparison in terms of pragmatic capacity and outage probability between two cases: i) each UT is served by only one satellite and each satellite serves only one UT (briefly reported in the legend as $N_{UC} = 1$) and, ii) $N_{UC} = 3$ and $N_{UT,MAX} = 5$ (briefly reported in the legend as $N_{UC} = 3$). In this last case, the results are reported versus the normalized transmitted power P_{SAT*}, computed from P_{SAT} by considering a constant penalty equal to the ratio of the average number of the respective employed satellites. This ratio, in the case of $N_{UC} = 3$, yields a value slightly higher than zero, since usually a few more satellites are used if the same UT is served by multiple satellites. For the scenario at hand, this power penalty was found to be 0.4 dB.[2] Therefore, it is evident that notable enhancements can be achieved in both pragmatic capacity and particularly in outage probability, as values as low as approximately 10% can be assured while saving power by roughly 5 dBW.

Regarding the performance of the OTFS detector detailed in Section III-B, in Figure 25, we compare the performance of the low-complexity IC$_G$ detector with the MMSE benchmark employing both the OFDM and the OTFS modulation formats. We assumed QPSK modulation for the information symbols and considered $N_{UC} = 1, 3$ satellites in visibility with the UT. Results are again provided in terms of pragmatic capacity, considering the same scenario previously described.

For the OFDM modulation, we considered an overhead of 6.4% due to the cyclic prefix (CP) and 7% due to pilot symbols. By contrast, OTFS achieves a significant reduction in CP overhead (down to 0.43%), since only one CP is required for each $N \times M$ symbol block. Finally, for the latter modulation format, the use of pilot symbols results in an overhead of 5%, according to the embedded pilot scheme of [114].

Figure 25 highlights the impact of satellite macro-diversity on performance. As shown in recent works [43], [60], transmission from multiple satellites (three in this case) improves link robustness. Furthermore, adopting OTFS modulation provides a substantial performance gain compared to OFDM, which not only suffers from higher sensitivity to Doppler effects induced by high mobility but is also heavily penalized by its non-negligible, yet essential, overhead. In addition, focusing on the two detection strategies under analysis, Figure 25 shows that the different receivers yield practically identical results for both modulation schemes. This outcome highlights the potential of the IC$_G$ detector, which drastically reduces the complexity of MMSE [44] without any loss in performance. The effectiveness of this approach is supported by the Ungerboeck observation model, which, by enforcing the compactness of the channel matrix, enables a simple interference-cancellation method to achieve satisfactory results.

[2]Therefore, basically $P_{SAT*} = P_{SAT} + 0.4$ dB in the case $N_{UC} = 3$ and $P_{SAT*} = P_{SAT}$ in the case $N_{UC} = 1$.

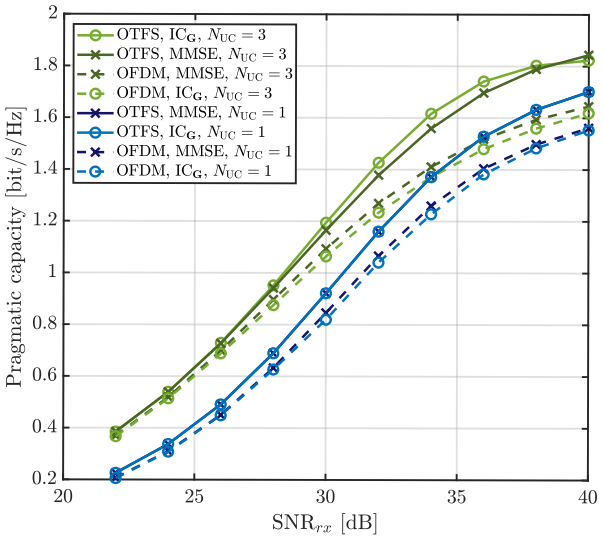

FIGURE 25. Performance comparison among OTFS and OFDM modulations in terms of pragmatic capacity.

TABLE 3. Selected parameters [88], [90].

ϱ_c	1/2	α	37 dB
ϱ_m	4	μ_1	2
P_T	100 mW	μ_2	1
G_T	10 dB	N_0	-160 dBm

B. THE CASE STUDY OF CE-MC WAVEFORMS FOR 6G NTNs: QUANTITATIVE (AND COMPARATIVE) PERFORMANCE EVALUATION

With reference to the considered case study of advanced PHY-layer design for 6G NTNs, intensive simulation trials have been performed to compare the performance of CE-multicarrier waveforms (CE-OFDM and CE-SC-OFDM) with that of conventional multicarrier ones (OFDM and DFT-s-OFDM) in a technically meaningful NTN transmission scenario. The related simulation results, expressed in terms of BER, have been fully reported and discussed in [66]. The following illustrates a representative sample of such results. The simulation scenario involves a downlink Ka-band LEO satellite transmission, where the user terminals are located in different dense urban sites, each characterized by different propagation conditions. For this reason, two different Ka-band NTN multipath channel models have been simulated: one of NLOS typology, namely, the 3GPP TDL-B model, and one of LOS typology, namely, the 3GPP TDL-D model [115]. The entire TX/RX chain simulator has been implemented in MATLAB^{TM} 2024 version. The comparative performance evaluation has been performed in two steps, following the same assessment strategy of [66]: a first step consists of the comparison of CE-MC and conventional MC waveforms in the presence of multipath propagation and AWGN only, focusing our attention on the multipath resilience and the influence of parameterization on CE-OFDM and CE-SC-OFDM behavior. The second step completes the simulation scenario with some significant hardware impairments typical of NTN links, namely, nonlinear amplification and phase noise. The analysis of spectral efficiency and computational complexity will conclude this subsection.

1) PARAMETRIC PERFORMANCE ASSESSMENT OF THE MULTIPATH RESILIENCE

The results concerning the first assessment step are shown in Fig. 26(a) and Fig. 26(b) for CE-OFDM and CE-SC-OFDM, respectively, in the NLOS propagation scenario. The corresponding results for the LOS scenario are shown in Fig. 27(a) for CE-OFDM and in Fig. 27(b) for CE-SC-OFDM. 4-QAM modulation has been considered in all the simulation trials. $M = 2047$ useful subcarriers (2048 for OFDM and DFT-s-OFDM) are used to transmit symbols, and the subcarrier spacing has been fixed to $15KHz$. According to [57], the numerical values chosen for the CE-MC oversampling factor are $F_{ov} = 4$ (black solid lines) and $F_{ov} = 8$ (red dashed lines), while a range of significant values of the modulation index has been tested for each F_{ov} and highlighted by a different choice of the markers. Finally, the spreading factor L_1 of DFT-s-OFDM has been set to 8.

In all the considered scenarios, the increase of F_{ov} does not look beneficial to improve BER performance. On the other hand, the increase in the modulation index is more beneficial, but it should not be arbitrary. This is a direct consequence of the nonlinear detection based on the arctangent function and the phase unwrapping. Apparently, the best parametric configuration is $F_{ov} = 4$, $2\pi h = 0.7$, for CE-OFDM, and $F_{ov} = 4$, $2\pi h = 0.5$, for CE-SC-OFDM, both in the NLOS and LOS cases. The increase in the modulation index above 0.7 rad degrades BER performance, resulting in a saturating trend due to residual unsolved phase ambiguities. It should be noticed that CE-SC-OFDM, thanks to the DFT precoding, can support modulation indexes higher than 1.0 rad without incurring in BER saturation, but the performance does not improve and even degrades. If the best parameterization is chosen, the comparison between CE-OFDM and CE-SC-OFDM is in favor of CE-SC-OFDM for high $\frac{E_b}{N_0}$ values. On the other hand, CE-OFDM generally outperforms its DFT-precoded version for low $\frac{E_b}{N_0}$. Regarding the comparison with conventional multicarrier waveforms (green dash-dotted curves), we can observe that, if the parameterization is appropriately set, both CE-OFDM and CE-SC-OFDM dramatically outperform OFDM at high signal-to-noise ratios thanks to the anti-multipath diversity offered by the constant-envelope multicarrier waveforms. A right choice of oversampling factor and modulation index also yields CE-MC to outperform DFT-s-OFDM, even though the improvement is less dramatic than in the previous case. Indeed, DFT-s-OFDM is substantially a cyclic-prefixed single-carrier waveform supported by FDE, thus capable of providing diversity against multipath propagation. It should be highlighted that OFDM and DFT-s-OFDM work better than CE-MC counterparts at low SNRs. This last is a consequence of the threshold effect, which

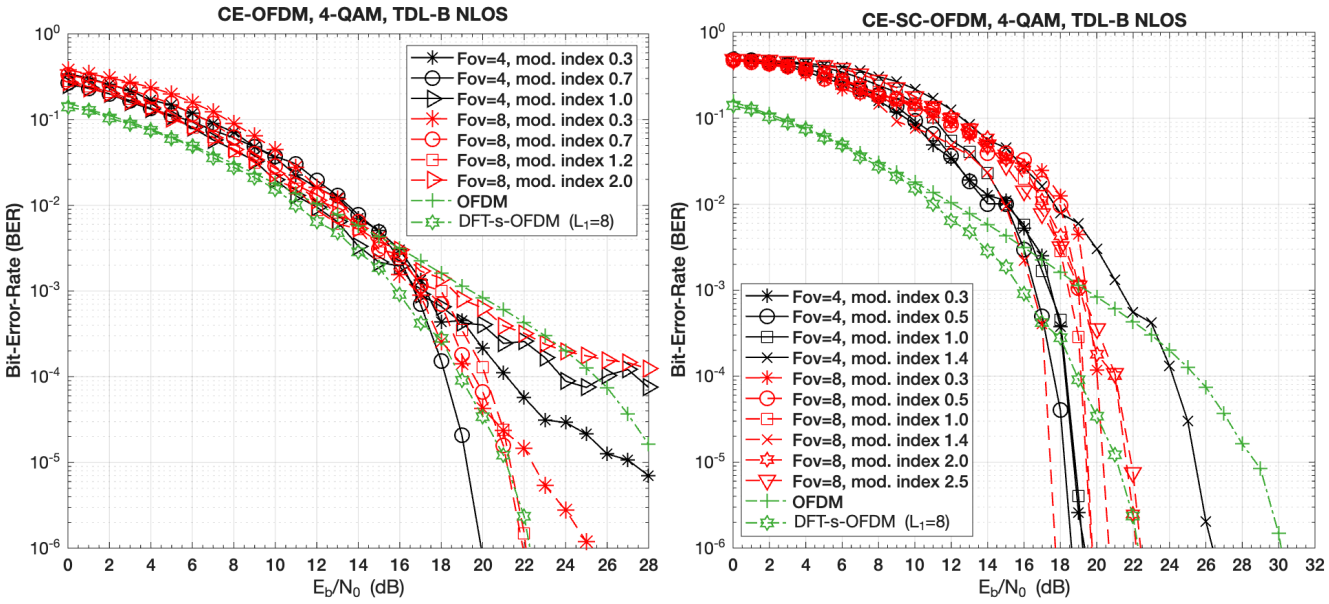

(a) (b)

FIGURE 26. BER performance achieved by CE-OFDM (a) and CE-SC-OFDM (b) compared to that achieved by conventional multicarrier waveforms (OFDM and DFT-s-OFDM) in the presence of AWGN and NLOS multipath propagation.

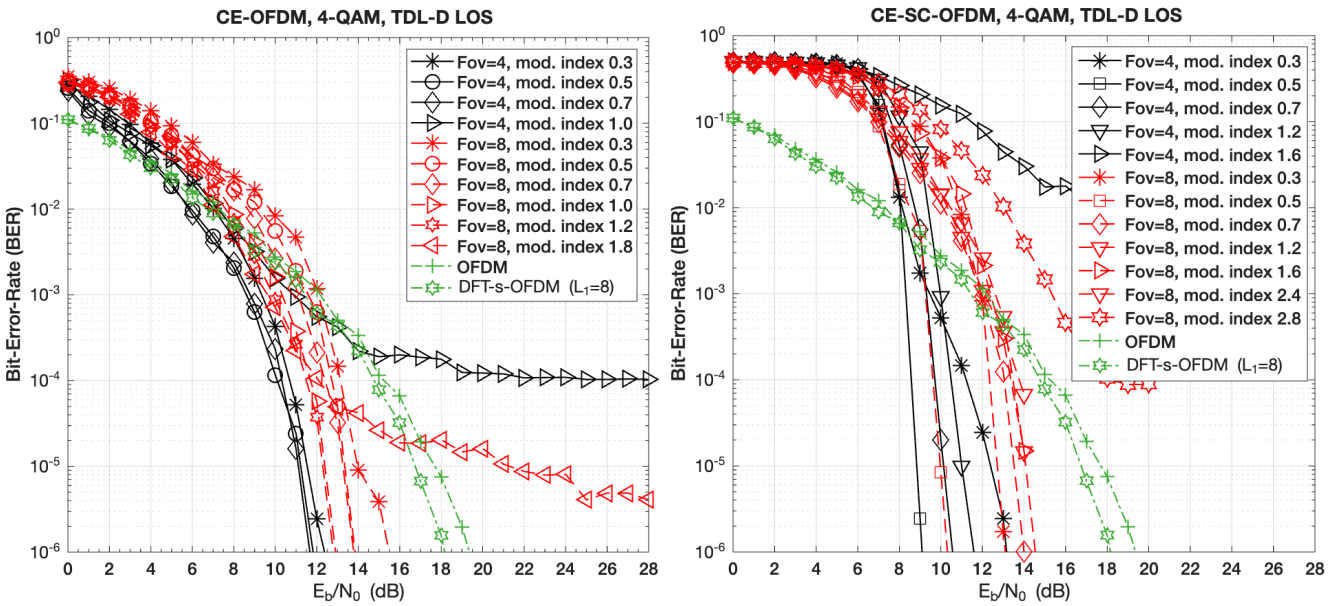

(a) (b)

FIGURE 27. BER performance achieved by CE-OFDM (a) and CE-SC-OFDM (b) compared to that achieved by conventional multicarrier waveforms (OFDM and DFT-s-OFDM) in the presence of AWGN and LOS multipath propagation.

increases the impact of background noise on link performance.

2) BER PERFORMANCE IN A REALISTIC NTN DOWNLINK TRANSMISSION SCENARIO

To complete the picture of the comparative link performance assessment, we are going to show and discuss in the following the outcomes of a second series of simulation trials, which, in addition to multipath propagation, considers the presence in the downlink scenario of nonlinear amplification and phase noise. A nonlinear amplifier has been introduced into the transmission chain by simulating the AM/AM characteristic of the Gallium-Nitride (GaN) Doherty power amplifier for Ka-band satellites described in [116]. Such a component features an output power of $35dBm$. As pointed out in [116], $10dB$ of IBO is required by such a component to resort to the linear amplification zone, with a corresponding OBO equal to $5dB$. Non-ideal RF carrier generation has also been considered by simulating the phase noise mask of the Ka-band local oscillator for high-throughput satellites presented

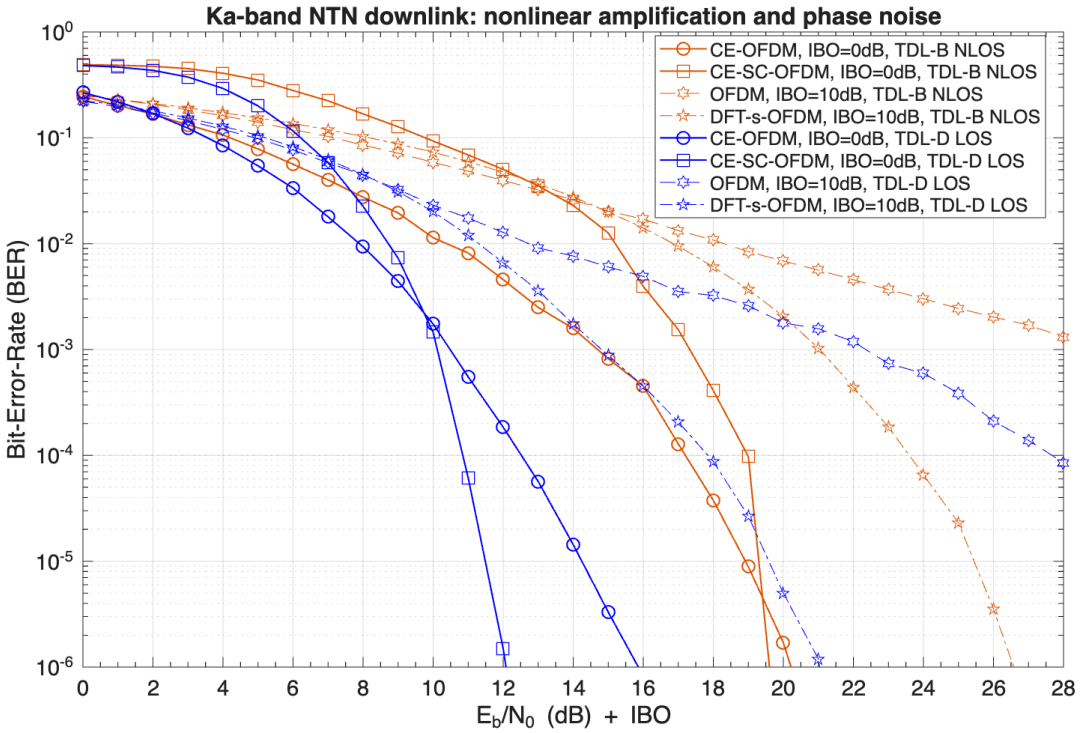

FIGURE 28. BER performance results achieved by conventional multicarrier modulations (OFDM, DFT-s-OFDM) and by constant-envelope (CE) multicarrier waveforms (CE-OFDM and CE-SC-OFDM) in a realistic Ka-band downlink satellite scenario where transmission is performed in a dense urban environment in the presence of multipath propagation, nonlinear distortion, and phase noise. The best parameterization of CE-MC waveforms has been set based on the plots of Figs. 26 and 27 for the NLOS and LOS scenarios respectively.

in [117]. The best values of oversampling factor and radian modulation index have been chosen for CE-OFDM and CE-SC-OFDM according to the outcomes of the previous series of simulation trials, namely: $F_{ov} = 4$ and $2\pi h = 0.7$ for CE-OFDM and $F_{ov} = 4$ and $2\pi h = 0.5$ for CE-SC-OFDM. The parameter L_1 of DFT-s-OFDM has been left equal to 8.

The related curves plotting the BER vs. $\frac{E_b}{N_0} + IBO$ are shown in Fig. 28. Regarding CE-MC waveforms (orange solid lines - NLOS case, blue solid lines - LOS case), we can observe a significant performance improvement as compared to the conventional MC counterparts, both in the NLOS and LOS scenarios. Such an improvement is mainly due to the capability of these advanced waveforms to exploit the amplifier at saturation without any need for IBO. Such a capability works in synergy with the increased diversity exhibited by these waveforms in multipath propagation scenarios. We can observe from Fig. 28 that CE-OFDM is overall preferable to CE-SC-OFDM in the NLOS case (a performance improvement is attained by CE-SC-OFDM only for $\frac{E_b}{N_0} > 20dB$), while CE-SC-OFDM looks better in the LOS case, at least for $\frac{E_b}{N_0} > 10dB$. On the other hand, traditional multicarrier waveforms (orange dashed lines - NLOS case, blue dashed lines - LOS case) are primarily impaired by the need to introduce a large IBO to the transmitted RF power to limit the impact of nonlinear distortion. The resulting OBO shifts to the right the related BER characteristics. As a consequence, the performance advantage shown at low SNRs by conventional MC waveforms in the case of linear amplification becomes much less significant when a nonlinear power amplifier is used. OFDM is jointly impaired by the intrinsic lack of diversity and the impact of phase noise, which introduces a saturating trend of BER curves due to inter-channel interference. DFT-s-OFDM appears more competitive as it exploits increased diversity gain and resilience to phase noise; however, it performs worse than CE-MC waveforms in the real downlink scenario, mainly due to the large IBO required.

3) COMPARISON IN TERMS OF SPECTRAL EFFICIENCY AND COMPUTATIONAL COMPLEXITY

The bandwidth occupied by the main lobe of the transmitted CE-MC signals is, in all the considered cases, estimated as 61.41 MHz, corresponding to a spectral efficiency of 1 b/s/Hz. The bandwidth occupied by conventional MC waveforms is half this value, namely: 30.72 MHz, with a correspondingly doubled spectral efficiency. As already mentioned in Section IV-D, the increased bandwidth occupation is the price to be paid to achieve the performance improvement attained by CE-MC waveforms.

Regarding computational complexity, CE-MC waveforms are more demanding than their conventional MC counterparts. The computational complexity of the CE-OFDM transmitter can be estimated as: $\mathcal{O}\left(N_{IFFT} \times log_2\left(N_{IFFT}\right)\right)$, which is F_{ov} times that of OFDM. At the receiver side, the FDE applied to the single-carrier signal increases the number of required elementary operations up to $F_{ov} \times M$ as compared

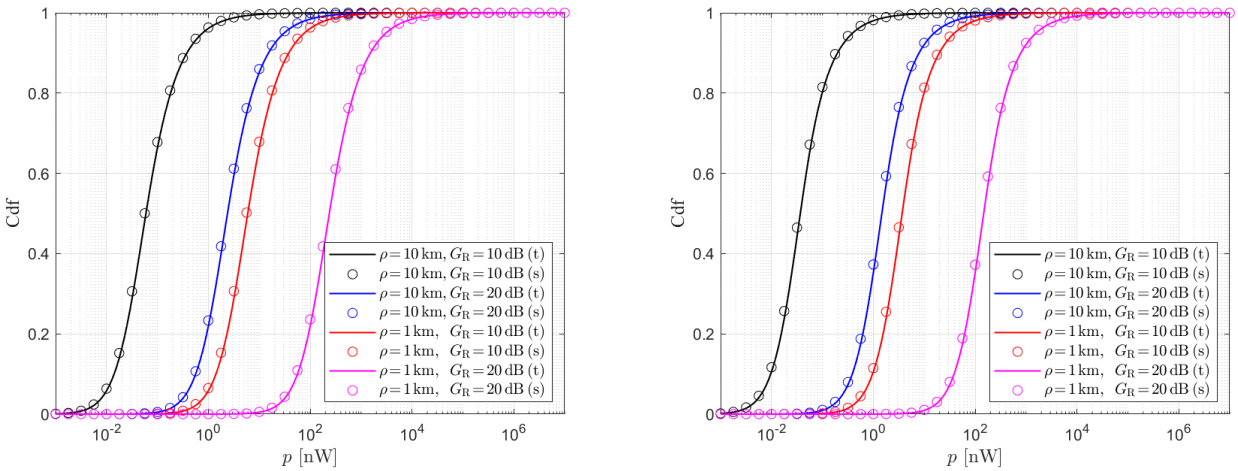

FIGURE 29. CDF of the power received by the destination from the single moving vehicle in air (a) and space (b) scenarios (t: theory, s: simulation).

to that required by the corresponding OFDM receiver. As compared to CE-OFDM, CE-SC-OFDM requires an additional computational burden involved by the DFT precoding (and decoding) at the TX/RX sides, whose order is quantified in $\mathcal{O}\left(M \log_2 (M)\right)$. The comparison of the computational load required by CE-MC waveforms and DFT-s-OFDM is substantially quantified by the ratio between F_{ov} and L_1. If the two values are comparable, the complexity of the generation and detection of the two typologies of waveforms becomes comparable as well.

4) WRAPPING UP

CE-MC waveforms have shown some favorable features that make them valuable candidates to support future NTN transmission applications (nonlinear distortion immunity and multipath resilience). The conceived SDR-based modular PHY-layer implementation makes the generation of CE-OFDM and CE-SC-OFDM easily derivable from the basic OFDM one. Moreover, the software-defined implementation of CE-MC receivers looks viable and does not incur the necessity of a problematic hardware implementation of nonlinear functions like arctangent and phase unwrapping. On the other hand, the tradeoff concerning increased bandwidth occupation and higher computational complexity should be conveniently appraised.

C. PD-NOMA THROUGHPUT

This subsection discusses the results derived from the semi-analytical model illustrated in Section V for the estimation of the PD-NOMA throughput in an NT distributed network. The model is implemented in MATLAB by assuming propagation channels complying with the recent proposals and measurement campaigns realized for aerial and space scenarios [88], [90]. The considered parameter values are listed in Table 3.

Fig. 29 reports the CDF of the power received by a centered destination from a single UAV in an aerial scenario (Fig. 29(a)) and from a single satellite in a space scenario (Fig. 29(b)), by considering different values of the radius topology ρ and of the receiving antenna gain G_{R}. Besides the theoretical curves, identified by lines and obtained by (17) for the air context and by (19) for the space one, the figure also shows the simulations, identified by markers and used to validate the analysis. Each simulated curve is derived by randomly generating $\Pi = 10^5$ realizations, whose overall running has required some seconds. The analytical evaluation has instead required just a few milliseconds. From a conceptual point of view, the obtained results confirm the significant impact of the antenna system capabilities and of the size of the region covered by the moving vehicles on the received power levels, even in the presence of random channel fluctuations (small-scale fading in the air case and ionospheric scintillation in the space case).

Fig. 30 shows the semi-analytical PD-NOMA throughput as a function of the offered load for $\rho = 10$ km and different receiving antenna gains. The curves are calculated considering, as reception criteria, the Shannon-based one (Fig. 30(a)) and the QPSK-based one (Fig. 30(b)), in which the i.i.d. received powers are generated according to (17) for the air scenario and according to (19) for the space scenario. These results reveal that a moderate performance degradation occurs when the ideal Shannon limit is replaced by a realistic code-modulation pair, even if the main impact on the achievable throughput is still due to the receiving antenna gain. The slight difference between the Shannon and QPSK cases may be explained by recalling the selected modulation order and code rate (Table 3), which leads to a selected rate equal to unity.

To investigate a more practical and hence nonideal scenario, Fig. 31 shows the semi-analytical PD-NOMA throughput as a function of the offered load for a QPSK modulation when $\rho = 10$ km, $G_{\mathrm{R}} = 20$ dB, and different interference residuals γ_{r} due to imperfect IC are present. This set of curves,

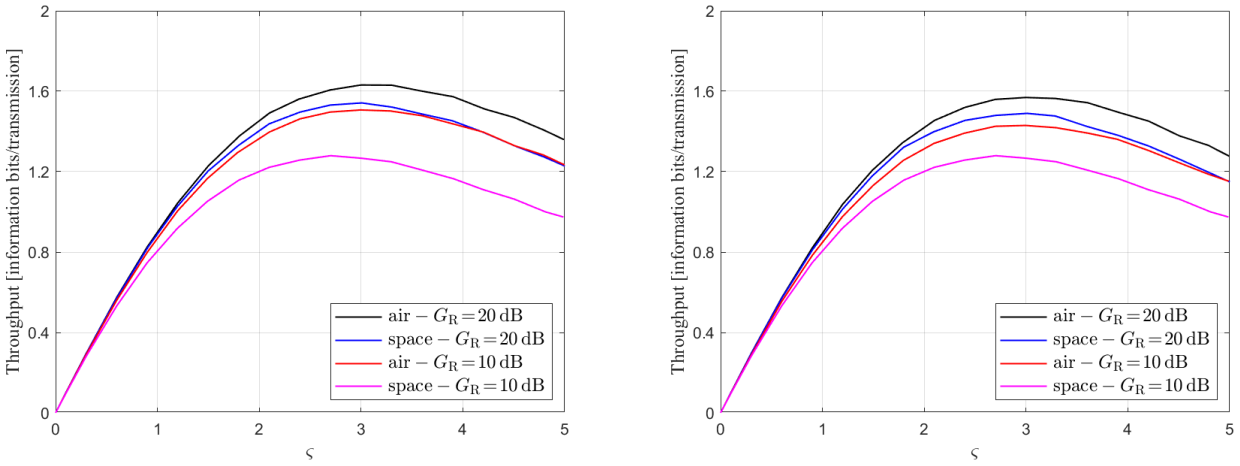

FIGURE 30. Semi-analytical PD-NOMA throughput as a function of the offered load: (a) Shannon-based, (b) QPSK with efficient code.

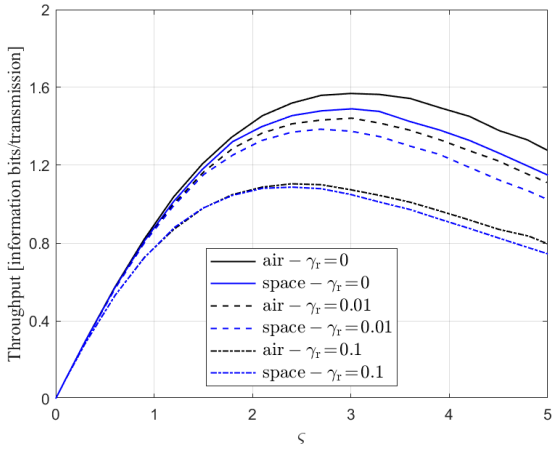

FIGURE 31. Semi-analytical PD-NOMA throughput as a function of the offered load using QPSK modulation under imperfect IC.

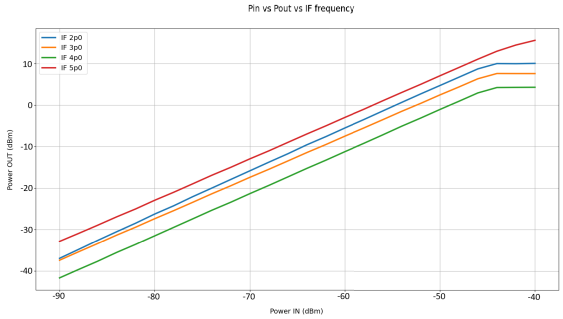

FIGURE 32. Measured RX input-output characteristics for different IF configurations.

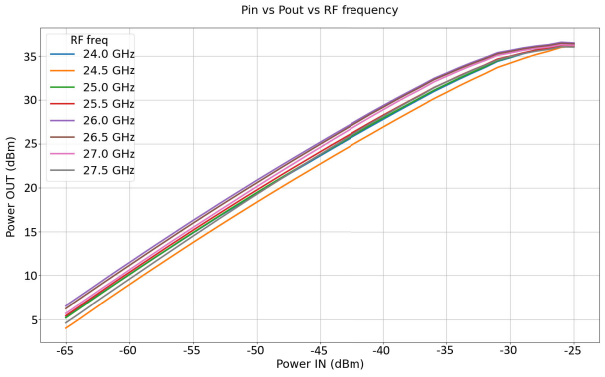

FIGURE 33. Measured TX input-output characteristics for different RF configurations (PA enabled).

which provides a quantitative estimation of the degradation suffered by a realistic air/space IC-based system, reveals that even receivers characterized by poor IC capabilities, i.e., with a 10% of residual interference, are able to provide acceptable throughput values in both non-terrestrial domains. This behavior confirms that, besides its conceptual simplicity, the PD-NOMA approach might also guarantee a certain robustness against cheap IC implementations and/or harsh propagation environments straining the system components.

D. MEASUREMENT RESULTS ON THE KA-BAND PoC FE

A measurement campaign has been carried out to validate the PoC FE and to extract the key RF parameters needed for system-level performance assessment under realistic hardware impairments. The transmitter/receiver chain has been tested across different IF operating points (see Fig. 32), showing no relevant performance degradation and reaching output power levels above 37 dBm with the PA enabled, as shown in Fig. 33. Phase noise has been measured at multiple RF output frequencies and IF configurations. The corresponding phase noise mask measured at TX is shown in Fig. 34. Finally, modulated-signal tests confirmed the feasibility of transmitting high-order modulations: a 32APSK signal (generated at IF with 120 MHz bandwidth) was transmitted at 37 dBm with EVM below 4%, as confirmed by the screenshots of Fig. 35.

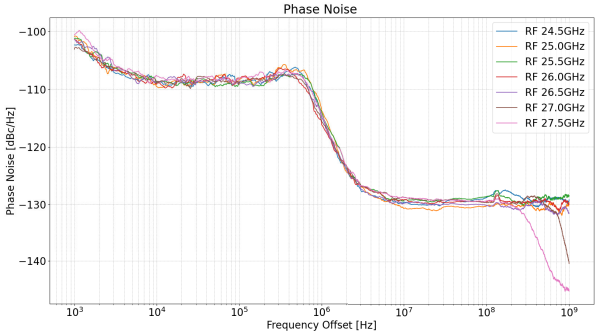

FIGURE 34. Measured TX phase noise across representative RF output frequencies.

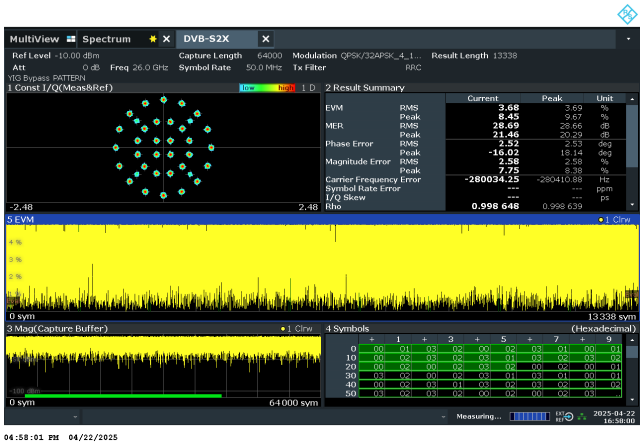

FIGURE 35. EVM measurements with 32APSK modulated signals for TX validation.

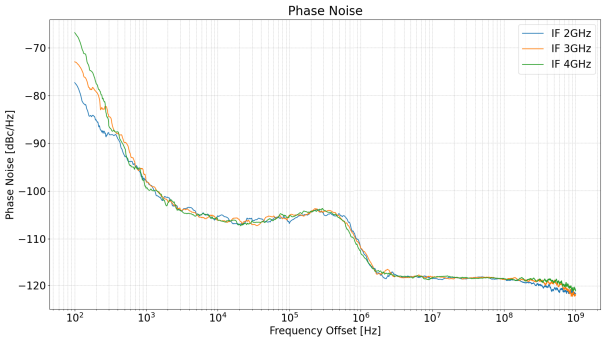

FIGURE 36. Measured RX phase noise across representative IF frequencies.

On the receiver chain, gain/linearity has been characterized via input-output measurements at representative RF frequencies. Phase noise has also been validated across different IF frequencies, and the related mask is shown in Fig. 36. The receive path was also validated with a 32APSK modulated signal at 26 GHz, which has been downconverted to 3 GHz IF, achieving EVM below 3% (see Fig.37).

Finally, in Table 4, a summary of measured PoC FE results is reported.

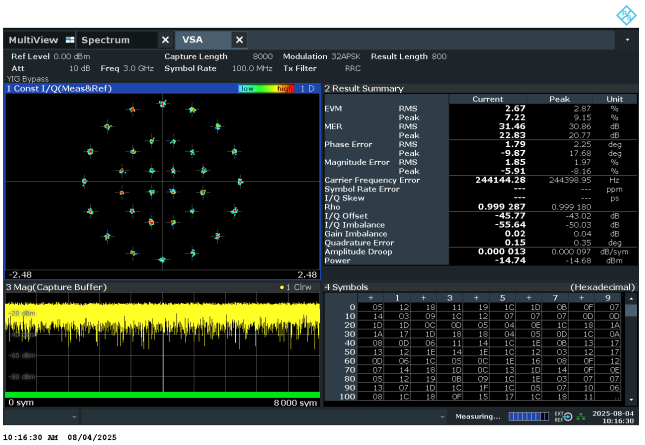

FIGURE 37. EVM measurements with 32APSK modulated signals for RX validation.

TABLE 4. Summary of measured PoC FE key results (representative configurations).

Metric	Measured value
TX output power (PA enabled)	> 37 dBm
TX EVM (32APSK, 120 MHz BW)	$< 4\%$
RX EVM (32APSK @ 26 GHz, IF=3 GHz)	$< 3\%$
TX spurious emissions (normalized)	< -40 dBc
Peak PoC power consumption	< 35 W

E. TERRESTRIAL VS. SPACE CLOUD ANALYSIS

This subsection presents the performance evaluation of terrestrial and space-based edge computing architectures by measuring the network latency of task requests from globally distributed user devices. We use the single terrestrial architecture as the baseline to compare it against three space clouds, using LEO satellites as MEC nodes. To highlight latency variations based on user location, results are grouped according to the geodesic distance between each user and the ground gateway.

Figure 38 shows the average latency $\overline{\lambda}_j$ as a function of the geodesic distance from each user to the ground gateway. As expected, latency for the terrestrial cloud increases with distance, due to longer propagation paths and additional inter-satellite hops. In contrast, the latency of space cloud configurations remains relatively stable, since data is processed in orbit and does not rely on terrestrial offloading. For users within 2000 km of the gateway, terrestrial cloud exhibits lower latency than space cloud alternatives. However, beyond 5000 km, all space cloud configurations outperform the terrestrial cloud. In the intermediate region (between 2000 km and 5000 km), the best-performing architecture varies depending on user location and the specific space cloud configuration.

On the other hand, to better compare architectural performance, we compute the relative latency gain of each space configuration compared to the terrestrial cloud:

$$\Delta\overline{\lambda}_j = \overline{\lambda}_j^{G} - \overline{\lambda}_j^{Si} \tag{27}$$

where $\overline{\lambda}_j^{G}$ is the average latency of the terrestrial cloud and $\overline{\lambda}_j^{Si}$ corresponds to one of the space cloud variants. Figure 39

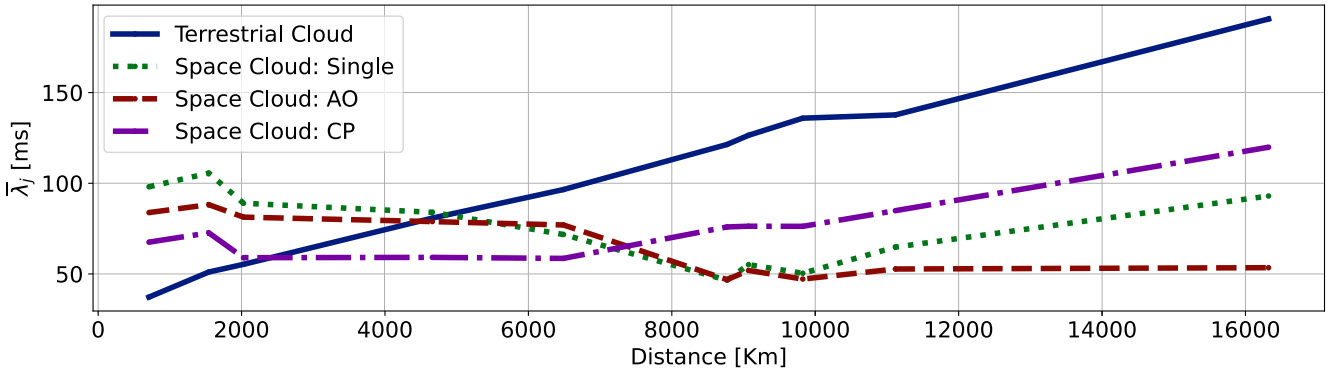

FIGURE 38. Mean network latency for terrestrial and space cloud architectures. The x-axis is the geodesic distance between the user and the gateway.

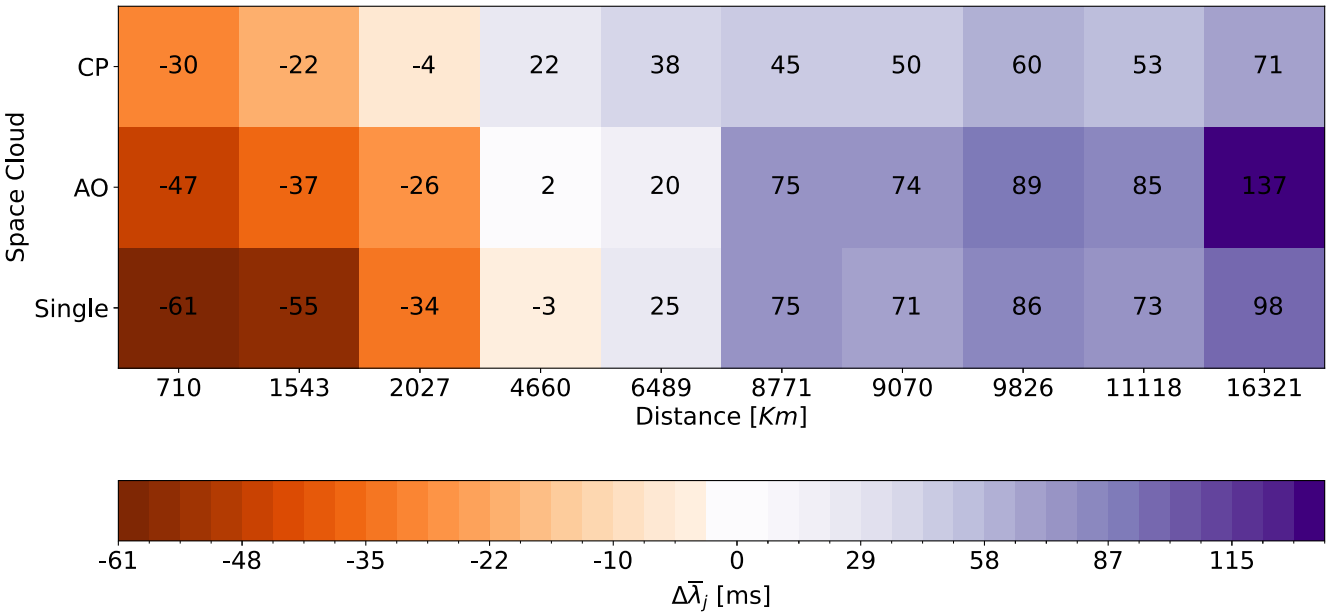

FIGURE 39. Latency difference between space and terrestrial clouds. Purple indicates that the space cloud outperforms the terrestrial architecture; orange indicates the opposite. The x-axis reflects the user-to-gateway geodesic distance.

shows $\Delta\overline{\lambda}_j$ for each user. Positive values (in purple) indicate a performance advantage for the space cloud; negative values (in orange) indicate that the terrestrial cloud is faster. Results confirm the existence of a transitional distance window, between 2000 km and 5000 km, where space cloud configurations yield latency improvements of up to 100 ms, depending on the user and configuration.

From the above-discussed results, it is noticeable that among the three space cloud configurations, no single distribution consistently achieves the lowest latency across all user locations. The Space Cloud CP configuration performs at best for users *u1*, *u2*, and *u3*, who are geographically closer to the gateway. The AO configuration outperforms the others for farther users. Interestingly, for users such as u4 and u5, the latency differences between the Single and multi-server space clouds are relatively small. This observation suggests that optimal server placement and replication depend heavily on user distribution and topology. In some cases, a single orbital edge server can offer comparable performance to more complex and distributed architectures. These findings emphasize the importance of adaptive, context-aware MEC orchestration in non-terrestrial networks.

F. ML-BASED NTN DISAGGREGATED NGRAN MONITORING

This subsection presents some results obtained using machine learning (ML) models to monitor and orchestrate 6G NTN disaggregated NGRAN environments using open-source network emulators. NTN networks with LEO satellite constellations extend terrestrial 6G networks by providing wide-area coverage and improved service continuity in remote regions. However, NTN integration introduces challenges stemming from long delays, Doppler shifts, intermittent connectivity, and rapidly changing network topologies. ML-based monitoring offers a promising approach to address these challenges by enabling predictive, topology-aware intelligence

across the satellite-terrestrial continuum. In our workflow, the KPIs used for training and evaluation are collected from a cloud-native disaggregated NGRAN testbed (containerized gNB-CU/gNB-DU functions) and then preprocessed to build the graph and time-series inputs used by the GNN and LSTM models for monitoring and orchestration.

In the ML-driven NTN disaggregated-RAN architecture, NGRAN functions are disaggregated between terrestrial cloud locations hosting gNB-CU units and satellite payloads hosting gNB-DU units. These components communicate via F1-over-Satellite Radio Interface (F1-over-SRI) links as shown in Fig. 19. One of the proposed monitoring frameworks leverages graph neural networks (GNNs) to represent disaggregated NGRAN components as graph-structured data. Nodes correspond to VNFs (e.g., gNB-CU, gNB-DU) deployed in Kubernetes-based testbeds, while edges represent F1-over-SRI and *Xn* connectivity. Node features include CPU, memory utilization, and signal strength, whereas edge features capture latency, packet loss, bandwidth, and jitter. Graph convolution layers propagate node and edge information across the topology to infer failures and routing bottlenecks. To obtain training/validation labels, we generate representative traffic and inject controlled degradations (e.g., delay/loss/bandwidth constraints); the collected KPIs are then modeled as a KPI-attributed graph (e.g., using NetworkX with node/edge attributes) and exported into adjacency and feature matrices consumed by the GCN/FedGNN pipeline. The GNN output (fault localization and alternative routing/traffic-steering decision) is exposed as an actionable intent to the orchestration plane, which can enforce rerouting and QoS-aware traffic steering across the satellite-terrestrial network.

A federated GNN (FedGNN) framework extends this capability by distributing local GCN models across terrestrial and satellite MEC nodes. Each local model observes local KPIs and shares only its learned parameters with a central aggregator, which updates a global GCN model and broadcasts the updated model back to the edge. This approach preserves data privacy, reduces backhaul load, and improves scalability in NTN systems. Fig. 40 illustrates the overall federated architecture. Beyond privacy assurance and overhead reduction, federated training across heterogeneous terrestrial/satellite MEC nodes improves generalization by aggregating diverse operating conditions (traffic patterns, link intermittency, and mobility-induced topology changes) without sharing raw data. Figure 41 shows the impact of FedGNN training on traffic routing across the satellite-terrestrial network. The average hop count decreases from 5 to 4.1 over the training rounds, while E2E latency improves from 30 ms to 20 ms. These improvements indicate that the GNN models progressively learn more efficient end-to-end paths across dynamic NTN topologies, consistent with proactive AI/ML frameworks that couple prediction with dynamic routing under varying network conditions [118]. This trend over training rounds is also an empirical indicator of adaptation beyond a single static snapshot, since the learned policy

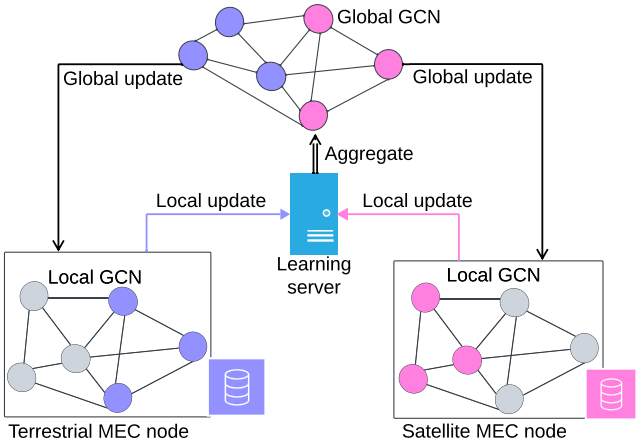

FIGURE 40. Federated GCN-based monitoring architecture with local GCNs at terrestrial and satellite MEC nodes, coordinated by a central learning server (courtesy of [107]).

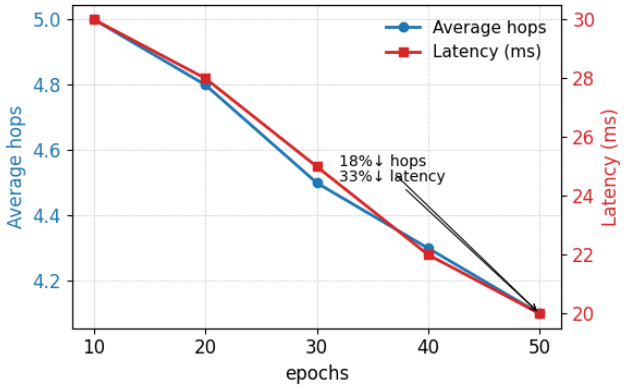

FIGURE 41. FedGNN-based traffic routing optimization and latency over training rounds.

improves as it is exposed to evolving topology and KPI distributions. Building on routing efficiency, the framework's resilience to LEO satellite mobility is evaluated in Fig. 42. Under fluctuating link quality and frequent handovers, the FedGNN model maintains robust performance; indeed, latency decreases from 40 ms to 25 ms, packet loss falls from 4% to 3%, and throughput steadily increases despite mobility-induced disruptions. These results demonstrate the model's adaptability to dynamic NTN conditions and its ability to sustain QoS across varying satellite trajectories. Importantly, these results reflect NTN-tailored adaptations (mobility-aware KPI graphs, intermittent F1-over-SRI/Xn connectivity, and MEC-assisted federated updates) rather than a purely static terrestrial setting. Complementing topology-aware and mobility-resilient monitoring, Long Short-Term Memory (LSTM) models are employed for predicting the time series of resource utilization in disaggregated NGRAN components. By learning temporal patterns in CPU, memory, and bandwidth usage, the LSTM model predicts future resource consumption to support proactive scaling and network function placement decisions in 6G NTN environments. Fig. 43 compares actual and predicted CPU usage for the gNB-DU

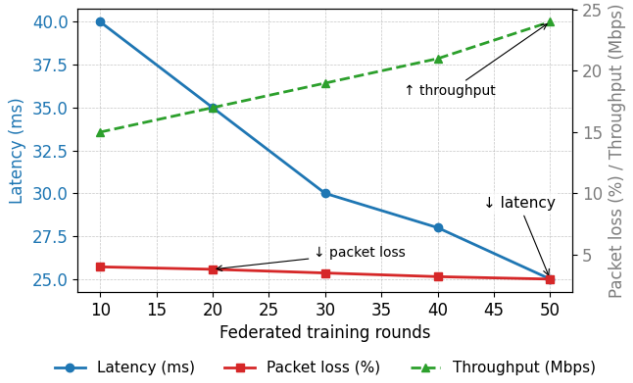

FIGURE 42. Resilience of the FedGNN-based routing policy under satellite mobility. Latency, packet loss, and throughput improve as the federated model adapts to dynamic LEO mobility conditions.

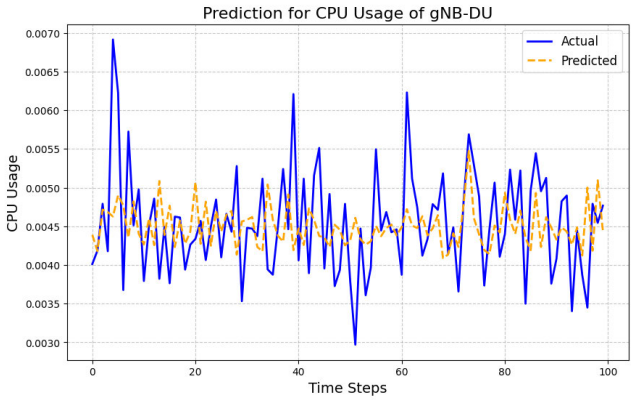

FIGURE 43. Predicted versus actual CPU usage for the gNB-DU F1 split using an LSTM-based time-series model.

component as a satellite payload, showing close alignment between predicted and observed values, with a mean absolute percentage error of 12.24%. With these utilization forecasts, a network operator can decide which disaggregated NGRAN function is feasible to deploy on the satellite payload under limited onboard computing, while accounting for payload and fronthaul constraints. Overall, the combined GNN and LSTM results demonstrate a cohesive ML-driven NTN Cloud-RAN monitoring stack capable of failure detection, routing optimization, mobility resilience, and proactive resource prediction, key requirements for self-optimizing 6G NTN systems. Moreover, the monitoring outputs can be exploited for orchestration intents (rerouting/traffic steering and payload-aware function placement), closing the loop between ML-based monitoring and software-defined control in integrated satellite-terrestrial networks.

IX. CONCLUSION, LESSONS LEARNED, AND FUTURE PERSPECTIVES

A. CONCLUDING REMARKS

The utilization of Space as a resource to extend the wireless connectivity worldwide is one of the main objectives of 6G. This work reviewed the most significant results achieved by INFINITE, the cascade-call project of the structural ITA-NTN project of the RESTART workprogramme. The research activities carried out during INFINITE considered a new eco-systemic approach to build broadband, flexible, and reconfigurable connections between terrestrial and non-terrestrial nodes, finalized to the true, seamless integration of terrestrial and non-terrestrial networks. The proposed ecosystem is based on the extended software-defined design of all network layers, adopting cutting-edge solutions encompassing advanced SDR-based waveform design, non-conventional NTN transmission configurations based on disruptive cell-free MIMO and NOMA concepts, use of multi-access edge computing, and AI tools for network management and monitoring. The various technologies and protocols involved in the ecosystem have been tested in the lab by means of realistic simulations upon specific key performance indicators. By the way, the vision emerging from the paper cannot be exhaustive; however, we think that it can represent a starting point to rethink Space connectivity as a sort of invisible glue connecting the unconnected. In the following of this concluding section, we shall try to summarize how such a starting point can be leveraged as a pitch for future developments going even beyond the 6G panorama.

B. LESSONS LEARNED

The various research aspects faced during the INFINITE project activities aim at contributing to a renewed vision of NTN connectivity, paving the road to future technology development in such a critical task of the forthcoming 6G standard [59]. In such a perspective, the lessons learned from the achieved results can be summarized as follows:

- Regarding the selection of the modulation format to use in future terrestrial and non-terrestrial communication systems, the well-established OFDM exhibits several drawbacks, which are exacerbated by the ever-increasing multitude of scenarios and applications, often extremely demanding in terms of challenges and requirements. For instance, in high mobility scenarios, such as moving vehicles served by LEO satellites, the continuously varying channel conditions strongly penalize the performance of OFDM, while other waveforms, like OTFS, are extremely robust in these cases. The complexity and variability of possible 6G NTN scenarios and applications also call for a shift of paradigm, from a traditional "cellular" system to a "cell-free" environment, where each user terminal can be connected to multiple base stations (terrestrial, non-terrestrial, or both), taking advantage of the additional rates and increased robustness arising from the reception of multiple signals. We also demonstrated that it is possible to achieve excellent detection performance with a very low receiver complexity, thus making it feasible to adopt alternative waveforms in real applications. Considering link impairments more inherent to the RF section of the NTN physical transceiver, open issues are related to the impact of nonlinear distortion and phase noise

on conventional multicarrier waveforms (OFDM and DFT-s-OFDM). The alternative solution represented by constant-envelope multicarrier waveforms (CE-OFDM and CE-SC-OFDM) offers immunity to nonlinear distortion, robustness to phase noise effects, and, in addition, multipath resilience. The performance losses of OFDM and DFT-s-OFDM due to the high IBOs and the possible error-floor caused by phase noise may justify the price paid by CE-MC in terms of increased bandwidth occupation and computational complexity. From a more general perspective of the implementation of a flexible NTN PHY-layer, where the waveform can be adaptively selected based on heterogeneous quality requirements and channel conditions, the proposed SDR-based modular framework should offer a viable solution. The software-defined modularity of the framework enables new and unexplored combinations of the elementary blocks to form unprecedented waveform formats. Of course, some significant implementation issues in terms of compatibility, overhead, synchronization, sustainability, and energy efficiency should be conveniently appraised and tackled.

- A cell-free MIMO NTN framework leveraging LEO satellites can effectively exploit macro-diversity when properly configured — for example, through the use of multi-antenna user terminals (UTs), zero-forcing beamforming, combining strategies, UT-satellite association policies that account for satellite load, and the generation of multiple ground-directed beams. Such a framework can substantially enhance both reliability and spectral efficiency in LEO-based non-terrestrial networks.
- NOMA is one of the breakthroughs of 5G and 6G. Being a capacity-oriented multi-access protocol, NOMA can overcome the spectrum shortcomings typical of the NTN environment. The main issue of NOMA is related to the multi-user interference mitigation. The literature offers many low-complexity and efficient solutions to this problem. It is expected that the synergy of SDR-based receiver implementation and machine learning could offer near-optimal approaches. NOMA may also solve one of the issues of CE-MC waveforms, namely, the impossibility of providing orthogonal multiple access in the uplink.
- The evolution of Non-Terrestrial Networks (NTN) beyond 5G opens transformative opportunities in edge computing and distributed task processing. By integrating NTN nodes — such as satellites and high-altitude platforms — into the edge computing ecosystem, computational resources can be dynamically extended to remote or underserved areas, reducing latency and enhancing real-time decision-making for applications like IoT analytics, autonomous systems, and AI-driven services. Lessons from early NTN deployments highlight the importance of adaptive resource allocation, seamless integration with terrestrial networks, and robust scheduling mechanisms to optimize task offloading. Looking forward, NTN-enabled edge computing promises a paradigm where computational power is ubiquitously available, enabling resilient, low-latency services across the globe and setting the stage for a truly pervasive digital infrastructure.
- Regarding the intelligent SDN-based NTN management, the results of our research demonstrate the effectiveness of ML-driven monitoring and orchestration for 6G NTN Cloud-RAN systems. The proposed GNN and FedGNN models enable accurate topology-aware fault detection, routing optimization, and mobility-resilient decision-making across dynamic LEO satellite environments, whereas the LSTM-based resource predictor supports proactive management of computational loads in disaggregated NGRAN components. Collectively, these approaches show that integrating distributed learning with cloud-edge intelligence can significantly enhance reliability, efficiency, and adaptability in future 6G NTN deployments, providing a practical foundation for scalable and self-optimizing 6G networks.

C. FUTURE R&D PERSPECTIVES

Future R&D work should go beyond the mere feasibility study by addressing the practical implementation of the investigated technologies, at least at a proof-of-concept (PoC) level. A first PoC is already available regarding the RF front-end (and described in Section VI). Another PoC will emulate in-lab the reconfigurable SDR-based NTN PHY-layer framework of Fig. 8 by open-source software tools (e.g., GNU-radio, Kubernetes clusters, etc.), as well as low-cost hardware devices such as National Instruments' Universal Software Radio Peripherals (USRP) boards. As far as the intelligent layer of the ecosystem is concerned, a third PoC should integrate the MEC section and the various AI tools assessed in the paper in an emulated Space cloud, capable of autonomously monitoring and controlling the underlying NTN layers. Such PoCs should represent the pitch for further R&D activities, whose objective is to transfer the technology from the lab to the Sky. In such a perspective, the involvement of big industrial actors, the liaison with international Space agencies, the proactive interaction with international standardization bodies – actions already planned and carried out in the framework of RESTART – will represent crucial factors to speed up the concrete technology development process.

ACKNOWLEDGMENT

The research activities presented in this article fall within the field of interest of the IEEE AESS technical panel on Glue Technologies for Space Systems.

REFERENCES

[1] S. Dang, O. Amin, B. Shihada, and M.-S. Alouini, "What should 6G be?" *Nature Electron.*, vol. 3, no. 1, pp. 20–29, Jan. 2020, doi: 10.1038/s41928-019-0355-6.

[2] *Measuring Digital Development, Facts and Figures*, International Telecommunication Union, Geneva, Switzerland, Jan. 2024.

[3] (2021). *Recovery Plan for Europe*. Accessed: Mar. 8, 2025. [Online]. Available: https://commission.europa.eu/strategy-and-policy/recovery-plan-europe_en

[4] (2023). *Research and Innovation on Future Telecommunications Systems and Networks, to Make Italy More Smart*. Accessed: Mar. 8, 2025. [Online]. Available: https://www.fondazione-restart.it/

[5] W. Chen et al., "5G-advanced toward 6G: Past, present, and future," *IEEE J. Sel. Areas Commun.*, vol. 41, no. 6, pp. 1592–1619, Jun. 2023.

[6] M. Giordani and M. Zorzi, "Non-terrestrial networks in the 6G era: Challenges and opportunities," *IEEE Netw.*, vol. 35, no. 2, pp. 244–251, Mar. 2021.

[7] M. Harounabadi and T. Heyn, "Toward integration of 6G-NTN to terrestrial mobile networks: Research and standardization aspects," *IEEE Wireless Commun.*, vol. 30, no. 6, pp. 20–26, Dec. 2023.

[8] C. T. Nguyen et al., "Emerging technologies for 6G non-terrestrial-networks: From academia to industrial applications," *IEEE Open J. Commun. Soc.*, vol. 5, pp. 3852–3885, 2024.

[9] A. Iqbal et al., "Empowering non-terrestrial networks with artificial intelligence: A survey," *IEEE Access*, vol. 11, pp. 100986–101006, 2023.

[10] R. G. Alavicheh, S. M. Razavizadeh, and H. Yanikomeroglu, "Integrated access and backhaul (IAB) in low altitude platforms," *IEEE Open J. Commun. Soc.*, vol. 5, pp. 5890–5904, 2024.

[11] A. Warrier, L. Aljaburi, H. Whitworth, S. Al-Rubaye, and A. Tsourdos, "Future 6G communications powering vertical handover in non-terrestrial networks," *IEEE Access*, vol. 12, pp. 33016–33034, 2024.

[12] Y. He, Y. Xiao, S. Zhang, M. Jia, and Z. Li, "Direct-to-smartphone for 6G NTN: Technical routes, challenges, and key technologies," *IEEE Netw.*, vol. 38, no. 4, pp. 128–135, Jul. 2024.

[13] H. Noh, H. Ju, and J. Lee, "6G repeaters for non-terrestrial network," in *Proc. Int. Conf. Electron., Inf., Commun. (ICEIC)*, Jan. 2024, pp. 1–3.

[14] D. Tuzi, T. Delamotte, and A. Knopp, "Satellite swarm-based antenna arrays for 6G direct-to-cell connectivity," *IEEE Access*, vol. 11, pp. 36907–36928, 2023.

[15] O. A. Amodu et al., "Technical advancements toward RIS-assisted NTN-based THz communication for 6G and beyond," *IEEE Access*, vol. 12, pp. 183153–183181, 2024.

[16] K. Guo, M. Wu, X. Li, Z. Lin, and T. A. Tsiftsis, "Joint trajectory and beamforming optimization for federated DRL-aided space-aerial-terrestrial relay networks with RIS and RSMA," *IEEE Trans. Wireless Commun.*, vol. 23, no. 12, pp. 18456–18471, Dec. 2024.

[17] M. Wu et al., "RIS-assisted SATINs with RSMA and DRL: A trade-off between spectral, secrecy, and energy efficiency," *IEEE Trans. Commun.*, vol. 73, no. 11, pp. 12380–12395, Nov. 2025.

[18] L. Zhi et al., "Self-powered absorptive reconfigurable intelligent surfaces for securing satellite-terrestrial integrated networks," *China Commun.*, vol. 21, no. 9, pp. 276–291, Sep. 2024.

[19] B. E. Y. Belmekki and M.-S. Alouini, "NOMA as the next-generation multiple access in nonterrestrial networks," *Proc. IEEE*, vol. 112, no. 9, pp. 1303–1345, Sep. 2024.

[20] C. Sacchi, K. Bhasin, N. Kadowaki, and F. Vong, "Toward the 'space 2.0' era [guest editorial]," *IEEE Commun. Mag.*, vol. 53, no. 3, pp. 16–17, Mar. 2015.

[21] C. Sacchi et al., "Glue technologies for space systems: An introduction to a new AESS technical panel," *IEEE Aerosp. Electron. Syst. Mag.*, vol. 35, no. 1, pp. 46–54, Jan. 2020.

[22] S. Basu, L. Oliviero, G. Cossu, C. Cantore, A. D'Orazio, and E. Ciaramella, "Prospects of optical wireless communications in non-terrestrial networks," in *Proc. 24th Int. Conf. Transparent Opt. Netw. (ICTON)*, Jul. 2024, pp. 1–4.

[23] E. Cianca et. al., "RESTART-integrated terrestrial and non terrestrial networks (ITA-NTN): D2.2 preliminary definition of UCS requirements and architecture," Ministero dell'Università e Della Ricerca, Rome, Italy, Tech. Rep., Nov. 2023.

[24] A. Guidotti et al., "Role and evolution of non-terrestrial networks toward 6G systems," *IEEE Access*, vol. 12, pp. 55945–55963, 2024.

[25] L. Bertaux et al., "Software defined networking and virtualization for broadband satellite networks," *IEEE Commun. Mag.*, vol. 53, no. 3, pp. 54–60, Mar. 2015.

[26] E. Cianca et al., "Softwarization and virtualization as enablers for future EHF/FSO high throughput satellites," in *Proc. IEEE Global Commun. Conf. (GLOBECOM)*, Dec. 2018, pp. 1–6.

[27] F. Patrone et al., "Data-driven network orchestrator for 5G satellite-terrestrial integrated networks: The ANChOR project," in *Proc. IEEE Global Commun. Conf. (GLOBECOM)*, Dec. 2021, pp. 1–6.

[28] M. M. Azari et al., "Evolution of non-terrestrial networks from 5G to 6G: A survey," *IEEE Commun. Surveys Tuts.*, vol. 24, no. 4, pp. 2633–2672, 4th Quart., 2022.

[29] S. Buzzi, C. D'Andrea, A. Zappone, and C. D'Elia, "User-centric 5G cellular networks: Resource allocation and comparison with the cell-free massive MIMO approach," *IEEE Trans. Wireless Commun.*, vol. 19, no. 2, pp. 1250–1264, Feb. 2020.

[30] H. Q. Ngo, A. Ashikhmin, H. Yang, E. G. Larsson, and T. L. Marzetta, "Cell-free massive MIMO versus small cells," *IEEE Trans. Wireless Commun.*, vol. 16, no. 3, pp. 1834–1850, Mar. 2017.

[31] U. T. Demir, E. BjErnson, and L. Sanguinetti, "Foundations of user-centric cell-free massive MIMO," *Found. Trends Signal Process.*, vol. 14, nos. 3–4, pp. 162–472, Jan. 2021.

[32] H. Q. Ngo, G. Interdonato, E. G. Larsson, G. Caire, and J. G. Andrews, "Ultradense cell-free massive MIMO for 6G: Technical overview and open questions," *Proc. IEEE*, vol. 112, no. 7, pp. 805–831, Jul. 2024.

[33] S. Buzzi et al., "Multi-satellite diversity through the use of OTFS," in *Proc. 39th Int. Commun. Satell. Syst. Conf. (ICSSC)*, Oct. 2022, pp. 273–274.

[34] S. Buzzi et al., "LEO satellite diversity in 6G non-terrestrial networks: OFDM vs. OTFS," *IEEE Commun. Lett.*, vol. 27, no. 11, pp. 3013–3017, Nov. 2023.

[35] Z. M. Bakhsh, Y. Omid, G. Chen, F. Kayhan, Y. Ma, and R. Tafazolli, "Multi-satellite MIMO systems for direct satellite-to-device communications: A survey," *IEEE Commun. Surveys Tuts.*, vol. 27, no. 3, pp. 1536–1564, Jun. 2025.

[36] K. Humadi, G. K. Kurt, and H. Yanikomeroglu, "Distributed massive MIMO system with dynamic clustering in LEO satellite networks," in *Proc. 6th Int. Conf. Commun., Signal Process., Their Appl. (ICCSPA)*, Jul. 2024, pp. 1–6.

[37] C. D'Andrea, T. Foggi, A. Piemontese, A. Ugolini, S. Buzzi, and G. Colavolpe, "Coherent vs. non-coherent joint transmission in cell-free user-centric non-terrestrial wireless networks," in *Proc. IEEE 25th Int. Workshop Signal Process. Adv. Wireless Commun. (SPAWC)*, Sep. 2024, pp. 636–640.

[38] L. Gaudio, G. Colavolpe, and G. Caire, "OTFS vs. OFDM in the presence of sparsity: A fair comparison," *IEEE Trans. Wireless Commun.*, vol. 21, no. 6, pp. 4410–4423, Jun. 2022.

[39] C. D'Andrea, T. Foggi, A. Piemontese, A. Ugolini, S. Buzzi, and G. Colavolpe, "Cell-free macro-diversity schemes in LEO non-terrestrial networks with OTFS and OFDM modulations," *IEEE Open J. Commun. Soc.*, vol. 6, pp. 10432–10448, 2025.

[40] G. Forney, "Lower bounds on error probability in the presence of large intersymbol interference," *IEEE Trans. Commun.*, vol. COM-20, no. 1, pp. 76–77, Feb. 1972.

[41] G. Ungerboeck, "Adaptive maximum-likelihood receiver for carrier-modulated data-transmission systems," *IEEE Trans. Commun.*, vol. COM-22, no. 5, pp. 624–636, May 1974.

[42] G. Colavolpe, D. Fertonani, and A. Piemontese, "SISO detection over linear channels with linear complexity in the number of interferers," *IEEE J. Sel. Topics Signal Process.*, vol. 5, no. 8, pp. 1475–1485, Dec. 2011.

[43] E. Conti, A. Piemontese, T. Foggi, G. Colavolpe, and A. Vannucci, "Efficient message-passing detection for multi-satellite systems using OTFS modulation," in *Proc. IEEE Aerosp. Conf.*, Mar. 2025, pp. 1–11.

[44] E. Conti, A. Piemontese, T. Foggi, G. Colavolpe, and A. Vannucci, "Detection techniques for OTFS transmissions over doubly-selective channels," *IEEE Trans. Wireless Commun.*, pp. 1–13, Nov. 2025.

[45] P. Raviteja, K. T. Phan, Y. Hong, and E. Viterbo, "Interference cancellation and iterative detection for orthogonal time frequency space modulation," *IEEE Trans. Wireless Commun.*, vol. 17, no. 10, pp. 6501–6515, Oct. 2018.

[46] D. Bandeira, D. Le Ruyet, M. Pischella, and J. Mota, "Performance evaluation of low-complexity algorithms for orthogonal time-frequency space modulation," *J. Commun. Inf. Syst.*, vol. 35, no. 1, pp. 138–149, Jun. 2020. [Online]. Available: https://www.jcis.sbrt.org.br/jcis/article/view/691

[47] L. Gaudio, M. Kobayashi, G. Caire, and G. Colavolpe, "On the effectiveness of OTFS for joint radar parameter estimation and communication," *IEEE Trans. Wireless Commun.*, vol. 19, no. 9, pp. 5951–5965, Sep. 2020.

[48] Z. Yuan, F. Liu, W. Yuan, Q. Guo, Z. Wang, and J. Yuan, "Iterative detection for orthogonal time frequency space modulation with unitary approximate message passing," *IEEE Trans. Wireless Commun.*, vol. 21, no. 2, pp. 714–725, Feb. 2022.

[49] H. Zhang and T. Zhang, "A low-complexity message passing detector for OTFS modulation with probability clipping," *IEEE Wireless Commun. Lett.*, vol. 10, no. 6, pp. 1271–1275, Jun. 2021.

[50] *Evolved Universal Terrestrial Radio Access (E-UTRA); Base Station (BS) Radio Transmission and Reception*, document 3GPP TS 36.104, Version 8.6.0, ETSI, Jul. 2009.

[51] M. S. J. Solaija, S. E. Zegrar, and H. Arslan, "Orthogonal frequency division multiplexing: The way forward for 6G physical layer design?" *IEEE Veh. Technol. Mag.*, vol. 19, no. 1, pp. 45–54, Mar. 2024.

[52] B. Farhang-Boroujeny and H. Moradi, "OFDM inspired waveforms for 5G," *IEEE Commun. Surveys Tuts.*, vol. 18, no. 4, pp. 2474–2492, 4th Quart., 2016.

[53] S. Hara and R. Prasad, "Overview of multicarrier CDMA," *IEEE Commun. Mag.*, vol. 35, no. 12, pp. 126–133, Dec. 1997.

[54] H. Myung and D. Goodman, *Single Carrier FDMA: A New Air Interface for Long Term Evolution* (Wireless Communications and Mobile Computing). Hoboken, NJ, USA: Wiley, 2008. [Online]. Available: https://books.google.it/books?id=Dotsv0dfH7kC

[55] Z. Wei, S. Li, W. Yuan, R. Schober, and G. Caire, "Orthogonal time frequency space modulation—Part I: Fundamentals and challenges ahead," *IEEE Commun. Lett.*, vol. 27, no. 1, pp. 4–8, Jan. 2023.

[56] T. Thaj, E. Viterbo, and Y. Hong, "Orthogonal time sequency multiplexing modulation: Analysis and low-complexity receiver design," *IEEE Trans. Wireless Commun.*, vol. 20, no. 12, pp. 7842–7855, Dec. 2021.

[57] S. C. Thompson, A. U. Ahmed, J. G. Proakis, J. R. Zeidler, and M. J. Geile, "Constant envelope OFDM," *IEEE Trans. Commun.*, vol. 56, no. 8, pp. 1300–1312, Aug. 2008.

[58] R. Mulinde, T. F. Rahman, and C. Sacchi, "Constant-envelope SC-FDMA for nonlinear satellite channels," in *Proc. IEEE Global Commun. Conf. (GLOBECOM)*, Dec. 2013, pp. 2939–2944.

[59] A. Rago et al., "Innovative multi-layer approaches for 6G integrated terrestrial and non-terrestrial networks," *IEEE Commun. Standards Mag.*, vol. 9, no. 2, pp. 39–47, Jun. 2025.

[60] C. Sacchi et al., "A unified software-defined radio framework for flexible waveform design in non-terrestrial networks," in *Proc. IEEE Aerosp. Conf.*, Mar. 2025, pp. 1–20.

[61] E. Cianca, T. Rossi, M. Ruggieri, and M. De Sanctis, "Space sustainability-by-design: Challenges and key-enablers," *IEEE Aerosp. Electron. Syst. Mag.*, vol. 40, no. 4, pp. 4–17, Apr. 2025.

[62] Y. Wang et al., "Covert communication for satellite aerial–ground integrated networks under imperfect limitations," *IEEE Internet Things J.*, vol. 13, no. 1, pp. 296–307, Jan. 2026.

[63] Z. Lin et al., "Wireless endogenous security for SAGINs: Achieving ubiquitous access and secure communication in symbiosis," *IEEE Netw.*, vol. 39, no. 6, pp. 155–163, Nov. 2025.

[64] M. Wu et al., "Federated learning-driven covert communication in satellite–terrestrial integrated networks: A privacy-preserving framework," *IEEE J. Sel. Areas Commun.*, vol. 44, pp. 2143–2157, 2026.

[65] Y. M. Worku, P. M. Tshakwanda, H. B. Tsegaye, C. Christodoulou, M. Devetsikiotis, and C. Sacchi, "Blockchain-enhanced security for LEO satellite firmware updates in beyond-5G NTN networks," in *Proc. IEEE 29th Int. Workshop Comput. Aided Model. Design Commun. Links Netw. (CAMAD)*, Oct. 2024, pp. 1–6.

[66] C. Sacchi, A. Tarable, G. Virone, and S. Morosi, "Constant-envelope multicarrier modulations vs. multicarrier modulations in non-terrestrial network scenarios," in *Proc. IEEE Aerosp. Conf.*, Oct. 2026, pp. 1–19.

[67] Z. Liu, "Maximum diversity in single-carrier frequency-domain equalization," *IEEE Trans. Inf. Theory*, vol. 51, no. 8, pp. 2937–2940, Aug. 2005.

[68] C. Sacchi, E. Cianca, T. Rossi, and M. De Sanctis, "Analysis and assessment of the effects of phase noise in constant envelope multicarrier satellite transmissions," in *Proc. IEEE Int. Conf. Commun. (ICC)*, Jun. 2015, pp. 922–927.

[69] A. Garcia Armada, "Understanding the effects of phase noise in orthogonal frequency division multiplexing (OFDM)," *IEEE Trans. Broadcast.*, vol. 47, no. 2, pp. 153–159, Jun. 2001.

[70] A. Carlson and P. Crilly, *Communication Systems* (McGraw-Hill Higher Education). New York, NY, USA: McGraw-Hill, 2009. [Online]. Available: https://books.google.it/books?id=8qOUCgAAQBAJ

[71] T. F. Rahman, C. Sacchi, S. Morosi, A. Mazzinghi, and N. Bartolomei, "Constant-envelope multicarrier waveforms for millimeter wave 5G applications," *IEEE Trans. Veh. Technol.*, vol. 67, no. 10, pp. 9406–9420, Oct. 2018.

[72] D. Palossi et al., "Fully onboard AI-powered human-drone pose estimation on ultralow-power autonomous flying nano-UAVs," *IEEE Internet Things J.*, vol. 9, no. 3, pp. 1913–1929, Feb. 2022.

[73] A. A. Zaid, B. E. Y. Belmekki, and M.-S. Alouini, "Aerial-terrestrial heterogeneous networks for urban air mobility: A performance analysis," *IEEE Open J. Veh. Technol.*, vol. 6, pp. 1–16, 2025.

[74] F. Y. Hadaegh, S.-J. Chung, and H. M. Manohara, "On development of 100-gram-class spacecraft for swarm applications," *IEEE Syst. J.*, vol. 10, no. 2, pp. 673–684, Jun. 2016.

[75] Y. He, Y. Liu, C. Jiang, and X. Zhong, "Multiobjective anti-collision for massive access ranging in MF-TDMA satellite communication system," *IEEE Internet Things J.*, vol. 9, no. 16, pp. 14655–14666, Aug. 2022.

[76] Z. Lin, Z. Feng, K. Guo, A. Nauman, D. Niyato, and J. Wang, "AI-driven seamless and massive access in space-air-ground integrated networks," *IEEE Wireless Commun.*, vol. 32, no. 3, pp. 72–79, Jun. 2025.

[77] Y. He, B. Sheng, H. Yin, D. Yan, and Y. Zhang, "Multi-objective deep reinforcement learning based time-frequency resource allocation for multi-beam satellite communications," *China Commun.*, vol. 19, no. 1, pp. 77–91, Jan. 2022.

[78] C. Xu, L. Ping, P. Wang, S. Chan, and X. Lin, "Decentralized power control for random access with successive interference cancellation," *IEEE J. Sel. Areas Commun.*, vol. 31, no. 11, pp. 2387–2395, Nov. 2013.

[79] L. Dai, B. Wang, Y. Yuan, S. Han, I. Chih-lin, and Z. Wang, "Non-orthogonal multiple access for 5G: Solutions, challenges, opportunities, and future research trends," *IEEE Commun. Mag.*, vol. 53, no. 9, pp. 74–81, Sep. 2015.

[80] Z. Ding et al., "Application of non-orthogonal multiple access in LTE and 5G networks," *IEEE Commun. Mag.*, vol. 55, no. 2, pp. 185–191, Feb. 2017.

[81] Z. Ding, X. Lei, G. K. Karagiannidis, R. Schober, J. Yuan, and V. K. Bhargava, "A survey on non-orthogonal multiple access for 5G networks: Research challenges and future trends," *IEEE J. Sel. Areas Commun.*, vol. 35, no. 10, pp. 2181–2195, Oct. 2017.

[82] W. Shin, M. Vaezi, B. Lee, D. J. Love, J. Lee, and H. V. Poor, "Non-orthogonal multiple access in multi-cell networks: Theory, performance, and practical challenges," *IEEE Commun. Mag.*, vol. 55, no. 10, pp. 176–183, Oct. 2017.

[83] Y. Liu, Z. Qin, M. Elkashlan, Z. Ding, A. Nallanathan, and L. Hanzo, "Nonorthogonal multiple access for 5G and beyond," *Proc. IEEE*, vol. 105, no. 12, pp. 2347–2381, Dec. 2017.

[84] Y. Cai, Z. Qin, F. Cui, G. Y. Li, and J. A. McCann, "Modulation and multiple access for 5G networks," *IEEE Commun. Surveys Tuts.*, vol. 20, no. 1, pp. 646–1629, 1st Quart., 2018.

[85] S. M. R. Islam, M. Zeng, O. A. Dobre, and K.-S. Kwak, "Resource allocation for downlink NOMA systems: Key techniques and open issues," *IEEE Wireless Commun.*, vol. 25, no. 2, pp. 40–47, Apr. 2018.

[86] X. Yue, Z. Qin, Y. Liu, S. Kang, and Y. Chen, "A unified framework for non-orthogonal multiple access," *IEEE Trans. Commun.*, vol. 66, no. 11, pp. 5346–5359, Nov. 2018.

[87] M. Comisso et al., "Power-domain non-orthogonal multiple access for distributed non-terrestrial networks: A semi-analytical throughput estimation," in *Proc. IEEE 12th Int. Workshop Metrol. Aerosp. (MetroAeroSpace)*, Jun. 2025, pp. 233–238.

[88] P. K. Sharma and D. I. Kim, "Random 3D mobile UAV networks: Mobility modeling and coverage probability," *IEEE Trans. Wireless Commun.*, vol. 18, no. 5, pp. 2527–2538, May 2019.

[89] V. V. Chetlur and H. S. Dhillon, "Downlink coverage analysis for a finite 3-D wireless network of unmanned aerial vehicles," *IEEE Trans. Commun.*, vol. 65, no. 10, pp. 4543–4558, Oct. 2017.

[90] F. D. Nunes and F. M. G. Sousa, "Generalized gamma fading simulation of scintillation disturbed GNSS signals," *IEEE Trans. Aerosp. Electron. Syst.*, vol. 54, no. 4, pp. 2025–2034, Aug. 2018.

[91] F. Babich, A. Soranzo, and F. Vatta, "Useful mathematical tools for capacity approaching codes design," *IEEE Commun. Lett.*, vol. 21, no. 9, pp. 1949–1952, Sep. 2017.

[92] M. Jia, D. Li, Z. Yin, Q. Guo, and X. Gu, "High spectral efficiency secure communications with nonorthogonal physical and multiple access layers," *IEEE Internet Things J.*, vol. 6, no. 4, pp. 5954–5961, Aug. 2019.
[93] M. Li et al., "Effects of residual hardware impairments on secure NOMA-based cooperative systems," *IEEE Access*, vol. 8, pp. 2524–2536, 2020.
[94] *Base Station (BS) Radio Transmission and Reception*, document 3GPP TS 38.104, version 17.2.0, 3GPP, Jul. 2021.
[95] Y. Mao, C. You, J. Zhang, K. Huang, and K. B. Letaief, "A survey on mobile edge computing: The communication perspective," *IEEE Commun. Surveys Tuts.*, vol. 19, no. 4, pp. 2322–2358, 4th Quart., 2017.
[96] P. Agbo and P. Weitkemper, "Analysis of different MEC offloading scenarios with LEO satellite in 5G networks," in *Proc. IEEE Int. Conf. Omni-Layer Intell. Syst. (COINS)*, Jul. 2023, pp. 1–6.
[97] SCNL. (2024). *Meteornet*. [Online]. Available: https://gitlab.com/camilo.rojas/meteornet
[98] M. Team. (2021). *Mininet: An Instant Virtual Network on Your Laptop*. Git. [Online]. Available: https://github.com/mininet/mininet
[99] D. Merkel, "Docker: Lightweight Linux containers for consistent development and deployment," *Linux J.*, vol. 2014, no. 239, p. 2, Mar. 2014.
[100] T. A. Limoncelli, "OpenFlow: A radical new idea in networking," *Commun. ACM*, vol. 55, no. 8, pp. 42–47, Aug. 2012, doi: 10.1145/2240236.2240254.
[101] P. Berde et al., "ONOS: Towards an open, distributed SDN OS," in *Proc. 3rd Workshop Hot Topics SDN*, 2014, pp. 1–6.
[102] R. K. Ahuja, K. Mehlhorn, J. Orlin, and R. E. Tarjan, "Faster algorithms for the shortest path problem," *J. ACM*, vol. 37, no. 2, pp. 213–223, Apr. 1990. [Online]. Available: https://doi-org.ezp.biblio.unitn.it/10.1145/77600.77615
[103] F. R. Hoots. (1980). *Spacetrack Report, no. 3, Models for Propagation of Norad Element Sets*. [Online]. Available: http://www.itc.nl/-bakker/orbit.html
[104] *5G NGRAN: Architecture Description*, document TS 1-38.401, 3GPP, Nov. 2020.
[105] H. B. Tsegaye, P. M. Tshakwanda, Y. M. Worku, C. Sacchi, C. Christodoulou, and M. Devetsikiotis, "LSTM-based resource prediction for disaggregated RAN in 5G non-terrestrial networks," in *Proc. IEEE Virtual Conf. Commun. (VCC)*, Dec. 2024, pp. 1–6.
[106] H. B. Tsegaye and C. Sacchi, "Graph neural network-based C-RAN monitoring for beyond 5G non-terrestrial networks," in *Proc. 11th Int. Workshop Metrol. Aerosp. (MetroAeroSpace)*, Jun. 2024, pp. 338–343.
[107] H. B. Tsegaye, P. M. Tshakwanda, Y. M. Worku, M. Devetsikiotis, C. Sacchi, and C. Christodoulou, "Federated learning and MEC for disaggregated RAN monitoring in the 5G non-terrestrial networks," in *Proc. IEEE Aerosp. Conf.*, Mar. 2025, pp. 1–11.
[108] Z. Liu and J. Zhou, *Graph Convolutional Networks*. Cham, Switzerland: Springer, 2020, pp. 23–32, doi: 10.1007/978-3-031-01587-8_5.
[109] S. Hochreiter and J. Schmidhuber, "Long short-term memory," *Neural Comput.*, vol. 9, no. 8, pp. 1735–1780, Nov. 1997.
[110] M. M. M. Freitas, S. Buzzi, and G. Interdonato, "Eliminating phase misalignments in cell-free massive MIMO via differential transmission," *IEEE Wireless Commun. Lett.*, vol. 14, no. 9, pp. 2718–2722, Sep. 2025.
[111] M. M. M. Freitas, S. Buzzi, and G. Interdonato, "UAV-empowered aerial cell-free networks robust to downlink phase misalignments," in *Proc. IEEE 26th Int. Workshop Signal Process. Artif. Intell. Wireless Commun. (SPAWC)*, Jul. 2025, pp. 1–5.
[112] V. Singh et al., "Diversity combining scheme for time-varying STBC NGSO multi-satellite systems," *IEEE Commun. Lett.*, vol. 28, no. 4, pp. 882–886, Apr. 2024.
[113] *Propagation Data Required for the Design Systems in the Land Mobile-Satellite Service*, document Recommendation ITU-R P.681-11, Aug. 2019. [Online]. Available: https://www.itu.int/rec/R-REC-P.681-11-201908-I
[114] P. Raviteja, K. T. Phan, and Y. Hong, "Embedded pilot-aided channel estimation for OTFS in delay–Doppler channels," *IEEE Trans. Veh. Technol.*, vol. 68, no. 5, pp. 4906–4917, May 2019.
[115] *Study on New Radio (NR) so Support Non-Terrestrial Networks*, document (TS) 38.811, 3GPP Technical Specification Group Radio Access Network, Sep. 2020.
[116] V. Valenta, I. Davies, N. Ayllon, S. Seyfarth, and P. Angeletti, "High-gain GaN Doherty power amplifier for Ka-band satellite communications," in *Proc. IEEE Topical Conf. RF/Microw. Power Modeling Radio Wireless Appl. (PAWR)*, Jan. 2018, pp. 29–31.
[117] A. Ahluwalia, D. N. Patel, R. Singh, J. Thakkar, and S. Sarkar, "Development of Hi-Rel Ka-band multipack downconverter assembly for high throughput satellite," in *Proc. IEEE Microw., Antennas, Propag. Conf. (MAPCON)*, Dec. 2023, pp. 1–5.
[118] P. M. Tshakwanda, S. T. Arzo, and M. Devetsikiotis, "Advancing 6G network performance: AI/ML framework for proactive management and dynamic optimal routing," *IEEE Open J. Comput. Soc.*, vol. 5, pp. 303–314, 2024.

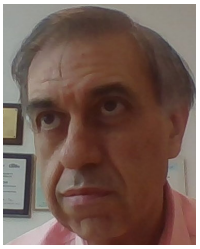

CLAUDIO SACCHI (Senior Member, IEEE) was born in Genoa, Italy, in 1965. He received the Laurea degree in electronic engineering and the Ph.D. degree in space science and engineering from the University of Genoa, Italy, in 1992 and 2003, respectively. From 1996 to 2002, he was a Research Cooperator with the Department of Biophysical and Electronic Engineering (DIBE), University of Genoa, and the National Italian Consortium in Telecommunications (CNIT), managing project activities in the field of multimedia surveillance systems and satellite communications. In August 2002, he joined the Department of Information Engineering and Computer Science (DISI), University of Trento, Italy, as an Assistant Professor, and was promoted to an Associate Professor in December 2020. Since January 2023, he has been got double affiliation with UNM, as a Research Professor. He has authored or co-authored more than 140 papers published in international journals and conferences. His main research interests include emerging satellite and aerospace communications and broadband mobile communications in 5G and 6G systems, software-defined radios, emergency communications, and mm-wave transmission in terrestrial and satellite applications. He is a member of IEEE ComSoc, IEEE BTS, IEEE VT, and IEEE AESS. Since 2019, he has been coordinating and chairing the IEEE AESS Technical Panel: "Glue Technologies for Space Systems," which was awarded by AESS as "Outstanding Panel of the Year" in 2020, 2021, and 2025.

CARMEN D'ANDREA (Member, IEEE) received the B.S., M.S., and Ph.D. degrees (summa cum laude) in telecommunications engineering from the University of Cassino and Southern Lazio, Italy, in 2013, 2015, and 2019, respectively. She is currently a tenure-track Assistant Professor (RTT) with the University of Cassino and Southern Lazio. In 2017, she was a Visiting Ph.D. Student with the Wireless Communications (WiCom) Research Group, Department of Information and Communication Technologies, Universitat Pompeu Fabra, Barcelona, Spain. In the spring of 2020, she spent three months as a Visiting Researcher with the Communication System Division, Department of Electrical Engineering, Linköping University, Sweden. Her research interests include wireless communication and signal processing, with an emphasis on mmWave communications, massive MIMO systems, and the study of waveforms for beyond-5G communication systems. In June 2023, she received the Best Paper Award at EUCNC and the 6G Summit 2023. In 2023, she received the Italian Scientific Habilitation (ASN) as an Associate Professor. From 2023 to 2025, she was in the World's Top 2% Scientists in the field of information and communication technologies—networking and telecommunications listed by Elsevier, Scopus, and Stanford University; and in the list of "100 Brilliant and Inspiring Women in 6G," in 2024. From 2019 to 2024, she served as an Associate Editor for IEEE OPEN JOURNAL OF THE COMMUNICATIONS SOCIETY. Since 2020, she has been an Associate Editor of IEEE COMMUNICATIONS LETTERS (an Exemplary Editor in 2022 and 2024). In 2025, she started serving as Associate Editor for IEEE TRANSACTIONS ON WIRELESS COMMUNICATIONS.

ELISA CONTI was born in Parma, Italy, in 1997. She received the B.Sc. and M.Sc. degrees (cum laude) in telecommunications engineering and the Ph.D. degree (cum laude) in information technology from the University of Parma, in 2019, 2021, and 2024, respectively. She is currently a Postdoctoral Researcher with the Department of Engineering and Architecture (DIA), University of Parma. Her research activity is in the area of digital communications and signal processing, with particular emphasis on iterative joint detection and decoding techniques based on factor graphs, message-passing algorithms, and multicarrier communications.

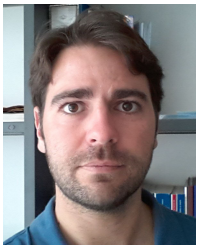

TOMMASO FOGGI received the master's degree in telecommunication engineering and the Ph.D. degree in information technology from the University of Parma, in 2003 and 2008, respectively. From 2009 to 2018, he was a Research Engineer with the National Inter-University Consortium for Telecommunications (CNIT), University of Parma Research Unit. He is currently an Associate Professor with the Engineering and Architecture Department, University of Parma. He was/is involved in many research projects funded by public authorities, such as MIUR, ESA, EU, and private companies, such as Ericsson, CGS, Inmarsat, and Huawei. He is the author of tens of peer-reviewed papers and several patents. His main research interests include electronic signal processing for optical and satellite communication systems. He has won the Best Paper Award in Optical Networks and Systems Symposium at IEEE International Conference on Communications (ICC 2008), Beijing, China, in May 2008.

AMINA PIEMONTESE received the Dr.-Ing. degree in telecommunications engineering from the University of Parma, Italy, in 2006, and joint the Ph.D. degree in information technology from the University of Parma and from Telecom Bretagne, Brest, France, in 2011. From 2011 to 2015, she held a post-doctoral position with the Department of Engineering and Architecture, University of Parma, where she is currently an Associate Professor. From May 2015 to May 2020, she was with the Department of Electrical Engineering, Chalmers University of Technology, Gothenburg, Sweden. Her research activity include various topics in digital communications, with particular emphasis on iterative joint detection and decoding algorithms, multiuser communications theory, and information theory. She received the Best Paper Award at Fifth Advanced Satellite Mobile Systems Conference, 11th International Workshop on Signal Processing for Space Communications (ASMS&SPSC 2010), and IEEE Wireless Communications and Networking Conference (WCNC); and the Marie Curie Individual Fellowship of European Commission.

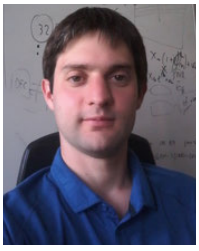

ALESSANDRO UGOLINI received the master's degree (cum laude) in telecommunications engineering and the Ph.D. degree in information technology from the University of Parma, in 2012 and 2016, respectively. In 2012, he received the National Inter-University Consortium for Telecommunications (CNIT) Grant and a Research Grant funded by the Department of Information Engineering (DII), University of Parma, for the study of synchronization algorithms for spectrally efficient systems. In 2016, he was a Post-Doctoral Researcher with DII. In 2017, he was a Visiting Researcher with the Communication and Antenna Systems Division, Chalmers University of Technology, Gothenburg, Sweden, and the Interdisciplinary Centre for Security, Reliability and Trust, University of Luxembourg. From 2016 to 2025, he was an Assistant Professor at the Department of Engineering and Architecture (DIA), University of Parma, where he is currently an Associate Professor. His main research interests include digital, wireless, and satellite communications, applied information theory, detection, and synchronization schemes. He received the best paper award at the IEEE Wireless Communications and Networking Conference (WCNC 2019).

ARMANDO VANNUCCI received the Dr.-Ing. degree (cum laude) in electronic engineering from the University of Rome "La Sapienza," in 1993, with a focus on digital analysis of speech signals applied to speech recognition, and the Ph.D. degree in information technology from the Polytechnic of Turin. He was a joint Ph.D. Student with the INFO-COM Department, University of Rome, and the University of Parma, joining an industrial research project on digital radio links, for which he holds two patents. His Ph.D. thesis titles "Sequence Estimation Receivers for Nonlinear Transmission Channels." In 2002, he became an Assistant Professor with the University of Parma. He took part in various research projects, both institutional and with industrial partners. He has been a Visiting Scientist with Alcatel Labs, Marcoussis, France, and the Université Laval, Quebec City, Canada; and a Visiting Lecturer with Hochschule, Karlsruhe, Germany. He is the author of two textbooks and has taught several courses (undergraduate, graduate, M.Sc., Ph.D., and summer schools) at the University of Rome, the University of Urbino, and the University of Parma, where he is currently in charge of "Signals and Systems." He is the author of more than 60 scientific publications, half of which on international journals. His research interests include variational techniques for the design of digital receivers, fiber optics transmission, polarization mode dispersion, optical amplifiers, and digital speech processing.

CAMILO ROJAS (Graduate Student Member, IEEE) received the degree in electrical engineering and the master's degree (Hons.) in computer science from the University of Chile. He is currently pursuing the Ph.D. degree in science and technology for electronic engineering and telecommunications with the Satellite Communications and Networking Laboratory (SCNL), University of Genoa. He has strong experience in programming, data visualization, digital communications, embedded systems, and Linux/Unix-based operating systems. As a bachelor student, he participated in the project Satellite of the University of Chile for Aerospace Investigation (SUCHAI), launched in June 2017, working on communications and on-board computer systems. From 2017 to 2020, he was a Researcher with the Advanced Laboratory for Geostatistical Supercomputing (ALGES) Laboratory. From 2017 to 2023, he conducted research with the Space and Planetary Exploration Laboratory (SPEL), developing flight software for upcoming satellites (SUCHAI II and III) and CI/CD tools for space and ground software systems. His main research interests include edge computing emulation, constellation emulation, space communications, and resource optimization using machine learning models.

NOUR BADINI (Member, IEEE) received the master's degree in computer and communication engineering from Lebanese University, Beirut, Lebanon, and the Ph.D. degree in science and technology for electronic and telecommunication engineering from the University of Genoa, Italy. She is currently a Post-Doctoral Researcher with the Satellite Communications and Heterogeneous Networking Laboratory, University of Genoa. Her main research interests include the routing and handover management in non-terrestrial networks, edge computing, emerging satellite and aerospace communications and broadband mobile communications in 5G and 6G systems, quality of service over satellite communications, the integration of non-terrestrial networks with the terrestrial infrastructure within 5G networks, and exploiting machine learning (ML)-based techniques for performance enhancement in heterogeneous networks.

FABIO PATRONE (Member, IEEE) is currently an Assistant Professor with the University of Genoa, Italy, and the Satellite Communications and Heterogeneous Networking Laboratory (SCNL). His main research activities include the design of resource allocation, routing, and handover solutions for non-terrestrial networks (NTN); study of integration solutions between terrestrial and non-terrestrial networks within the B5G/6G framework involving the edge computing paradigm; study of the Internet of Things (IoT) solutions for aerial communication networks; and design of machine learning (ML)-based solutions for cybersecurity, focusing on ML-based intrusion detection systems (IDS) and physical-layer device identification (RF device fingerprinting).

MARIO MARCHESE (Senior Member, IEEE) is currently a Full Professor with the University of Genoa, Italy; the Vice-Rector for the Ph.D. studies and relationship with the companies; and the Head of Research with the Satellite Communications and heterogeneous Networking Laboratory (SCNL). He is the author of the book *Quality of Service Over Heterogeneous Networks* (John Wiley & Sons, Chichester); and the author/co-author of more than 400 scientific works, including international magazines, international conferences, and book chapters. His main research interests include networking, quality of service over heterogeneous networks, non-terrestrial networks, and networking security. He was the Chair of the IEEE Satellite and Space Communications Technical Committee from 2006 to 2008.

FULVIO BABICH (Senior Member, IEEE) received the Laurea degree (cum laude) in electrical engineering from the University of Trieste, in July 1984. After graduation, he was with Research and Development Laboratories, Telettra, where he was engaged in optical fiber communications. Then, he joined Zeltron, where he was a Communication System Engineer, responsible for the activities within the ESPRIT Program. In 1992, he joined the Department of Electrical Engineering (DEEI), University of Trieste, where he is currently a Full Professor of digital communications and wireless networks. He has been the Vice Director of the Department of Engineering and Architecture. He is the Coordinator of the Ph.D. Program for Industrial and Information Engineering with the University of Trieste. He was a Board Member of National Telecommunications and Information Theory Group–GTTI and the Directive Board Member of the National Inter-University Consortium for Telecommunications (CNIT). His current research interests are in the field of wireless networks and millimeter wave communications. He is involved in channel modeling, multiple access techniques, channel encoding, error control techniques, and cross-layer design.

MASSIMILIANO COMISSO (Member, IEEE) received the M.Sc. degree in electronic engineering and the Ph.D. degree in information engineering from the University of Trieste, Italy, in 2003 and 2007, respectively. He was with Alcatel, on DWDM systems and with Danieli Automation, on electromagnetic NDE models. Currently, he is an Associate Professor in communication networks and waveguide/optical systems with the Department of Engineering and Architecture (DIA), University of Trieste. He is the author/co-author of more than 100 international scientific papers. His research interests include distributed wireless networks, millimeter-wave communications, antenna array synthesis, and small antennas. He has been a Best Paper Award (BPA) Student Finalist at IEEE GLOBECOM'06 and received the BPA at IEEE CAMAD 2009. He serves as a referee/TPC member for several IEEE journals and conferences.

ALBERTO CARINI (Senior Member, IEEE) received the Laurea degree (summa cum laude) in electronic engineering and the Ph.D. degree in information engineering from the University of Trieste, Trieste, Italy, in 1994 and 1998, respectively. From 1996 to 1997, he was a Visiting Scholar with the University of Utah, Salt Lake City, UT, USA. From 1997 to 2003, he was a DSP Engineer with Telit Mobile Terminals SpA, Trieste. In 2003, he was with Neonseven srl, Trieste. From 2001 to 2004, he was also a Contract Professor of digital signal processing with the University of Trieste. From 2004 to 2018, he was an Associate Professor with the University of Urbino. Since 2018, he has been an Associate Professor with the University of Trieste. His research interests include digital signal processing, system identification, nonlinear filtering, and adaptive filtering for electronics, audio, and telecom applications. He is a member of EURASIP. His professional activities include the following: the Member-at-Large with the IEEE SPS Conference Board (2009–2010); a member of the IEEE SPS Signal Processing Theory and Methods Technical Committee (2006–2011 and 2015–2020); the Program Co-Chair of signal processing area at 2009 International Symposium on Image and Signal Processing and Analysis (ISPA) and 2013 International Symposium on ISPA; an Editorial Board Member (Handling Editor) of *Signal Processing* (2005–2021); and an Associate Editor of *EURASIP Journal on Advances in Signal Processing* (2023–2024). Since 2022, he has been serving as an Area Editor for *Digital Signal Processing*.

FRANCESCO ADAMO received the joint M.Sc. degree in electronic engineering from the University of Perugia, Italy, in collaboration with Huawei Italia Srl. He is currently pursuing the Ph.D. degree with the National Ph.D. Program in Space Science and Technology, University of Trento. His master's thesis titles ''Design of an E-Band Resistive Mixer in GaAs HEMT Technology. He is conducting the Ph.D. research with PicoSaTs s.r.l., Trieste, in collaboration with the University of Trieste. His work focuses on 5G satellite telecommunications payloads for the future integration of non-terrestrial networks. As part of his Ph.D. activities, he is also involved in in-lab emulation and validation of hardware systems for SATCOM 5G at European Space Agency ESTEC Facility, The Netherlands.

SIMONE PAULETTO was born in 1997. He received the B.Sc. degree (magna cum laude) in electronics and computer science engineering from the University of Trieste, Italy, in 2019, where he is currently pursuing the M.Sc. degree in electronics and computer science engineering. He joined PicoSaTs s.r.l., Trieste, where he is studying electronic systems for small satellites through a research grant. His main area of study is power electronics, specifically switching circuits, such as class D power amplifiers and SMPSs.

HENOK BERHANU TSEGAYE (Member, IEEE) received the B.S. degree in electrical and computer engineering and the M.S. degree in communication engineering from Jimma University, Ethiopia, in 2016 and 2019, respectively, and the joint Ph.D. degree from the Information Engineering and Computer Science (IECS) School, University of Trento, Italy, in collaboration with Bruno Kessler Foundation (FBK), in November 2024. He was an Assistant Lecturer with the Department of Electrical and Computer Engineering, Jimma University; and a Satellite Ground Station Operator with Ethiopian Space Science and Technology Institute (ESSTI). He is currently a Post-Doctoral Fellow with the Department of Electrical and Computer Engineering, The University of New Mexico. His research interests include network monitoring and orchestration, virtualization, resilient non-terrestrial networks, beyond 5G/6G communications, software-defined radio and networking, cloud-edge continuum frameworks, and blockchain for network security.

PETRO MUSHIDI TSHAKWANDA (Senior Member, IEEE) received the M.Sc. degree in financial engineering from World Quant University, New Orleans, LA, USA, the another M.Sc. degree in information systems management from the University of Liverpool, Liverpool, U.K., and the Ph.D. degree in engineering (Hons.) from the Department of Electrical and Computer Engineering, The University of New Mexico, Albuquerque, NM, USA. He is a distinguished figure in education, research, and technology leadership, with a rich expertise spanning artificial intelligence and machine learning, intelligent network systems, the Internet of Things, and network automation. His scholarly pursuits have been marked by groundbreaking research in designing intelligent network systems through multi-agent systems. His contributions have been published in prestigious journals and presented at esteemed conferences, exemplifying his pivotal role in advancing network optimization and management.

MICHAEL DEVETSIKIOTIS (Fellow, IEEE) received the Dipl.-Ing. degree in electrical engineering from the Aristotle University of Thessaloniki, Greece, in 1988, and the M.S. and Ph.D. degrees in electrical engineering from North Carolina State University, Raleigh, NC, USA, in 1990 and 1993, respectively. Since July 2016, he has been a Professor and the Chair of the Department of Electrical and Computer Engineering, The University of New Mexico, Albuquerque, NM, USA. He is a renowned researcher, with a focus on the design and performance evaluation of telecommunication networks, complex socio-technical systems, cyber-physical systems, and smart grid communications. His research has received funding from prestigious organizations, such as the National Science Foundation (NSF), the Natural Sciences and Engineering Research Council of Canada (NSERC), and industry leaders, such as Cisco and IBM. He has garnered significant recognition for his contributions, with more than 10 000 citations. In 2017, he was inducted into the NC State ECE Alumni Hall of Fame. His extensive body of work includes over 50 refereed journal articles, 130 conference papers, and 61 invited presentations. His work continues to shape emerging areas, such as smart cities, the IoT, and socio-technical system modeling and simulation.